Hillslope response to climate-modulated river incision and the role of deep-seated landslides in post-glacial sediment flux: Waipaoa Sedimentary System, New Zealand

---

A thesis submitted in partial fulfilment of the requirements for the
Degree of
Doctor of Philosophy in Geology

By

Eric Leland Bilderback

University of Canterbury
Christchurch, New Zealand

July, 2012

View along one of the tributaries to the Waingaromia River in the upper Waipaoa catchment. Landscape features include deep-seated landslides of different size (foreground and middle distance) and last glacial aggradation terrace remnants (right side of the image) perched above the Waingaromia River.

Table of Contents

List of Figures

List of Tables

Digital Appendices

Acknowledgements

Funding for this research, including scholarship and research costs, was provided by the Ministry of Science and Innovation (formerly the Foundation for Research, Science and Technology) contract C05X0705: Terrestrial Landscape Change: MARGINS Source-to-Sink New Zealand led by Dr. Nicola Litchfield. In addition, lidar topography for part of the study area was provided as an academic exchange with Dr. Josh Roering and Dr. David Schmidt at the University of Oregon, USA from an NSF - MARGINS grant (OCE-0841111) to study sediment production via landsliding. Without these funding sources, this research would not have been possible.

Throughout my studies at the University of Canterbury, my wonderful wife, Alexandra, and sweet daughter, Chani, have provided me unwavering support. In addition to being a caring mother and supportive wife, Alexandra has been an incredible field assistant and an understanding partner while living so far from her Chicago, USA-based family in the earthquake-ravaged city that we have come to love. Alexandra's parents, Edmond and Julie Feldy, have been wonderfully supportive and loving throughout our time in New Zealand. Chani has been an absolute joy and a much needed distraction from long days in the office, and while she may not remember much of Christchurch, earthquakes, or hikes in the Southern Alps, her first years in New Zealand have been truly wonderful.

The Department of Geological Sciences at the University of Canterbury has been a singularly vibrant academic environment over the course of my studies. From the enthusiasm of staff, lasting friendships, and support for research, I have been overwhelmed by how positive the environment has been. The Department was also proactive in recognizing the research potential after the 4th, September 2010 M_w 7.1 Darfield Earthquake and was supportive after the more destructive 22nd, February 2011 Christchurch earthquakes.

My supervisory team of Jarg Pettinga, Nicola Litchfield, and Mark Quigley have been excellent, and I thank Jarg and Nicola for imagining this project, securing funding and being very supportive. I thank Mark for insight in the field, pushing me to think large,

and for being a great friend. Jarg, Nicola, and Mark worked well as a team using their diverse research talents to their fullest to bring the best out of this research.

Other researchers who have provided data, suggestions or support have also been invaluable to the success of this project. These include: Mike Marden at Landcare Research who is the Waipaoa-Guru; Josh Roering at the University of Oregon, USA who provided a sounding-board in the field and incredible lidar topography; Oliver Korup at the Institute of Earth and Environmental Sciences, Potsdam University, Germany who supplied much needed guidance in statistical techniques for landslide volumetric estimates; Alan Palmer at Massey University gave guidance and provided tephra sample standards; Mike Page at GNS Science gave much guidance; and Ben Crosby at the Idaho State University, USA provided guidance and knickpoint data.

Access to field areas around the Mangatu River was generously provided by Integrated foods, who manage the Mangamaia, Maungahaumi, and Komihana Stations that form most of the western study site. Access to field areas around the Waingaromia River was provided by Waitangi-Terrace Station and Toromiro Station, which collectively encompass most of the eastern study site. Station managers and staff, who are intimately familiar with these properties, provided invaluable insight about history, geomorphology, and land use issues.

I would also like to acknowledge some of my fellow Doctoral Candidates at the University of Canterbury, Brendan Duffy, Tim Stahl, and Tom Brookman, wonderful colleagues who provided feedback on this research and extraordinary friendship.

Finally to Diane and David Bilderback, there is no way for your son to express the gratitude he feels for your continued support and outstanding editing skills.

Abstract

Quantifying how hillslopes respond to river incision and climate change is fundamental to understanding the geomorphic evolution of tectonically uplifting landscapes during glacial-interglacial cycles. Hillslope adjustment in the form of deep-seated bedrock landslides can account for a large proportion of the regional sediment yield and denudation rates for rapidly uplifting landscapes. However, the timing and magnitude of the response of hillslopes to climatic and tectonic forcing in moderate uplift temperate maritime catchments characteristic of many active margins worldwide is not well quantified. This study seeks to investigate how hillslopes respond to climate-modulated river incision and to quantify the magnitude of the sediment flux from this response in a typical active margin setting.

The non-glacial Waipaoa Sedimentary System (WSS) on the East Coast of the North Island of New Zealand consists of river catchments, coastal foothills to uplifting mountain ranges, and terrestrial and marine sediment depocentres collectively underlain by relatively young (Cretaceous and younger) sedimentary rocks within a tectonically active setting and temperate maritime climate. These attributes make the WSS similar to many coastal catchments on oceanic-continental convergent margins worldwide. However, because of widespread destruction of primary forests for conversion to pasture lands by the mid 20th Century, the WSS is currently a globally significant source of sediment to the world's oceans. Because of these factors, the WSS was selected as one of two global study sites for the international, NSF supported, MARGINS Source-to-Sink initiative designed to investigate the transfer of sediment from terrestrial source to marine sink. Previous studies on the WSS have shown a strong link between climate change and geomorphic response in the system. River incision since the last glacial coldest period has generated a significant amount of topography, leaving small remnants of the ca.18,000 cal. yr BP last glacial aggradation terrace scattered up to 120 m above modern rivers.

In this study, the hillslope response to river incision is quantitatively examined using new high resolution topographic data sets (lidar and photogrammetry) in combination with

field mapping and tephrochronology. Hillslopes are found to be coupled to river incision and adjusted to rapid incision through the initiation and reactivation of deep-seated landslides. In the erodible marine sedimentary rocks of the terrestrial WSS, post-incision deep-seated landslides can occupy over 30% of the surface area. Many of these slides show evidence of multiple "nested" failures and landslide reactivation. The ages of tephra cover beds identified by electron microprobe analysis show that following an initial 4,000 to 5,000 year time lag after the initiation of river incision, widespread hillslope adjustment started between the deposition of the ca. 13,600 cal. yr BP Waiohau tephra and the ca. 9,500 cal. yr BP Rotoma tephra. Tephrochronology and geomorphic mapping analysis indicates that river incision and deep-seated landslide slope adjustment is synchronous between mainstem rivers and headwater tributaries. Tephrochronology further shows that many slopes have continued to adjust to channel incision into the late Holocene. Hillslope response in the catchment can involve the entire hillslope from river to ridgeline, with some interfluves between incising sub-catchments being dramatically modified through ridgeline retreat and/or lowering. Using the results of the landform tephrochronology and geomorphic mapping, a conceptual time series of hillslope response to uplift and climate change-induced river incision is derived for a timeframe encompassing the last glacial-interglacial cycle.

Using the same high resolution topography datasets, in-depth field analysis, and tephrochronology, the 18,000 year sediment yield from terrestrial deep-seated landslides in the WSS is estimated in order to investigate the magnitude of hillslope response to climate-modulated, uplift driven river incision. This completes one of the first process-based millennial time-scale sediment budgets for this class of temperate maritime, active margin catchments. Fluvial and geomorphic modelling is applied to reconstruct pre 18,000 cal. yr BP topography in 141 km^2 of detailed study area and the resulting volumetric estimates from 207 landslides are used to estimate deep-seated landslide sediment flux for the broader system. An estimated 10.2 km^3 of deep-seated landslide-derived sediment with a multiplicative uncertainty of 1.9 km^3 (+9.2 km^3, -4.8 km^3) was delivered to terrestrial and marine sinks. This accounts for between 10 and 74% of the total mass of the terrestrial WSS budget of ca. 91,000 Mt (+37,000 Mt, -26,000 Mt). Combining the deep-seated landslide results with other studies of terrestrial sediment sources and terrestrial and shelf sinks, the estimated terrestrial source load ranges from

1.2 to 3.7 times larger than the mass of sediment sequestered in terrestrial and shelf depocentres. This implies that off-shelf transport of sediment is important in this system over the last 18,000 cal. yr BP, as it is today for anthropogenic reasons. Based on the derived sediment budget, the denudation rate for the terrestrial WSS of 0.8 mm yr^{-1} (+0.3 mm yr^{-1}, -0.2 mm yr^{-1}) is indistinguishable from the average terrestrial Waipaoa late Quaternary uplift rate, indicating an approximate steady-state balance between denudation and uplift. This thesis provides a quantitative analysis of the role of deep-seated landslides in an active margin catchment that is used to improve the understanding of landscape and terrestrial source-to-marine-sink sediment transfer dynamics.

Chapter 1: Introduction and thesis organization

1.1 Introduction

The sensitivity of landscapes to environmental change and to the geomorphic processes controlling sediment generation and storage is important to our understanding of evolving landscapes, and can be illuminated by inclusive landscape-wide sediment budget studies (e.g. Gomez et al., 2001; Kuehl et al., 2003, 2006; Carter et al., 2010). Landscapes responding to tectonics (long-term uplift and periodic seismic events) and/or climate change alter erosion patterns, shift the availability of water for agricultural and forestry resources, and expose people and public resources to geologic hazards. The role of deep-seated landslides in the evolution of landscapes is important because these large erosional processes connect ridgetops and hillslopes to river systems and valley floors, acting as agents to transmit change in the fluvial systems to the rest of the landscape. There is an emerging consensus that deep-seated landslides can account for a large proportion of the regional sediment yield for very high uplift landscapes such as the Himalayas, the Southern Alps of New Zealand, and Taiwan (e.g. Burbank et al., 1996; Hovius et al., 1997; Hewitt, 1998; Hovius et al., 2000; Korup et al., 2004; Korup, 2006), but the role of deep-seated landslides in moderate uplift, temperate maritime catchments that characterize many active margins is not well quantified.

The propensity of large deep-seated landslides to impact the morphology and resources of the East Coast of the North Island of New Zealand, a typical temperate maritime active margin, has been long recognized (e.g. Guthrie-Smith, 1969; Gage and Black 1979). However, the concept for quantifying the timing and long-term (post 18,000 cal. yr BP) impact on landscape evolution of these features, a main focus of this study, grew out of the development of the USA National Science Foundation's MARGINS Source-to-Sink initiative. This broad science initiative attempted to quantify mass fluxes of sediment across the Earth's continental margins by providing funding, research objectives, and community access to oceanographers, geochemists, geologists, and geomorphologists interested in the role that climate, tectonics and eustasy play in shaping the Earth's surface (Gomez et al., 2001). Discussions within the scientific community interested in sediment budget approaches to interdisciplinary Source-to-Sink

questions led to the selection of two systems for focused research; the Waipaoa Sedimentary System (WSS) in the North Island of New Zealand and the Fly River System in Papua New Guinea. The advantages of the WSS are that the primary sources and sinks of sediment have good access and are generally are open to investigation, permitting the opportunity to close sediment budgets and connect landscape evolution to stratigraphy (Gomez et al., 2001).

After an initial round of targeted research, a knowledge gap with respect to the role of large-scale deep-seated landslides in the WSS was identified (e.g., Litchfield et al., 2008). Research into the marine environments and terrestrial fluvial systems was progressing but the role of deep-seated landslides in production, transferral, and sediment storage was still poorly understood. This was highlighted in conferences preceding the funding of this project and was further noted in a concluding remark for a study investigating post-glacial river incision in the WSS. Marden et al. (2008) found that postglacial channel incision represents only ca. 25% of the volume of sediment stored in terrestrial and marine depocentres in the WSS, and suggested that unquantified hillslope erosion processes are likely to make up the difference. The impression left by this statement, that there is an apparent sediment budget deficit (i.e. not enough source for the amount of sediment in the sink), is in fact not technically correct. As shown in Chapter 3, Marden et al. (2008) compared volumes of low density marine Latest Pleistocene to Holocene deposits to higher density terrestrial source materials, whereas sediment mass should have been compared instead. However, the statement and research paper did help to highlight the fact that post ca. 18,000 year river incision had exported large volumes of material from the terrestrial WSS to marine environments but that an equally obvious geomorphic process in the WSS, deep-seated landslides, was unquantified. Since research on the WSS terrestrial and marine depocentres was complete or progressing (e.g. Brown 1995; Foster and Carter, 1997; Orpin et al., 2006; Marden 2008; Gerber et al., 2010; Wolinsky et al., 2010), quantifying the role of deep-seated landslides in the WSS presented a unique opportunity to pursue a process based quantitative landscape evolution project that would tie in with the sediment budget approach to a broader interdisciplinary Source-to-Sink study.

This research seeks to quantify hillslope response to climate-modulated river incision

and the role of deep-seated landslides in the sediment flux of the Waipaoa Sedimentary System. The geologic timeframe for this investigation is limited to the last glacial-interglacial cycle (ca. 28,000 cal. yr BP to present). This is because the geomorphic record of landscape change in the WSS is best preserved for this period and the post-glacial (ca. 18,000 cal. yr BP) depocentres are reasonably well defined.

The objectives for this project are to:

1. Investigate the relationship between river incision and deep-seated landslides.
2. Evaluate how deep-seated landslides have contributed to the geomorphic evolution of hillslopes.
3. Develop a chronology of hillslope response to climate-modulated uplift-driven river incision.
4. Develop a conceptual model for how hillslopes have responded to tectonic uplift and climate change during the last glacial-interglacial transition.
5. Approximate the sediment flux from deep-seated landslides over the last glacial-interglacial cycle.
6. Explore the contributions of deep-seated landslides to the wider WSS sediment budget.
7. Synthesize the implications of the sediment budget estimate on the dispersal of sediment within the WSS.

To accomplish these objectives, I use new high resolution topographic data sets (lidar and photogrammetry), in combination with field mapping and tephrochronology, to determine the timing and extent of post ca. 18,000 year deep-seated landsliding. Landslide volumes and their relationship to river incision were calculated through paleo-topographic reconstructions using detailed geomorphic mapping and aspects of stream profile analysis. Landslide population statistics and volume-area scaling relationships were then applied to the landslide dataset to evaluate the magnitude of sediment generated by these landslides.

These techniques were applied to two study areas of reasonable size and access with contrasting lithology, structural setting, and relief which were considered to be

representative of general hillslope processes in the WSS. The study area results were then scaled-up to the entire terrestrial WSS and combined with estimates of the magnitude of other erosional processes and previous depocentre investigations to calculate the ca. 18,000 year sediment budget for the entire system. Finally, the implications of the sediment budget for landscape evolution and the transferral of sediment from terrestrial source-to-marine-sink are discussed.

1.2 Thesis organization

This thesis is presented in three main chapters that address the timing and conceptual evolution of the hillslope response to river incision, the role of deep-seated landslides in the WSS, and geomorphic evidence for differential uplift across the terrestrial WSS. The chapters are self contained and have been written to facilitate publication. Therefore, much of the introductory aims, scope, and previous research information related to the individual chapters are contained in the chapters, and are not repeated here. In addition, Litchfield et al. (2008) produced a review of the research conducted and future direction of WSS studies, so an exhaustive literature review is not included in this chapter.

Chapter 2 “Hillslope response to climate-modulated river incision in the Waipaoa Catchment” and Chapter 3 “The role of deep-seated landslides in post-glacial sediment flux from the Waipaoa Sedimentary System” represent the main body of work addressing the Source-to-Sink sediment budget of the WSS and the role of deep-seated landslide in the overall system. Because of the detail of both of these chapters, abstracts have been included at the start of the chapters as a means of summarizing these significant sections.

Chapter 4 “Stream profile analysis and uplift in the Waipaoa and Waimata catchments” developed out of stream profile research done for aspects of Chapter 3 and is written as a more standard thesis chapter, rather than the largely stand-alone works in Chapters 2 and 3.

Chapter 5, Conclusions, presents summaries of the conclusions of Chapters 2 to 4 and is the final section of the thesis.

Digital appendices are also included of the tabular results of the electron probe

microanalysis for landform tephrochronology, Geographic Information System layers (ESRI ArcGIS®) of much of the spatial analysis data, and photos of soil profiles from sites used in the tephrochronology. The appendices are provided as a repository of data collected and analyzed for this work but are not specifically referred to in the text because examples of these data and analysis are provided in the main body of the thesis.

Chapter 2: Hillslope response to climate-modulated river incision in the Waipaoa Catchment, East Coast North Island, New Zealand

2.1 Abstract

Quantifying hillslope response to the interplay between river incision and climate change is fundamental to understanding the evolution of uplifting landscapes during glacial-interglacial cycles. The non-glacial Waipaoa River catchment located in the exhumed inner forearc of an active subduction margin on the east coast of the North Island of New Zealand is an ideal area to investigate the dynamics between uplift, river incision, and hillslope response. Parts of the catchment have been incised up to 120 m since the last glacial coldest period (LGCP) leaving small remnants of the ca.18,000 cal. yr BP LGCP aggradation terrace scattered throughout the landscape. New high resolution topographic data sets (lidar and photogrammetry) combined with field mapping and tephrochronology in the upper Waipaoa catchment indicate that hillslopes adjusted to this rapid incision through the initiation and reactivation of deep-seated landslides. In the erodible marine sedimentary rocks of the Waipaoa, post incision deep-seated landslides can occupy over 30% of the surface area. Many of these slides show evidence of multiple "nested" failures and landslide reactivation. The ages of tephra cover beds identified by electron microprobe analysis show that following an initial 4,000 to 5,000 year time lag after the initiation of river incision, widespread hillslope adjustment started between the deposition of the ca. 13,600 cal. yr BP Waiohau tephra and the ca. 9,500 cal. yr BP Rotoma tephra. Tephrochronology and geomorphic mapping analysis indicates that river incision and deep-seated landslide slope adjustment is synchronous between main stem rivers and headwater tributaries. Tephrochronology further shows that many slopes have continued to adjust to channel incision into the late Holocene. Hillslope response in the catchment can include the entire slope from river to ridgeline, with some interfluves between incising sub-catchments being dramatically modified through ridgeline retreat and/or lowering. Using the results of the landform tephrochronology and geomorphic mapping, I derive a conceptual time series of hillslope response to uplift and climate change-induced river incision over the last glacial-interglacial cycle.

2.2 Introduction

An understanding of the erosive response of hillslopes to river incision coupled to uplift and climate change in climatically sensitive and active tectonic areas is fundamental, with a majority of the world's erosive activity taking place at these locations (Milliman and Farnsworth, 2011). It is hillslope processes delivering sediment to streams and rivers that make the sediment discharge from sensitive small mountainous catchments globally significant (Milliman and Syvitski, 1992). The Waipaoa Sedimentary System (WSS) on the North Island East Coast (NIEC) of New Zealand (Fig. 2.1) is one such small mountainous river system. Poorly indurated and highly fractured sedimentary rocks underlying much of the WSS have contributed to some of the highest sediment yields ever recorded (Griffiths, 1982; Walling and Webb, 1996; Hicks et al., 1996). Sensitivity to external forcing such as changing storm frequency and deforestation (Gage and Black, 1979; Page and Trustrum, 1997; Page et al., 1999; Wilmshurst et al., 1999) played a role in the selection of this system as part of a larger international initiative investigating terrestrial to marine sediment response and transfer called the MARGINS Source-to-Sink (Gomez et al., 2001; Kuehl et al., 2003, 2006; Carter et al., 2010). The sensitive, rapidly responding Waipaoa Sedimentary System is

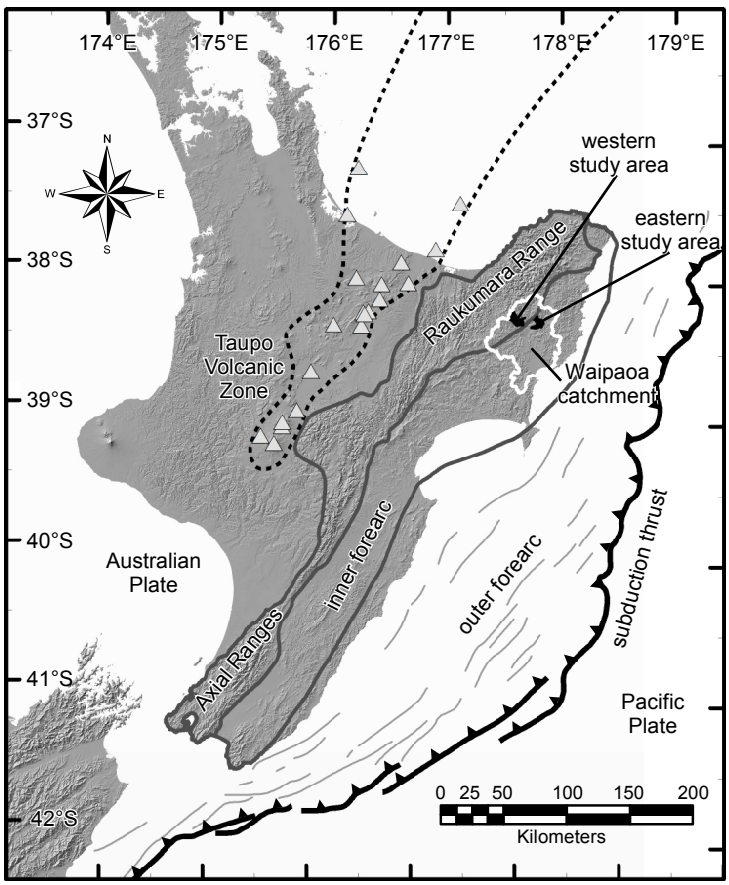

Figure 2.1. Location and regional tectonic setting of the Waipaoa catchment (white outline) and the two representative study areas on the Hikurangi Subduction Margin, east coast North Island of New Zealand. Triangles are locations of volcanoes in the Taupo Volcanic zone. Figure modified from Litchfield et al. (2007).

an ideal location to investigate the response of hillslopes to large scale (glacial-interglacial) climate change and ongoing tectonic uplift on an active margin.

The change from the last glacial to the current interglacial climate increased annual precipitation and temperature and reduced seasonality over much of New Zealand (e.g. Shulmeister et al., 2004; Drost et al. 2007). In North Island river catchments this led to increased annual discharge but a decrease in the erodibility of upland slopes due to the rapid spread of podocarp forest (Newnham and Lowe, 2000; McGlone, 2001, 2002; Litchfield and Berryman, 2005, 2006; Alloway et al., 2007). In the terrestrial WSS the changing climate resulted in an incision of up to 120 m in trunk and tributary channels (Berryman et al., 2000; Eden et al., 2001; Marden et al., 2008). The incision dramatically increased tributary relief and over-steepened valley walls. This incision occurred in all of the North Island east coast catchments studied by Litchfield and Berryman (2005) and small scale incision-induced gravitational instability has been observed in east coast catchments other than the Waipaoa (e.g. Pettinga and Bell,1992; Lacoste et al., 2009). Underlain by soft marine sedimentary rocks, hillslopes in the terrestrial WSS are prone to deep-seated mass movement (Gage and Black, 1979; Pearce and Black, 1981, Gomez and Livingston, 2012). Understanding the interplay between hillslope processes, such as deep-seated landslides, and episodes of river incision and aggradation can shape a broader understanding of landscape evolution.

To study the modes and timing of hillslope response to climate-modulated uplift-driven river incision, I chose two geologically and geomorphologically distinct study areas to represent the ca. 2500 km^2 two major river catchments that comprise the terrestrial WSS. These are the Waipaoa and Waimata river catchments (Figs. 2.1 and 2.2). The study areas encompass terrain ranging from the lower reaches of two of the three main upper tributary sub-catchments of the Waipaoa River catchment to 1^{st} order basins. These areas include remnants of the last glacial coldest period (LGCP) (ca. 28,000 - 18,000 cal. yr BP) aggradation terrace (Berryman et al., 2000; Marden et al. 2008) and numerous lithologic and non-lithologic knickpoints (Crosby and Whipple, 2006). These features are markers of previous landscapes and are benchmarks that can be used to measure change.

I use geomorphic mapping based on field investigation, air photo interpretation and new photogrammetric and lidar topography in the two study areas to investigate post river incision deep-seated landslides. Slope activity in response to the last episode of incision is differentiated from older activity based on landform tephra cover and cross cutting relationships with last glacial aggradation terraces. In the last ca. 25,500 years the WSS has been the recipient of ash fall from many (up to 19) major volcanic eruptions in the Taupo and Okataina volcanic centres (e.g. Lowe et al., 1999; Shane et al., 2003; Lowe et al., 2008, Vandergoes et al., 2013) which are west of and upwind of the WSS. During deposition, these tephra deposits blanket the landscape (Gage and Black, 1979, Pearce and Black, 1981); later mass movement modifies this cover by disrupting stratigraphic coherence and/or partially or completely stripping tephra from the landscape. The tephra cover has enabled me to assign minimum stabilization ages to some landslides in a landscape largely devoid of sufficient quartz for cosmogenic exposure ages and radiocarbon material for dating of landslide deposits. In addition, by investigating a population of landslide stabilization ages, I can infer the timing of hillslope response to river incision.

In this chapter I: (1) connect deep-seated landslide related hillslope erosion to post LGCP river incision in the tectonically active and climatically sensitive WSS; (2) discuss the geomorphic evolution of WSS valley walls and interfluves from the LGCP to present; (3) present a chronology of slope response based on tephra cover; and (4) present a conceptual model for catchment evolution in the context of river incision and uplift over the last glacial-interglacial cycle.

2.3 Tectonic, geologic and climatic setting

2.3.1 Tectonic setting

The WSS straddles the active inner forearc of the Hikurangi subduction margin with its headwaters in the actively uplifting axial ranges of the North Island (Raukumara Range) (Fig. 2.1). The majority of the terrestrial WSS is drained by the Waipaoa and Waimata river catchments (ca. 2500 km^2 out of 3200 km^2). Other small coastal catchments contribute to a common WSS marine sediment depocentre, but for consistency with other studies (eg. Kuehl et al., 2006; Marden et al. 2008) this chapter focuses on the Waipaoa and Waimata catchments. In this study, I define the Waipaoa catchment as the

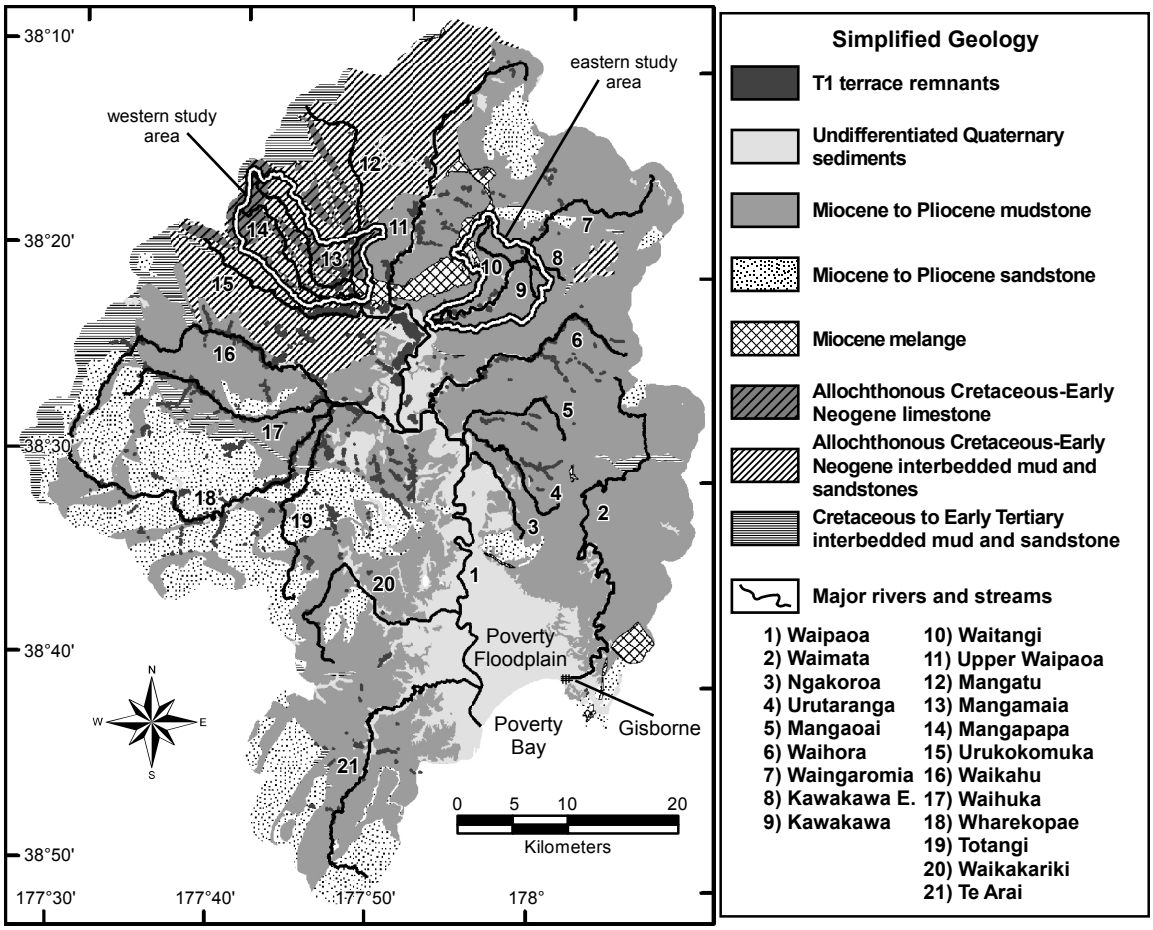

Figure 2.2. Simplified geologic map of the Waipaoa and Waimata catchments. Major tributaries are named and the study areas are outlined. Geologic map modified from Mazengarb and Speden (2000).

ca. 2500 km^2 that includes both the Waipaoa and Waimata rivers (Fig. 2.1). The Waimata River is included because this river flows into the same marine depocentre and was likely a tributary to the Waipaoa during sea-level lowstands. West of the Raukumara Range divide is the active Taupo Volcanic Zone (TVZ) which is a continental rift that has been one of the most active rhyolitic eruptive systems in the latest Pleistocene and Holocene (Smith et al., 2005) (Fig. 2.1). The Raukumara Peninsula is cut by active normal, reverse, and strike-slip faults. Ruptures on these, as well as the subduction interface, could cause significant ground motions in the WSS (Modified Mercalli Intensity 8+) (Litchfield et al., 2009). Uplift is variable across the WSS and is discussed below and in Chapter 4.

2.3.2 Geology and rock properties

The inner forearc sequence underlying the terrestrial WSS is mostly composed of imbricate-thrust Miocene-Pliocene marine mud and sandstones (e.g. Lewis and Pettinga,

1993; Mazengarb and Speden, 2000). Diapiric, chaotic melange that probably originated from Miocene under-compacted shales underlies the north central and coastal eastern areas of the Waipaoa catchment (Neef and Bottrill, 1992; Mazengarb and Speden, 2000) (Fig. 2.2). A highly deformed allochthonous sequence of Cretaceous to Early Neogene marine mudstones, sandstones, and limestones underlie about 15% of the catchment, mostly in the northwest (Fig. 2.2). Swelling smectite clays are present in the mudstones of the region (Gage and Black, 1979; Pearce and Black, 1981; Pettinga and Bell, 1992; Lacoste et al., 2009). These tectonically crushed, compacted but poorly cemented, interbedded marine sediments of the NIEC forearc sequence are prone to slaking disintegration through wetting and drying cycles and can weather to thick (ca. 5 - 15 m in convergent areas) clay-rich residual soil (Gage and Black, 1979).

Unweathered mudstone and sandstone outcrops in the terrestrial WSS exhibit a Hoek and Brown (1997) geological strength index (GSI) of 15 to 35. GSI in this range for these lithologies generally relates to rock with friction angles less than about 33º and low uniaxial compressive strength (between 5 and 35 MPa) (Hoek and Brown, 1997). This is corroborated by uniaxial compression tests done on sandstone and siltstone samples from the NIEC (Pettinga and Bell, 1992; Lacoste et al, 2009)

2.3.3 Morphology

The overall form of the Waipaoa catchment is highly concave with tributaries eroding back into uplands radially from the mainstem Waipaoa River. The maximum altitude of the terrestrial WSS is 1,200 m. Mean altitude is ca. 300 m, but only about 16% of the Waipaoa catchment is over 500 m. Relief is highest in the northwest of the catchment, approaching 600 m from valley bottom to ridge top. Areas mapped as allochthonous marine mudstone, sandstone and limestone correspond to the areas of highest relief (Fig. 2.2) (Mazengarb and Speden, 2000). Limestone ridges in this area exhibit the steepest slopes (up to 60°), while the Miocene melange exhibits the lowest relief and gentlest slopes of any of the pre-Quaternary geologic units. Most of the rest of the catchment has maximum hillslope relief of ca. 300 m.

The WSS exhibits many varied landforms including deep-seated landslides, aggradation (fill) terraces, fill-cut terraces, strath terraces, and knickpoints. For the purposes of this

study, I define deep-seated landsides as landslides typically involving organic and inorganic soils (regolith) and varying amounts of weathered or unweathered bedrock. In many cases this can be generalized as landslides failing to a depth of more than about 3 m. Deep-seated landslides of many sizes and types, which are described in detail in the following sections, are pervasive in the terrestrial WSS (e.g. Gage and Black, 1979; Pearce and Black, 1981; Pettinga and Bell, 1992; Page and Lukovic, 2011). Small, discrete aggradation and degradation terrace remnants are preserved above many tributaries and are described in more detail below. The landslides and the repeated cycles of aggradation and incision give the terrestrial WSS hillslopes a distinctly hummocky morphology (landslides) separated by discrete areas of stepped topography (terraces). In addition, knickpoints related to river incision or lithology can be found throughout the catchment and indicate a landscape in transition (Crosby and Whipple, 2006).

Four generations of river aggradation are preserved as remnant terraces in the terrestrial WSS (Berryman et al., 2000; Marden et al., 2008). Because of clear regional correlation of the timing of these terraces across different river catchments in the NIEC (Litchfield and Berryman, 2005), I adopt the terminology of T1 to T4 for these terraces from Litchfield and Berryman (2005). This is opposed to the local Waipaoa terminology, Waipaoa-1 (W-1) to Waipaoa-4 (W-4) of Berryman et al. (2000), Eden et al. (2001), and Marden et al. (2008). The LGCP T1 terrace is by far the best preserved aggradation (fill) terrace and can be found in many tributaries above the Poverty Floodplain where this former valley bottom has been buried by more recent terrestrial aggradation and marine transgression (Fig. 2.2) (Berryman et al., 2000; Marden et al., 2008). The T1 terrace is comprised of a ca. 3 to 20 m thick package of sand, gravel, and cobble-bearing conglomerate covered by overbank silts and air-fall tephra. The thickness of the T1 gravel is generally less than 20% of the total post T1 river incision (Marden et al., 2008). T1 aggradation began between the deposition of the Omataroa and the Kawakawa tephra, ca. 33,000 to 25,500 cal. yr BP and ceased between the deposition of the Okareka and the Rerewhakaaitu tephra, ca. 22,000 to 18,000 cal. yr BP (Berryman et al., 2000; Eden et al., 2001; Litchfield and Berryman, 2005; Marden et al., 2008). Marden et al. (2008) note that the cessation of aggradation was followed by a period of incision that cut up to two degradation (fill-cut) terraces that are preserved in a small number of locations along major tributaries before the deposition of the Rerewhakaaitu tephra (ca. 17,625 cal. yr BP).

2.3.4 Uplift

Regional-scale uplift of the Raukumara Range is primarily driven by deep-seated subduction processes including: oceanic plateau subduction, seamount subduction, tectonic erosion and sediment underplating (Walcott, 1987; Reyners et al., 1999; Upton et al., 2003; Litchfield et al., 2007). Local Quaternary uplift is non-uniform across the catchment with parts of the lower catchment (southern Poverty Floodplain) undergoing tectonic subsidence, while uplift of the headwaters approaches 4 mm yr^{-1} (Brown, 1995; Litchfield and Berryman, 2006). Uplift rates for the upper Waipaoa catchment have been estimated by comparing the elevations of two generations of aggradation terraces, T3 and T1, that are correlated to high $\delta^{18}O$ cool Marine Isotope Stages 4 and 2 and with periods of glacial advance in the South Island (Berryman et al., 2000; Litchfield and Berryman 2005; Litchfield and Berryman 2006). Aggradation terraces T3 and T1 are dated at ca. 55,000 and 18,000 cal. yr BP, respectively, using tephrochronology techniques similar to those described below (Litchfield and Berryman, 2005). Assuming that the current difference in elevation between these two terraces is due to tectonic uplift, late Pleistocene uplift rates for the middle of the catchment in both field areas are estimated at between 1 and 2 mm yr^{-1} (see figure 10, Litchfield and Berryman, 2006).

2.3.5 Climate

Modern climate in the WSS is temperate maritime with mean annual temperatures of 12.5° to 15° C at the coast and lowlands and 7.5° to 12.5° C in the uplands (Leathwick et al. 2002). The mean annual minimum temperature is 2.5° to 5° C and 0° to 2.5° C and the mean annual maximum is temperature is 20° to 22.5° C and 17.5° to 20° C in the lowlands and uplands, respectively. Westerly winds shadow the Poverty Floodplain behind the Raukumara Range with mean annual precipitation of less than 1000 mm in Poverty Floodplain (Leathwick et al. 2002). Mean annual precipitation in the mid elevations is 1000 to 1500 mm and 1500 to 2500 mm in the headwaters of the WSS (Leathwick et al. 2002). High intensity rainstorms and cyclones occur frequently in the WSS averaging ca. 1 every 5 years throughout the Holocene (Page et al., 2010) and play a significant role in the WSS as evidenced by the widespread landsliding, flooding and sedimentation from Cyclone Bola in 1988 (Page et al., 1994a, b).

Broad paleoclimatic conditions in the WSS can be inferred from a number of

paleoclimate studies using proxy data such as pollen assemblages, changes in sedimentation and stable isotope ratios from sites around the NIEC and the North Island (Fig. 2.3). Holocene records include speleothems from the Hawke's Bay region (Lorrey et al., 2008), sediment cores from Lake Tutira (Page et al., 2010, Orpin et al., 2010), and a sediment core from Repongaere Swamp within the Waipaoa catchment (Wilmshurst et al., 1999). Latest Pleistocene to Holocene paleoclimate proxy data from around the NIEC are derived from sediments from Kaipo Bog (Hajdas et al., 2006; Newnham and Lowe, 2000; Lowe et al., 1999), Lake Poukawa (McGlone, 2002), and marine cores P69 (McGlone, 2001) and MD97-2121 (Carter et al., 2002) (Fig. 2.3). To assess the regional nature of the climate signal and to draw on other proxy records that span the last glacial-interglacial transition, these records can be compared with other North Island Latest Pleistocene to Holocene records including the Onepoto and Pukaki maars in the Auckland region (Augustinus et al., 2011; Sandiford et al., 2003) and Otamangakau wetland (McGlone et al., 2005) on the central North Island (Fig. 2.3). The closest terrestrial long record of environmental change and tephra deposition for this study is Kaipo Bog located about 70 km west of the Waipaoa field areas at an elevation of 980 m a.s.l (Fig. 2.3). This record exhibits high preservation of tephra and pollen with excellent age control and geochemically identified tephras (Lowe et al., 1999; Newnham and Lowe, 2000; Hajdas et al., 2006).

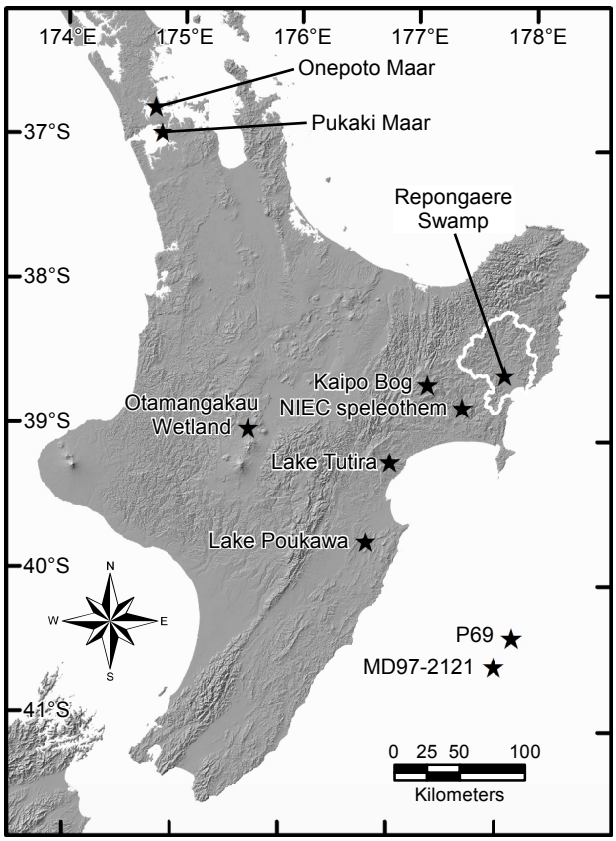

Figure 2.3. Location map of relevant paleoclimate studies referred to in the text.

Many of these high resolution paleoclimate records are summarized in Alloway et al. (2007), who produced a composite climate record for New Zealand. There is a high degree of correlation for paleoclimatic events between these records. The LGCP in New

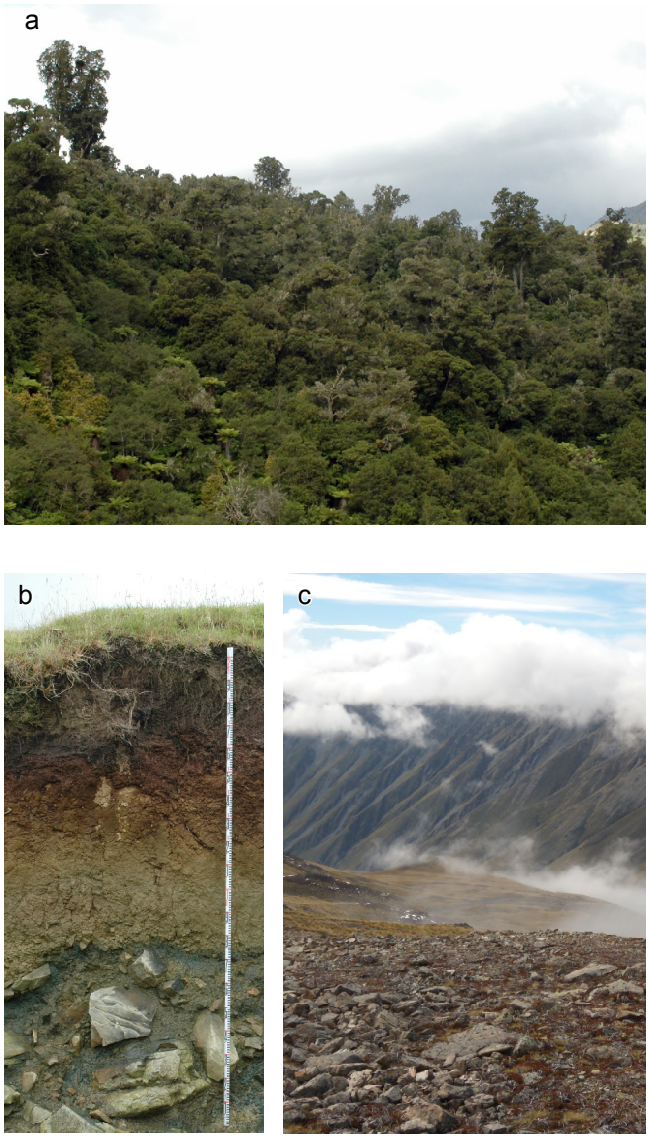

Figure 2.4. a) Current native podocarp-angiosperm forest completely covering hillslopes around the WSS at ~ 650 m a.s.l. b) Soil profile showing LGCP scree buried below tephric soils at 630 m a.s.l in the upper WSS western study area. The measuring rod is 2 m long. The basal tephra above the ancient scree is the 17,625 ± 425 cal. yr BP Rerewhakaaitu tephra identified by electron probe microanalysis. c) modern scree above treeline in the central South Island, New Zealand as a visual analog for upland conditions in the LGCP WSS.

Zealand began ca. 28,000 cal. yr BP and terminated at ca. 18,000 cal. yr BP. The transition from the LGCP to Holocene interglacial conditions was from ca. 18,000 cal. yr BP to ca. 11,600 cal. yr BP and included a Late-glacial climate reversal between ca. 13,500 and 11,600 cal. yr BP. The current Holocene interglacial period has had two phases of greatest warmth between ca. 11,600 and 10,800 cal. yr BP and from ca. 6,800 to 6,500 cal. yr BP (Alloway et al., 2007).

2.3.6 Vegetation

Vegetation cover on the hillslopes of the terrestrial WSS has varied dramatically during these different climate phases and because of the short-lived impacts (50 to 200 years) of multiple volcanic eruptions in the Taupo Volcanic Zone (Newnham and Lowe, 2000, Carter et al., 2002). During the LGCP, pollen assemblages in the basal sandy mud of the Kaipo Bog are dominated by grasses, other herbs, and sub-alpine shrubs with relatively little large tree pollen (Newnham and Lowe, 2000). Other lines of evidence that support sub-alpine conditions in the uplands of the WSS come from ancient scree buried beneath the latest Pleistocene tephras at elevations above about 500 m a.s.l. in the western field area and the upper WSS (Fig. 2.4b) (Gage and Black, 1979) and the fact that the Kaipo Bog at 980 m a.s.l. was non-depositional during the LGCP (Alloway et al., 2007). The ancient scree may be related to periglacial processes and lack of deposition at Kaipo Bog suggests that at these upper elevations very little vegetation cover existed (perhaps analogous to that shown in Fig. 2.4c).

After ca. 18,000 cal. yr BP mixed podocarp-angiosperm-beech forests expanded reaching a pre-late-glacial reversal maximum at ca. 15,500 cal. yr BP (Newnham and Lowe, 2000). However, the pre Late-glacial reversal ratio of lowland-montane podocarp pollen to upland grass pollen at Kaipo Bog was still less than half that after ca. 11,600 cal. yr BP., indicating that full Holocene forest conditions were not reached until after 11,600 cal. yr BP. This record of a full Holocene forest expansion and increasing mild and wet conditions after ca 11,600 cal. yr BP is echoed in the Auckland maar records (Augustinus et al., 2011; Sandiford et al., 2003). Based on the Kaipo Bog and Auckland records, it appears that the climatic optimum for podocarp-angiosperm forests (Fig. 2.4a) at mid to high elevations was not reached until after the Late-glacial climate reversal at ca. 11,600 cal. yr BP. Modern vegetation in the terrestrial WSS consists mainly of pasture land and exotic forest plantations. Fire may have been use as a forest clearance tool by early Polynesian (Maori) settlers but major deforestation began in the mid 19th Century by European settlers with wholesale conversion to pasture by the mid 20th Century (e.g. Pullar, 1962; Wilmshurst et al., 1999; Dymond et al., 1999).

2.4 Methodology

Two study areas of contrasting lithology and structural setting were chosen as representative of the post LGCP river incision and hillslope processes that characterize the upper WSS. The 57 km^2 eastern study area in the lower Waingaromia River catchment includes several complete tributary basins and is underlain by Miocene-Pliocene marine mudstones and diapiric melange (Fig. 2.2). The 84 km^2 western study area stretches from the lower Mangatu River to the catchment divide, includes two large tributaries to the Mangatu, and is underlain mostly by allochthonous Cretaceous-Early Neogene marine mudstone, sandstone, and limestones (Fig. 2.2).

2.4.1 Geomorphic mapping

Geomorphic mapping in both study areas was accomplished using a combination of field investigation, air photo interpretation, and interpretation of high resolution topography. The high resolution topographic data sets used are: 1) Eastern area - 2.5 m vertical accuracy photogrammetric topography from predominantly clear ground (deforested) photography acquired in the late 1970's and early 1980's. Contours in this area were processed to a 5 m grid using ESRI ArcGIS® software; 2) Western area - sub-metre airborne lidar (light detection and ranging) topography was acquired during the 2010 Australasian autumn by NZ Aerial Mapping Limited. Funding for the lidar was provided by NSF MARGINS grant OCE-0841111 (Sediment production via landsliding). For this study, bare earth lidar return data was processed to a 2 m grid using free software tools available through the NSF Open Topography Portal (http://www.opentopography.org/). Field mapping of geomorphic features such as landslides, terraces and knickpoints complemented and verified mapping and stream profile analysis based on photography and high-resolution topography. Most mapped features were field verified (e.g., 60% of the mapped landslides) during field campaigns in 2009 and 2010. All features mapped were digitised into a geographic information system (GIS) for analysis using ESRI ArcGIS®.

2.4.2 Tephrochronology and age control

First order age control for landslides active since the LGCP is possible by mapping slides that cross-cut the T1 LGCP aggradation surface (Marden et al., 2008). Based on this cross-cutting relationship these landslides must have experienced at least some

Tephra name	Mid-point of 2σ age-range (cal. yr BP)	TVZ Volcanic Center
Kaharoa	636 ± 12	Okataina
Taupo	1,717 ± 13	Taupo
Whakaipo - Unit-V	2,960 ± 190	Taupo
Waimihia	3,410 ± 40	Taupo
Whakatane	5,530 ± 60	Okataina
Mamaku	8,005 ± 45	Okataina
Rotoma	9,505 ± 25	Okataina
Waiohau	13,635 ± 165	Okataina
Rotorua	15,425 ± 325	Okataina
Rerewhakaaitu	17,625 ± 425	Okataina
Okareka	21,800 ± 500	Okataina
Kawakawa/Oruanui	25,360 ± 160	Taupo
Omataroa	32,755 ± 1415	Okataina
Mangaone	32,285 ± 755	Okataina
Rotoehu	ca. 55,000	Okataina

Table 2.1. Macro tephra deposits identified in the Waipaoa catchment by previous studies (Gage and Black, 1979; Wilmshurst et al., 1999, Berryman et al., 2000; Eden et al., 2001; Marden et al., 2008; Berryman et al., 2010). Ages are calibrated from C^{14} dates on proximal deposits (Newnham et al., 2004; Smith et al., 2005; Lowe et al., 2008; Vandergoes et al., 2013).

movement since the initiation of river incision. Datable organic material entrained in landslides was found to be scarce, with only three samples collected (one angiosperm and two podocarp logs). In this landscape lacking sufficient quartz for cosmogenic exposure ages and radiocarbon in landslide deposits, finer resolution age control of geomorphic features is possible through tephrochronology. At the high preservation depositional environment of Kaipo Bog, 16 tephra deposits younger than 18,000 cal. yr BP have been identified. Time between deposition in this record range from 100 cal. yr to 2,200 cal. yr (Lowe et al., 1999; Newnham and Lowe, 2000; Hajdas et al., 2006; Lowe et al., 2008). Older tephras are also present in the region; these enable the classification of more stable older surfaces (Litchfield and Berryman, 2005). In practice, not all of the tephras present in the high preservation environment of Kaipo Bog have been described as macroscopic layers in soil profiles on landforms in the terrestrial WSS. However, enough of the tephras are macroscopically present that tephrochronology in the WSS is an effective dating technique for LGCP to present landforms (Table 2.1) (Gage and Black, 1979; Wilmshurst et al., 1999, Berryman et al., 2000; Eden et al., 2001; Marden et al.,

2008; Berryman et al., 2010).

Tephrochronology of landforms in the terrestrial WSS is based on four main assumptions: 1) tephra erupted by TVZ volcanoes blankets the landscape of the WSS immediately after deposition; 2) tephras are chemically or otherwise distinguishable; 3) shallow erosion processes, such as sheet wash, shallow landslide, or soil diffusion, do not completely remove all tephra from the landform; and 4) deep-seated slope failures significantly disrupt or completely entrain the surficial tephra cover. The last three of these assumptions can be tested by detailed investigation of tephra cover. If all of the assumptions are satisfied, the age of the oldest tephra on a landform is a minimum stabilization age for that landform (Lang et al., 1999). To test these assumptions and to collect tephra for identification, 80 tephra samples were collected from 173 soil test pits and 64 soil auger sites across the two study areas. Test pits and auger sites were located on the largest expanse of low slope ground available on a sampled landform in order to obtain samples from areas with the best tephra preservation potential. Test pit samples were discrete, consisting of no more than 4 cm thick slices, and auger samples

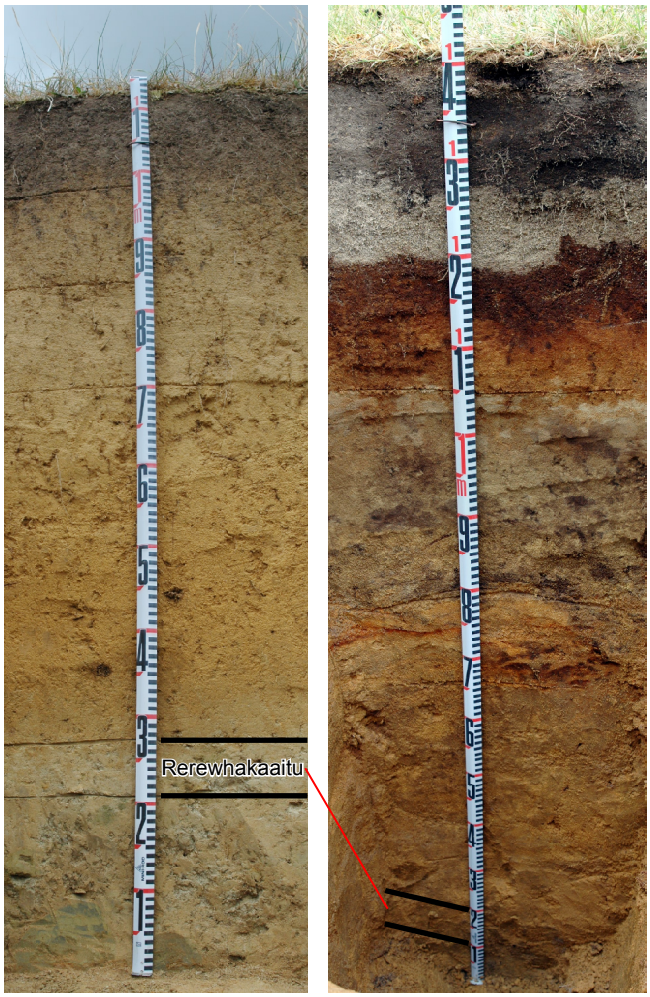

Figure 2.5. Examples of tephra profiles. Profiles are both located in the western study area on LGCP aggradation terraces and bottom in gravels. The numbers on the measuring rod show 10 cm increments. EMPA results from both sites show that the basal tephra is the 17,625 ± 425 cal. yr BP Rerewhakaaitu tephra. The sites are located less than 5 km apart and at less than 150 m elevation difference. All Rerewhakaaitu to present tephras listed in table 2.1 are probably present in these profiles. Color and to some extent texture difference are due to secondary alteration. There are no paleo O or A horizons in either profiles making visual differentiation of individual tephras difficult.

averaged no more than 10 cm thick. All of the sites have been logged and located by differential global positioning systems (DGPS).

2.4.3 Tephra identification

Tephra identification is difficult in the field because many of the tephras are not visually distinct, are altered to different extents and paleo O and A horizons are absent from tephra soil profiles in all but the most ideal depositional environments (Fig. 2.5). The absence of paleo O and A horizons is probably due to secondary alteration as there is enough time between deposition of individual tephras for organic soils to develop (ca. 500 to 4,000 years between major eruptions) (Table 2.1). In many profiles of the slightly acidic tephra soils in the oxidising environments of the East Coast North Island, organic carbon decreases dramatically (almost completely absent below ca. 50 cm) and secondary clay mineral content increases with depth (Bakker et al., 1996, Alloway, et al., 2007). Additionally, iron-manganese nodules, a product of mineral dissolution, are present lower in the profiles indicating weathering and alteration. The differing degree of alteration can change the color and to a lesser degree the texture of the tephra from location to location. Because of the difficulty of field identification, tephras are positively identified primarily by electron probe microanalysis (EMPA) of major oxide glass chemistry assisted by stratigraphy and ferromagnesian mineralogy.

EMPA was conducted using the JEOL JXA-8230 SuperProbe Electron Probe Microanalyser at Victoria University of Wellington. Wavelength dispersive X-ray spectrometry was used for all samples. Basic procedures for sample preparation and EMPA followed Lowe (2011). Analysis was calibrated on natural and synthetic glass standards, VG-568 and ATHO-G (Jarosewich et al., 1980; Jochum et al., 2006), and standards were analyzed between all samples to track calibration. Multiple glass shards from each sample were analyzed with a defocused 20 μm diameter beam of 8.0 nA at 15 kV accelerating voltage. Sixty-seven unknown samples from 56 sites were analysed along with 16 previously identified latest Pleistocene and Holocene tephras collected from type sections (Vucetich and Pullar, 1964, 1969). The previously identified tephras include all of the tephras listed in Table 2.1 except for the Rotoehu, Whakatane, and Whakaipo tephras, for which appropriate type section samples were not available. For these three tephras, samples were compared with published glass chemistry results (Smith etal., 2005; Smith et al., 2006; Lowe et al. 2008).

EMPA results from unknown (field collected) samples were compared with results from previously identified samples and results from literature on major oxide bi-plots. All results were normalized to 100% to minimize the effects of secondary hydration. For Taupo and Okataina Volcanic Centre rhyolitic tephras K_2O, CaO and FeO appear to be the most diagnostic of the major oxides (Smith et al., 2005; Smith et al., 2006; Lowe et al. 2008). Okataina tephras from this age range are distinctively higher in K_2O and lower in CaO than Taupo tephras. For three of the Okataina centre tephras (Rotoma, Mamaku, and Whakatane) that have significant glass chemistry and ferromagnesian assemblage overlap (Smith et al., 2006), stratigraphy, field texture, and glass chemistry bi-plot pattern were used to identify individual tephras.

2.5 Results

2.5.1 Geomorphic mapping

I identified 236 deep-seated landslides that have been active since the end of the LGCP in the two study areas (Fig. 2.6). The landslides are not limited to one mode of movement, and there are numerous examples of complex failure combining rotational, translational, and earthflow deep-seated mass movement mechanisms. The identified deep-seated landslides range in size from 2,760 m^2 to 1,745,660 m^2 and can have widely varying length to width aspect ratios ranging from 0.3 to 12.8. Many of the landslides show evidence of multiple generations of movement in the form of internal changes in vegetation recovery, morphology, and internal discrete shear zones. Even though many deep-seated landslides show evidence of multiple "nested" failures and landslide reactivation, I have concentrated on mapping the larger features with clearly defined scarps. In my inventory I have included 23 of the largest and most prominent reactivation features that are inside the mapped boundaries of larger landslides where these features illustrate multiple generations of movement on a hillslope (Fig. 2.6). Only six of the mapped non-nested landslides are clearly up-stream from any LGCP river incision (Fig. 2.6).

Landslides make up 35% of the surface area (3D not planimetric) of the lower relief Miocene-Pliocene mudstone terrain of the eastern study area. The higher relief, older, limestone and mudstone dominated western study area, by contrast, has only 13% of its

surface area affected by post-LGCP landslides. The vast majority of mapped landslides toe-out into streams directly coupling them to the fluvial system. This indicates significant sediment delivery to the WSS (Chapter 3). Most also have large portions of their mass movement bodies located under the projected elevation of the T1 LGCP aggradation surface (Fig. 2.6).

Landslide aspect is not closely linked with bedding structure. Of the 123 landslides where bedrock (bedding attitude) measurements could be obtained from nearby (within 0.5 km) (Mazengarb and Speden, 2000), only ca. 25% could be considered dip-slope landslides. Sliding surfaces for landslides are generally not exposed but, based on morphology and two exposures, sliding surfaces slope to and intersect with incising streams.

Twenty-five T1 aggradation terrace remnants were mapped, many of which were originally identified by Marden et al., (2008). Terrace remnants are found above modern tributaries from the main stems to headwater areas (Fig. 2.6). Terrace remnants, including portions of paleo alluvial fans grading to the T1 aggradation surface, range in size from 274 m^2 to 180,645 m^2 and range in height above the modern fluvial system from 12 m to 116 m.

Fifty-eight non-lithologic post-LGCP river incision knickpoints were mapped and used to and help define the LGCP aggradation surface (Fig. 2.6). Non-lithologic knickpoints are located high up in the tributary system, as noted by Crosby and Whipple (2006). Contrary to theory of detachment limited channels responding to increased uplift through knickpoint retreat where knickpoints remain at similar elevations (Whipple and Tucker, 1999; Niemann et al., 2001), knickpoints in the study area are not located at similar elevations. In just the eastern study area, for example, the difference in elevations between the 47 knickpoints on different tributaries is over 50% that of the total elevation difference of the stream network. The knickpoints in the study areas are located between ca. 55 and 75 km from the Waipaoa River mouth and there are two orders of magnitude difference between the areas of the largest and smallest drainage basins upstream of a knickpoint. These observations are consistent with results from Crosby and Whipple (2006).

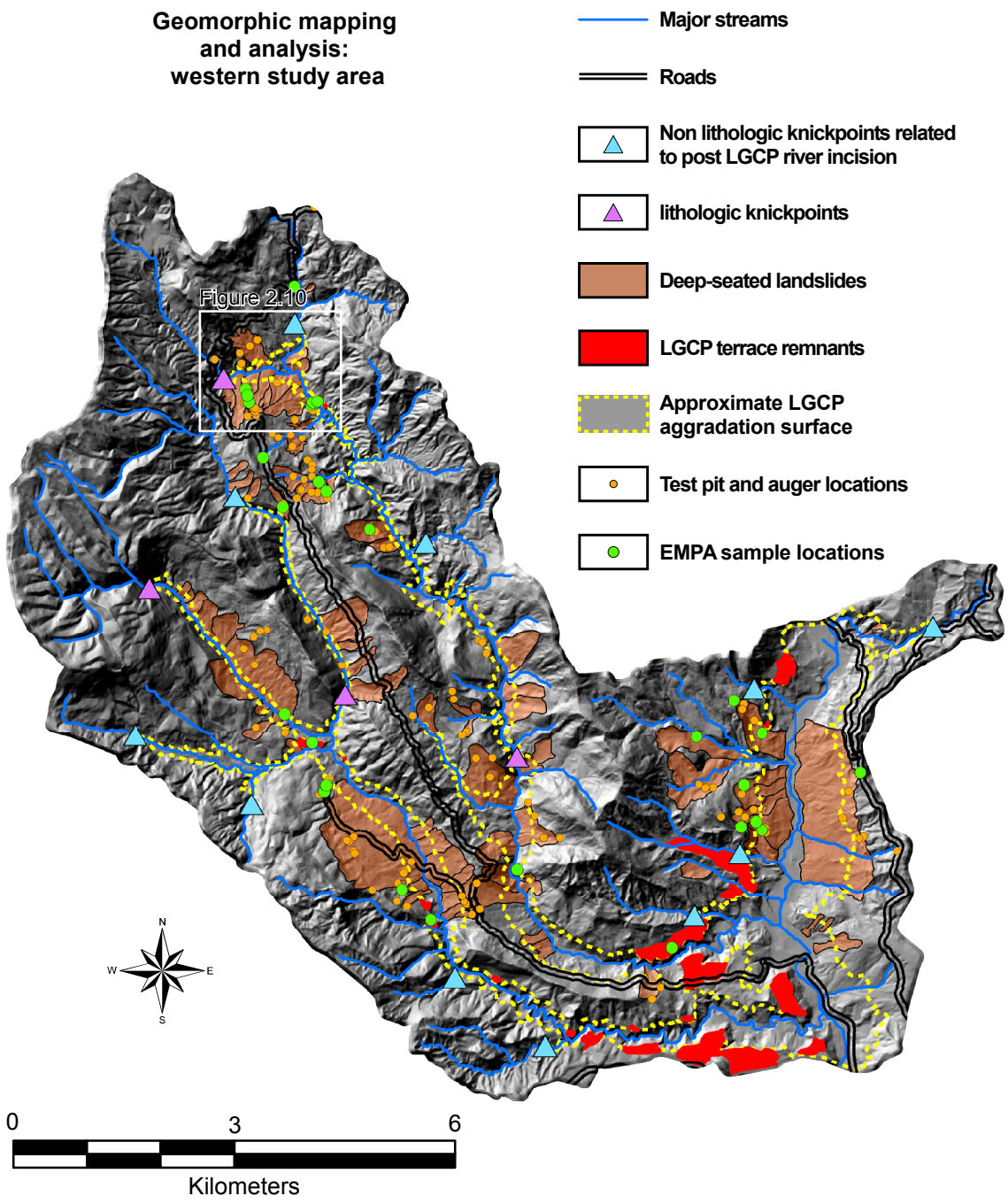

Figure 2.6. Geomorphic mapping and analysis for the western study area (this page) and the eastern study area (next page). Shown are deep-seated landslides, T1 aggradation terrace remnants, knickpoints and the approximate outline of the LGCP aggradation surface based on terrace remnants and knickpoints in the two study areas. Also shown are test pit and auger locations, tephra sample sites analyzed by EMPA, the location of the area presented in Figure 2.10, and the location of the cross sections shown in Figure 2.11.

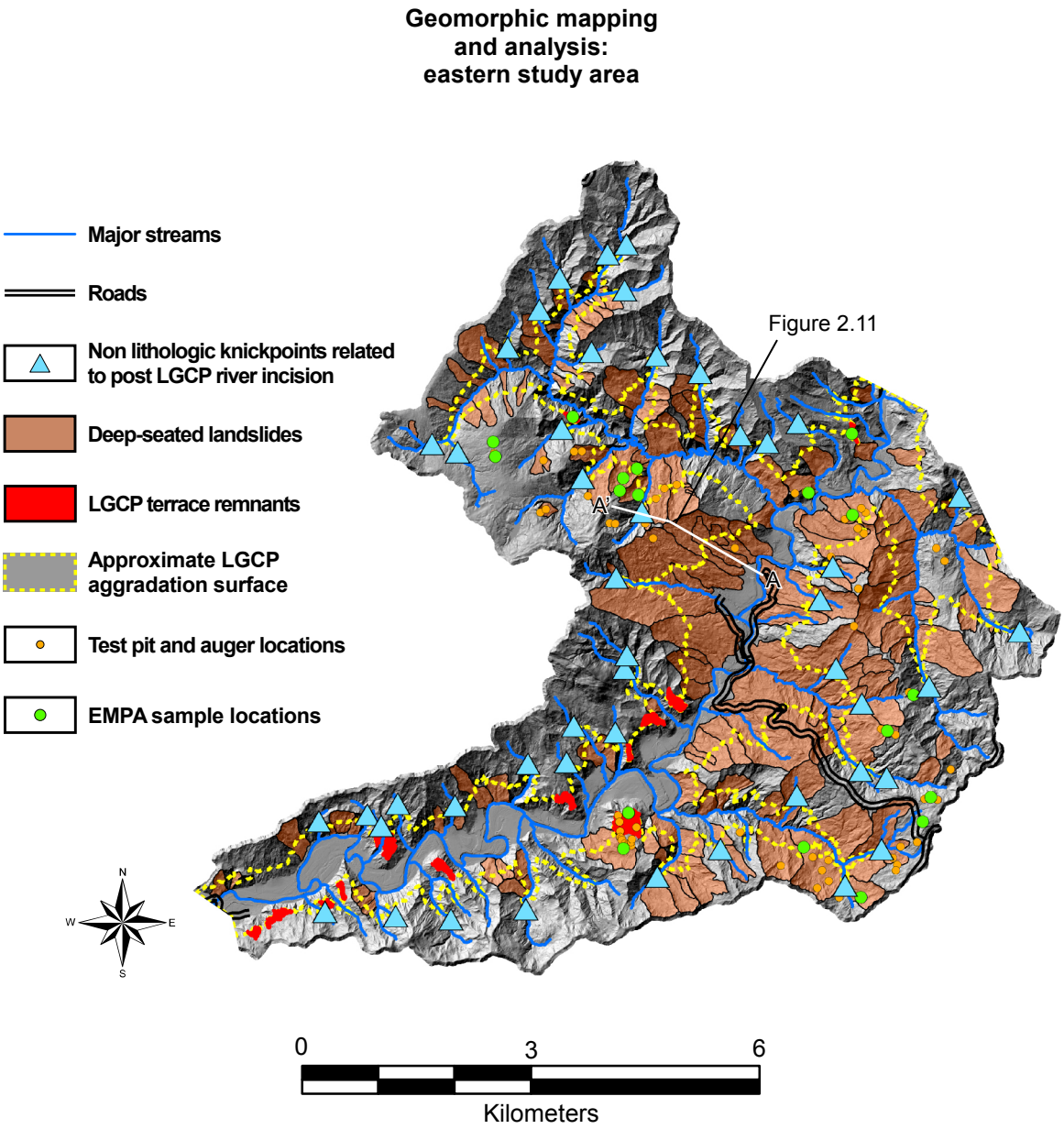

Figure 2.6. See previous page for caption.

2.5.2 Landform tephrochronology

Of the sixty-seven tephra samples analyzed by EMPA, only two appear to be very mixed samples containing shards from multiple tephras out of stratigraphic sequence. These two samples were from landslide bodies. Many samples do include a small percentage of shards from generally overlying (younger) tephras, but this does not preclude the identification of the majority tephra in the sample (Fig. 2.7).

After completing the EMPA on the collected samples, it became apparent that located and logged sites that had not been analyzed could still be assigned a probable oldest tephra based on texture/thickness relationships and the number of colour/texture horizons present. For test pits dug in all localities except sag ponds, Taupo (ca. 1700 cal. yr BP) and Kaharoa (ca. 630 cal. yr BP) tephras are present only scattered in the soil O or A horizons. In this case, the O and A horizons are not thicker than 15 cm combined. All of the sites that have a concentrated tephra comprising the inorganic portion of the A horizon show a layer of grey to dark brown coarse lapilli rich tephra that can be 10 to 50 cm thick. In all locations where 10 cm or less of this horizon is present, EMPA results indicated the presence of Whakaipo (ca. 2900 cal. yr BP) or Waimihia (ca. 3400 cal. yr BP) tephra. In all locations where this coarse layer is more than 10 cm thick, basal sample EMPA results indicated the presence of the Whakatane (ca. 5500 cal. yr BP) tephra. If a tephric B horizon is present below the coarse horizon, it is a fine to medium light grey to pinkish white generally stiff tephra. EMPA results indicate that where this horizon is less than 30 cm thick, it contains the Mamaku (ca. 8000 cal. yr BP) or Rotoma (ca. 9500 cal. yr BP) tephras, and where it is more than 30 cm thick, it most likely contains the Waiohau (ca. 13,600 cal. yr BP) or Rerewhakaaitu (ca. 17,600 cal. yr BP) tephras. Profiles containing Waiohau or Rerewhakaaitu tephras also often show some other colour/texture changes at depth. Biotite can often be seen in the Rerewhakaaitu tephra with a hand lens. Profiles that have Kawakawa (ca. 25,500 cal. yr BP) or older tephras are often well over 1 m thick. The Omataroa tephra (ca. 32,700 cal. yr BP) is readily distinguishable in the field as it is always more than a metre deep in a soil profile, is very coarse yellowish lapilli, and is ≥50 cm thick. From these relationships and from the EMPA results, I produced six stabilization categories that are valid for the two study areas (table 2.2). These categories were used to make stabilization age estimates for landslides that had been investigated by test pit or soil auger but did not have EMPA results.

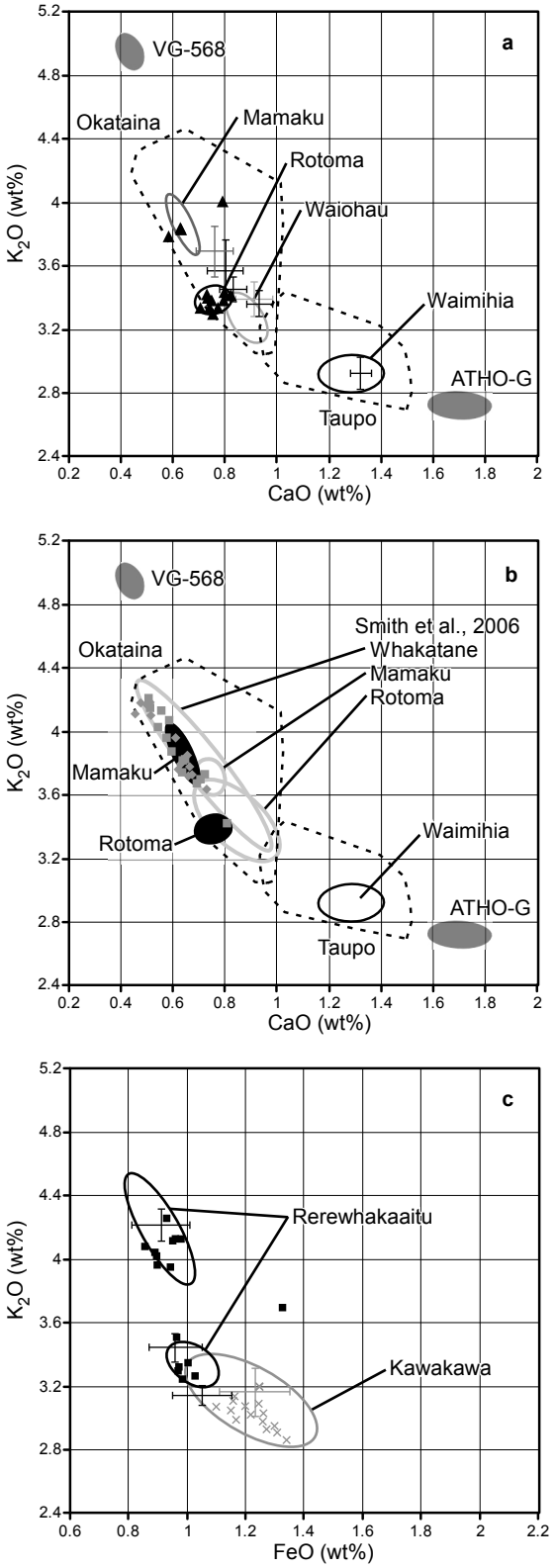

Figure 2.7. Biplots of select EMPA results. Dashed polygons are convex hulls of all the known Okataina and Taupo Volcanic center results used in this study, except for the distinctly bimodal Rotorua tephra, showing distinct glass chemistry. Ovals are 95% ellipses from EMPA analysis of known tephras ($n \geq 10$). Crosses are 2σ error bar results for the same tephras from a different instrument (Lowe et al., 2008). VG-568 and ATHO-G are glass standards used for calibration. a) Unknown sample (black triangles) interpreted to be the Rotoma tephra based on the tight cluster overlapping the Rotoma 95% ellipse. b) Unknown samples (grey squares and diamonds) interpreted to be Whakatane tephra based on similar glass chemistry pattern of Smith et al. (2006) (grey 95% ellipses), field stratigraphic relationships and clear Okataina source. c) Unknown samples represented by black squares and grey crosses interpreted to be the bimodal Rerewhakaaitu tephra and the Kawakawa tephra, respectively.

Soil profile observation	Typical total profile depth range (cm)	Probable oldest tephra	Estimated landform stabilization age range (cal. yr BP)
No tephra observed	3 to 10	No tephra	younger than 636
Lapilli scattered in the O and A horizon	5 to 15	Taupo and/or Kaharoa	2,960 to 636
Thin coarse lapilli rich A horizon tephra	12 to 20	Waimihia and/or Whakaipo	5,530 to 2,960
Thick coarse lapilli rich A horizon tephra	30 to 60	Whakatane	8,005 to 5,530
Thin fine to medium B horizon tephra	40 to 65	Mamaku and/or Rotoma	13,635 to 8,005
Thick fine to medium B horizon tephra	60 to 130	Waiohau and/or Rerewhakaaitu	Greater than 13,635
More than 3 distinct tephra layers with a total thickness of over a metre	100+	Older than Waiohau	Greater than 13,635

Table 2.2. Texture-depth relationships for estimating probable basal tephra for hillslopes in the Waipaoa catchment. Developed from EMPA analysis and field observations.

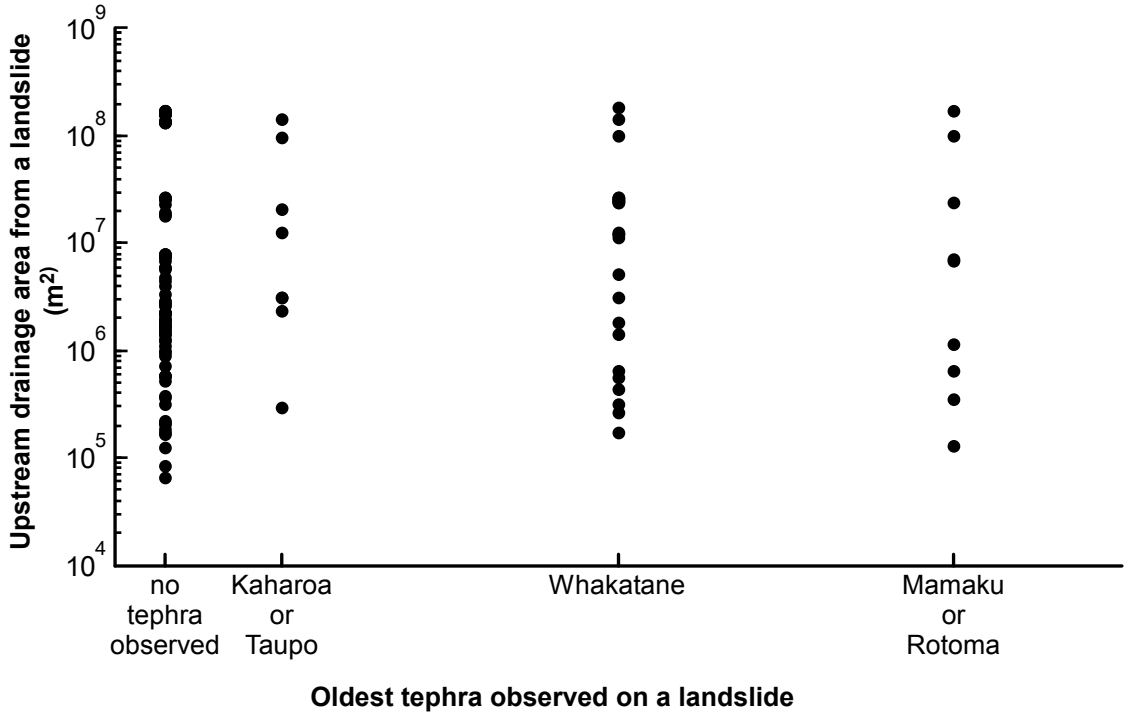

Figure 2.8. The oldest tephra identified on a landslide body plotted against the upstream location of the landslide (log drainage area above the point where the landslide toe intersects the stream). Spacing on the x-axis is proportional to the time between tephras. The Waimihia tephra was only confirmed as the oldest basal tephra on one landslide and was not included in the figure. There is no clear pattern showing a decrease in the stabilization age of upstream (lower drainage area) landslides. In fact, it appears that position in the drainage network has very little to do with the stabilization age of the landslide.

Field and EMPA assessment of 141 of the 236 mapped post-LGCP deep-seated landslides indicates that no tephra older than Rotoma (ca. 9500 cal. yr BP) is present on the body of these slide masses (Fig. 2.8). Seventy percent of these landslides have accumulated only Taupo (ca. 1700 cal. yr BP) and Kaharoa (ca. 630 cal. yr BP), Kaharoa only, or no tephra. There is no discernible spatial pattern to the oldest tephra observed on any of the landslide masses investigated (Fig. 2.8). For example, landslides located at both high and low elevations in the fluvial drainage network have Mamaku (ca. 8,000 cal. yr BP) or Rotoma (ca. 9,500 cal. yr BP) as the oldest tephra on the slide mass (Fig. 2.8).

With the exception of one sample of Waiohau Tephra (ca. 13,600 cal. yr BP), the Rerewhakaaitu Tephra (ca. 17,600 cal. yr BP) is the basal tephra coverbed on all of the prospective T1 terrace remnants analyzed. In the western study area, the observation that three terrace treads all have Rerewhakaaitu as the basal tephra (Marden et al., 2008) can be extended up to the headwaters of the catchment above a prominent lithologic

knickpoint. The uppermost of these three treads is the T1 LGCP aggradation terrace sensu stricto, and two lower (by up to 13 m) terraces are interpreted to be degradation terraces (fill-cut terraces, after Bull, 1991) cut into the T1 surface.

Stable landforms such as terrace remnants, broad ridge tops, or catchments upstream of knickpoints related to post LGCP river incision (EMPA results from 31 sites) are all overlain by thick tephra sequences with a basal tephra of Rerewhakaaitu (ca. 17,600 cal. yr BP) or older. The Rerewhakaaitu tephra overlies ancient scree deposits that can be found in other locations in the headwaters of the WSS (Gage and Black, 1979) (Fig. 2.4b). These thick older tephra sequences can be preserved on very steep (≥30°) slopes. Many interfluves flanked on both sides by landslides exhibit an extremely truncated tephra profile characterised by either no tephra or a thin sequence of post-Waimihia tephras (ca. 3,400 cal. yr BP). Notably, some truncated interfluve profiles exist in close proximity with multiple other sites overlain by the entire Rerewhakaaitu (ca. 17,600 cal. yr BP) to present sequence. This lack of tephra cover in areas where a full sequence is expected is most prominent in the eastern study area.

2.6 Discussion

2.6.1 Hillslope instability

Mapping of post-LGCP large deep-seated landslides shows that slope instability has affected large areas of the upper WSS, with many slides extending from valley floor to ridge crest (Fig. 2.6). Analysis of tephra cover stratigraphy indicate that some of the interfluves which are flanked on either/both sides by landslides are also recently stabilized landforms, suggesting that many of the ridgelines have been lowered or retreated through mass movement on both sides of drainage divides.

Landslides are generally not bedding controlled and where observable, slide planes are visible at incised streams. This means that before river incision the current slide planes for many of the mapped deep-seated landslides would have been many metres beneath intact bedrock without any free (not buttressed) surface to facilitate sliding. In addition, the accommodation space for the sliding mass did not exist before river incision. I therefore conclude that slopes underlain by low strength and highly sheared bedrock were debuttressed by river incision and responded by gravitational collapse. Figure 2.9 shows the difference between hillslopes where river incision is present and where it is

not. The provision of accommodation space for deep-seated landslides by river incision is illustrated by the example in figure 2.10 where the headscarp height and the amount of river incision are approximately the same (ca. 25 m), indicating the river incision was the primary cause of landsliding. This is consistent with theories for threshold hillslopes where vertical river incision into bedrock over-steepens hillslopes with gradients near threshold angles leading to increasing relief until gravitational stress exceeds mountain scale material strength and deep-seated bedrock landsliding ensues (e.g. Schmidt and Montgomery, 1995; Burbank et al., 1996, Montgomery, 2001; Montgomery and Brandon, 2002; Binnie et al., 2007; Larsen and Montgomery, 2012). Deep-seated landslides in the WSS may have been triggered by intense or long duration precipitation events common to the WSS (Page et al., 2010) or by seismic events but the underlying causes for the observed widespread landsliding are river incision and low bedrock mass strength.

2.6.2 Timing of hillslope response

Minimal tephra was found on the body of landslides, while thick sequences of multiple tephras are preserved on other stable landforms (e.g. terraces). Incomplete tephra stratigraphy was found on about a third of the landslides analyzed (Fig. 2.8) suggesting that at least portions of these slides have been stable since the time between the deposition of the oldest tephra on the landslide and the preceding tephra and that tephrochronology is a valid method for dating these surfaces. Tephra older than Rotoma (ca. 9,500 cal. yr BP) was not found on the body of any landslide. While unambiguous evidence of the absence of a tephra is difficult to prove, I propose that the discovery of every major tephra younger than the Waiohau Tephra (ca. 13,600 cal. yr BP) present as undisturbed layers on landslides makes the absence of the Waiohau and Rerewhakaaitu (ca. 17,600 cal. yr BP) tephras notable. This absence means that either: 1) landslides initiated before the deposition of these tephras and did not stabilize for long enough to preserve any undisturbed tephra, or 2) widespread slope instability did not initiate until

Figure 2.9 (next page). Two small catchments (ca. 1.5 km^2) in the WSS that illustrate the connection between river incision and hillslope deep-seated landsliding. Both catchments are underlain by marine sedimentary rocks. Because of their small drainage areas, river incision in both catchments is most significant when local base level is lowered. This did not occur for the catchment pictured on the left (a) because it is at a point in the drainage network above a threshold for significant river incision (not enough discharge). The tributary in the catchment on right (b), did experience significant river incision because it is connected to a larger tributary, draining almost 10 km^2, that has experienced over 90 m of river incision. Hillslopes are relatively stable in the catchment on the left (a) and hillslope debuttressing due to river incision has activated a number of large deep-seated landslides in the catchment on the right (b).

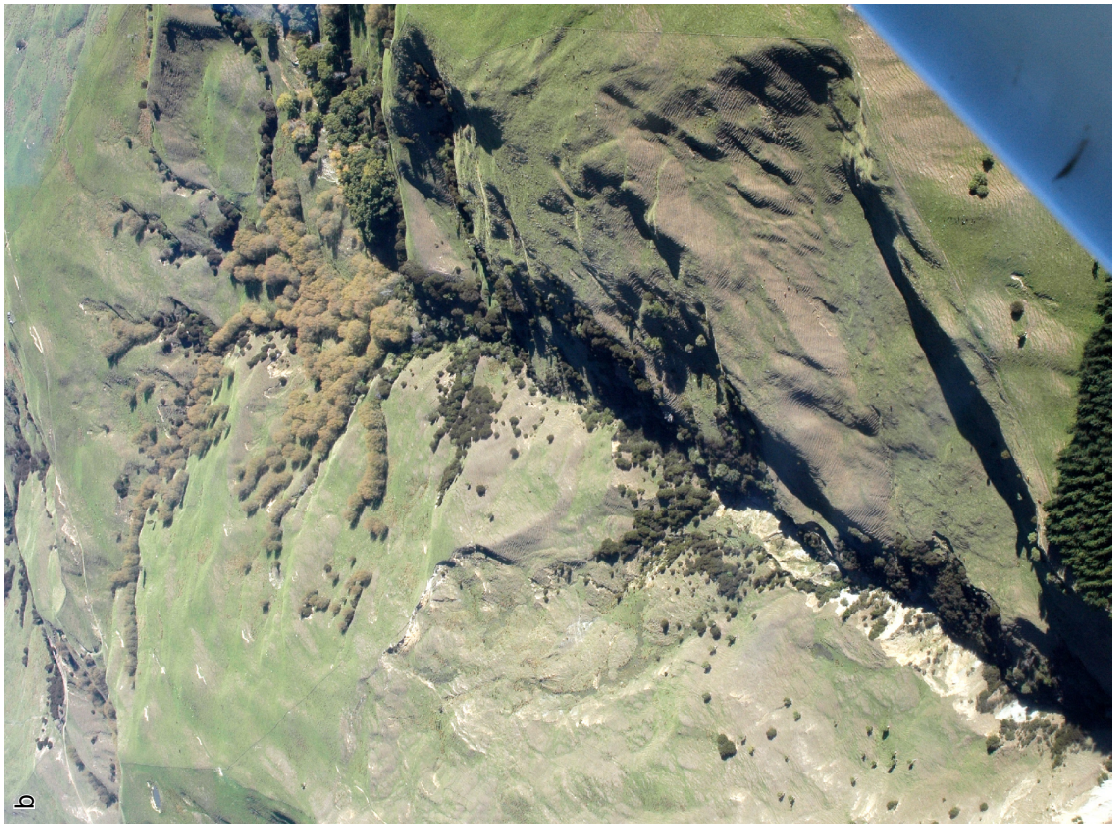

Figure 2.9. See previous page for caption.

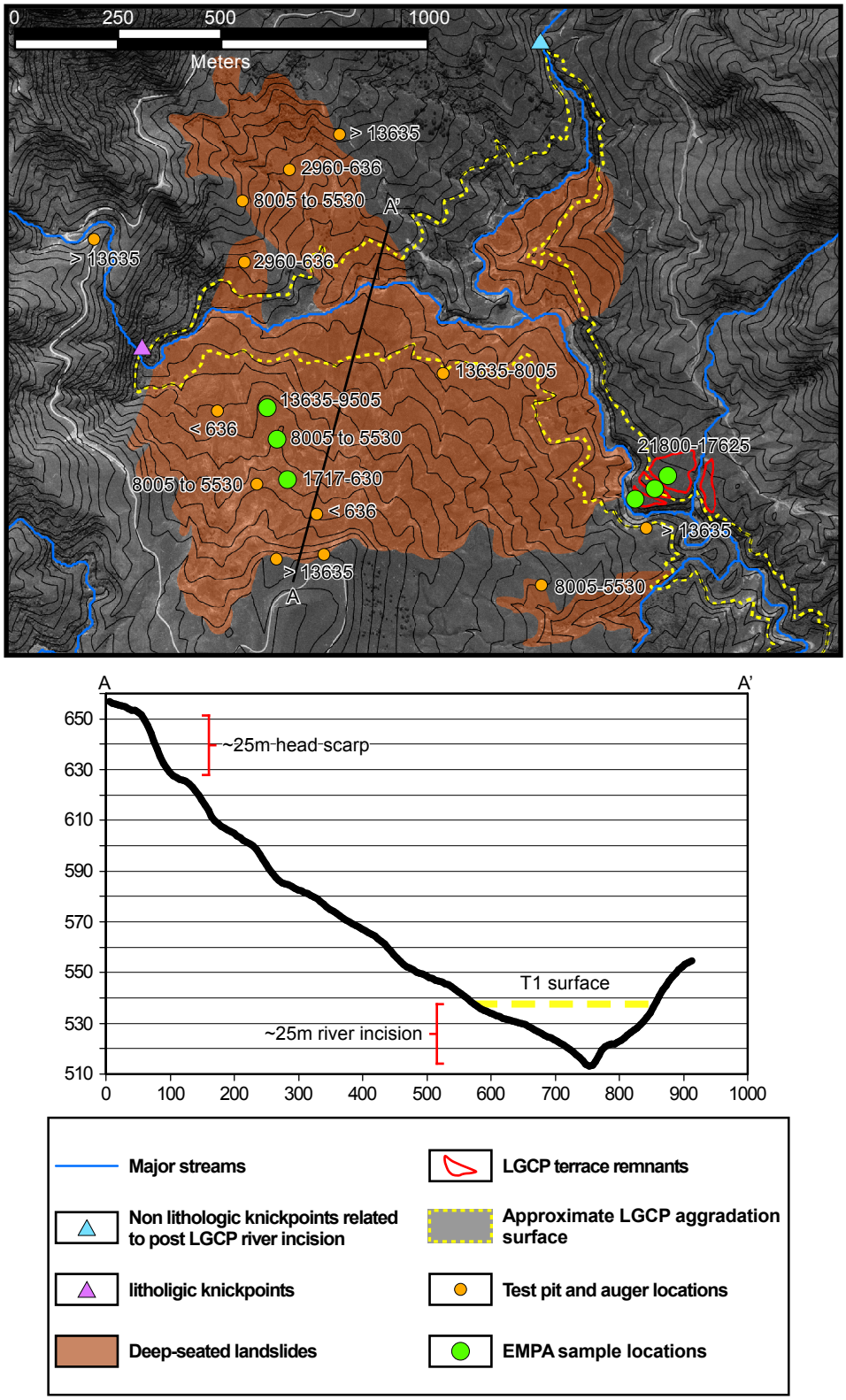

Figure 2.10. Landslides and LGCP terrace remnants in the headwaters of the Mangatu River (Mangamaia tributary). Stabilization age ranges (cal. yr BP) are noted next to the test pit locations. Contour interval is 10 m. In the lower right corner, note the 2 clear pre Rerewhakaaitu (ca. 17,600 cal. yr BP) degradation terrace treads separated by ca. 13 m of elevation difference from the upper T1 fan surface. These are mapped by GPS and dated by tephrochronology. The bedrock strath outcrops 4 m below the surface of the lowest tread at this location. Cross section A-A' shows that the ca. 25 m height of the head scarp on the large central landslide closely matches the ca. 25 m of post-LGCP river incision. It also shows that without incision there would have been no accommodation space for the body or toe of the landslide.

after the deposition of the Waiohau tephra. The link between slope instability and river incision described above means that the timing of river incision can help to inform which of these hypotheses are more likely.

River incision initiated between ca. 21,800 cal. yr BP and 17,600 cal. yr BP and cut 1-2 degradation terrace treads separated by up to 15 m before deposition of Rerewhakaaitu tephra (ca. 17,600 cal. yr BP) (Fig. 2.10) (Marden et al., 2008). This initial incision, however, did not completely cut through the T1 aggradation gravels at most locations, keeping the river's erosive capacity decoupled from bedrock (Fig. 2.10) (Marden et al., 2008). The initial incision was followed by relatively slow river incision with terraces overlain by Waiohau tephra (ca. 13,600 cal. yr BP) typically less than 4-8 m below the lowest degradation terrace overlain by Rerewhakaaitu tephra (Marden et al., In prep.). The most rapid incision through significant amounts of bedrock (below the T1 aggradation gravels), occurred after the deposition of the Waiohau tephra (ca. 13,600 cal. yr BP) (Marden et al., In prep.). This period of rapid incision occurs prior to the deposition of the oldest basal tephra on landslides (Rotoma, ca. 9,500 cal. yr BP), suggesting the lack of Waiohau tephra on post-LGCP landslides likely relates to the post-Waiohau debuttressing of hillslopes due to rapid river incision into bedrock. I infer that widespread post-LGCP slope instability initiated in the period after the deposition of the Waiohau tephra (ca. 13,600 cal. yr BP) and before the deposition of the Rotoma tephra (ca. 9,500 cal. yr BP).

The signal of rapid incision and debuttressing appears to be near synchronous in the upper WSS from the headwaters to the mainstem (Fig. 2.8). This is at odds with a hypothesis of migrating knickpoints translating the incision response through the landscape (Crosby and Whipple, 2006; Berryman et al., 2010). Tephrochronology indicates that the initial rapid incision occurred at almost the same time on the mainstem as at the headwaters of the Mangatu River (Fig. 2.10) (Marden et al., 2008). Further, degradation terraces cut into the T1 aggradation surface in the headwaters that are the same age as main stem degradation terraces are upstream of a major lithologic knickpoint (Fig. 2.6). Such a lithologic barrier would limit the upstream advance of a stream power or base level fall induced migrating knickpoint. The lack of any progressively younger landslide tephra coverbeds upstream (Fig. 2.8) also indicates that deep-seated landsliding, which I have shown is strongly coupled to river incision, was

near synchronous and not translated by migrating knickpoints. The non-lithologic knickpoints correlated to the incision since the LGCP in the WSS probably initiated at a threshold stream power high up in the fluvial network and have had a relatively slow retreat rate as alternatively proposed by Crosby and Whipple (2006).

The timing of the initiation of river incision, the onset of rapid bedrock incision and large scale hillslope response closely match the timing of the transition from the LGCP and the climatic amelioration following the late glacial climate reversal observed in many climate proxies (e.g., Alloway et al., 2007). Dramatic changes in upland erodibility between ca. 21,800 cal. yr BP and 17,600 cal. yr BP (Fig. 2.4) provide a mechanism for linking climate with aggradation and incision by replacing bed load over-capacity with under-capacity (Berryman et al., 2000; Eden et al., 2001; Litchfield and Berryman, 2005; Marden et al., 2008; Gomez and Livingston, 2012; Upton et al., in press). Widespread destabilization of hillslopes, however, did not commence until after the transition to full podocarp-angiosperm forest cover after the late glacial climate reversal at ca. 11,600 cal. yr BP. At this time hillslope sediment undersupply was presumably at a maximum, and the rivers and tributaries of the WSS had reengaged with bedrock after scouring the remaining T1 aggradation gravels from their beds.

Conceptually, the upper WSS was primed for significant post LGCP incision. Since the beginning of LGCP aggradation at ca. 28,000 cal. yr BP to resumption of incision into bedrock after ca. 12,000 cal. yr BP, uplift of ca. 1-4 mm/yr proceeded while rivers and streams were decoupled from bedrock by aggradation gravels. During this time when river incision was out of equilibrium with ongoing tectonic uplift, a ‘backlog’ of river incision developed and hillslopes buttressed behind aggradation fill most likely attained an equilibrium slope profile through ongoing periglacial or shallow mass movement processes producing and moving sediment from uplands. In this model, during the LGCP valley floors became aggradation plains and experienced net surface uplift, hillslopes continued to erode and likely attained some degree of slope equilibrium.

2.6.3 Conceptual time-series for hillslope response

The likely causative effect of vegetation change on river incision allows me to further refine my tephra-based chronology of hillslope response to infer that significant incision induced destabilization of hillslopes progressed after the transition to full podocarp-

Figure 2.11. See next page for caption.

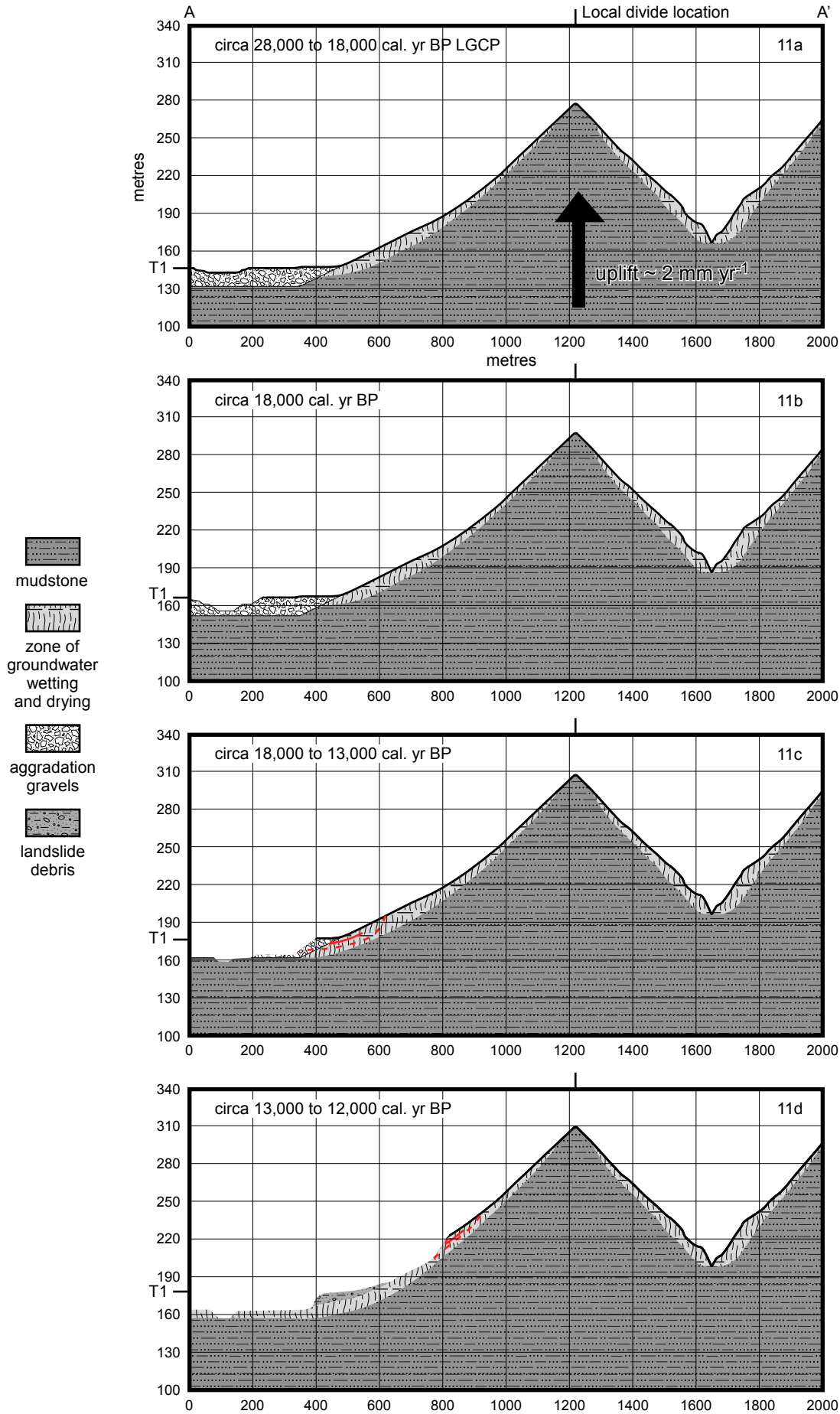

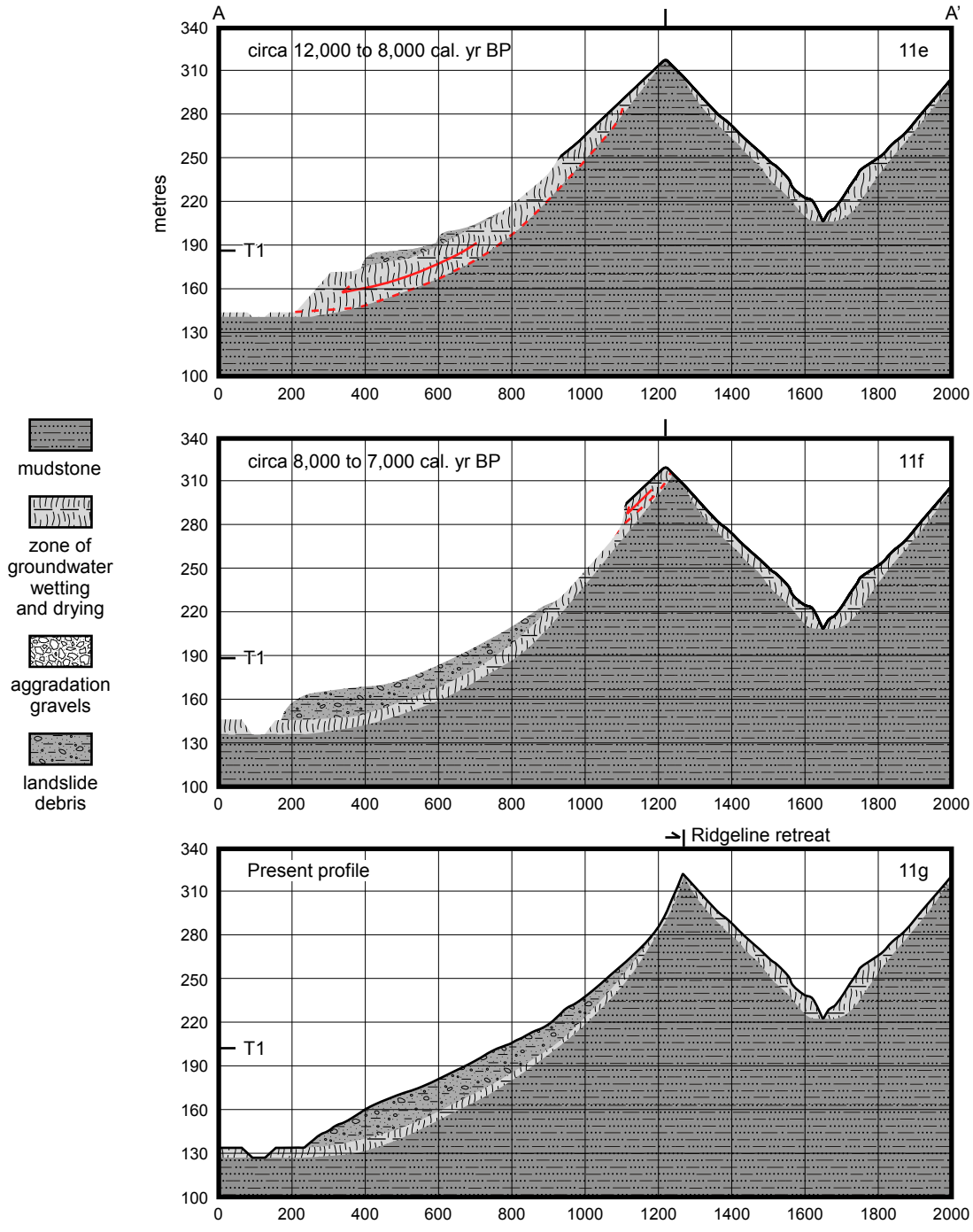

Figure 2.11a-g. Conceptual time-series of the magnitude of hillslope response to climate change induced river incision referred to in the Discussion section. Profile A-A' is modeled off the present day profile across a hillslope and interfluve adjacent to the Waingaromia River shown in Figure 2.6. The cross section crosses the smaller tributary on the right above the post LGCP incision related knickpoint, thus no change in basic hillslope geometry is expected in this area. Red dashed lines are landslide slip planes and arrows indicate sense of moment.

beach-angiosperm forest cover occurring after the late glacial climate reversal at ca. 11,600 cal. yr BP. This enables the development of a conceptual model of the timing and magnitude of hillslope response to climate change induced river incision (Fig. 2.11).

In this model tectonic uplift drives river incision over glacial-interglacial cycles, but river incision is modulated by climate change within glacial and interglacial cycles. During the LGCP (ca. 28,000 to 18,000 cal. yr BP) minimal forest cover, possible periglacial weathering in the uplands, and increased seasonality lead to sediment over capacity and aggradation. At this time, uplift continued without significant river incision because rivers and streams were decoupled from bedrock by thick deposits of aggradation gravel. This created a situation where erosion progressed on hillslopes and interfluves, but the floors of valleys experienced net surface uplift, creating a 'backlog' of river incision (Fig. 2.11a). The transition to interglacial conditions from ca. 18,000 to 12,000 cal. yr BP included the lateglacial climate reversal between ca. 13,500 and 11,600 cal. yr BP (Alloway et al., 2007). During this time changes in vegetation and possibly precipitation triggered a switch from mainly aggradation to river incision as hillslopes were vegetated, and rivers experienced sediment undersupply. T1 aggradation gravels were scoured away, but incision into bedrock was minimal (Fig. 2.11b, c). As river incision over-steepened hillslopes, threshold angles for mass-wasting were approached. Hillslopes debuttressing began, but the hillslope response was limited to the lower slopes (Fig.2.11c, d). After ca. 11,600 cal yr BP. podocarp-angiosperm-beech forests expanded to the maximum upland extent. Sediment starved rivers (under supply) caused rapid and large scale river incision into bedrock (Fig 2.11e). This also potentially increased the depth of the damage zone for groundwater wetting and drying by dropping the effective hillslope groundwater table (Fig 2.11e). Debuttressed, threshold hillslopes caused widespread landsliding triggered by heavy and/or long duration precipitation events and possibly earthquakes (Fig. 2.11e, f). In the Holocene hillslope response continued as rivers incised to balance tectonic uplift, and local base-level drop progressively propagated upslope. In places, interfluves lowered and retreated away from areas of greatest local base level fall due to the upslope propagation of landslides (Fig. 2.11g). Through the response to climate-modulated, tectonic uplift-driven river incision, the morphology of the upper WSS was modified, releasing large amounts of sediment from hillslope storage and transferring it to storage in terrestrial and marine depocentres (Chapter 3).

2.7 Summary and conclusions

I have identified 236 deep-seated landslides that have been active since the end of the LGCP (ca. 18,000 cal. yr BP) in 141 km^2 of detailed upper Waipaoa catchment study areas (Fig. 2.6). Depending on the underlying geology, landslides make up between 13% to 35% of the surface area of these study areas. I have found that landslide aspect is not closely linked with bedding structure. Dip-slope landslides are approximately randomly correlated to underlying geologic structure with only ca. 25% of landslides with proximal bedrock attitude measurements considered dip-slope landslides. Further, deep-seated bedrock landslides are spatially and temporally correlated with post LGCP river incision. I conclude that slopes underlain by low strength and highly sheared bedrock were debuttressed by river incision and as hillslopes reached threshold gradients, they responded by gravitational collapse. These deep-seated bedrock landslides may have been triggered by intense or long duration precipitation events or by seismic events, but the underlying causes for the widespread landsliding observed are river incision and low bedrock mass strength.

Landform tephrochronology indicates that widespread slope instability did not initiate until after the deposition of the ca. 13,600 cal. yr BP Waiohau tephra. My results further indicate that the signal of rapid incision and debuttressing appears to be near synchronous in the upper WSS from the headwaters to the mainstem (Fig. 2.8). Within the limits of the tephrochronology, there is good agreement between the timing of hillslope debuttressing and other independent terrace-based degradation estimates of the timing of most rapid river incision after the LGCP (Berryman et al., 2010; Marden et al., in prep). Through investigation of the timing of coupled river incision and landslide activity, confirmation of similar incision histories at the mainstem and headwaters, and assessment of the minimum age of ancient scree exposures, I bolster the argument that climate change leading to alterations in upland vegetation influenced the morphology of the terrestrial WSS through changes in sediment supply to and, possibly, discharge of rivers (Berryman et al., 2000; Edan et al., 2001; Litchfield and Berryman, 2005; Marden et al., 2008; Gomez and Livingston, 2012). These investigations also indicate that the non-lithologic knickpoints observed in the modern WSS (Crosby and Whipple, 2006) did not initiate in mainstems and propagate throughout the fluvial network, but rather, initiated at a threshold stream power high up in the fluvial network and the retreated at

slow rates to their current locations (Crosby and Whipple, 2006) .

I have produced a conceptual model that shows how hillslopes in the WSS responded to climate and vegetation change during the last glacial-interglacial transition. Widespread deep-seated landsliding caused by slope oversteepening and debuttressing resulted from climate-modulated, uplift-driven river incision. These post LGCP deep-seated landslides shaped the modern morphology of the WSS to the extent that even interfluves were, in places, shifted and lowered. Through this work I have shown how climate and tectonic uplift have shaped hillslope morphology. This has implications for the timing and magnitude of the transfer of sediment from the terrestrial Waipaoa Sedimentary System to terrestrial and marine depocentres that is the subject of Chapter 3.

Chapter 3: The role of deep-seated landslides in post-glacial sediment flux from the Waipaoa Sedimentary System, New Zealand

3.1 Abstract

Deep-seated bedrock landslides can account for a large proportion of the regional sediment yield and denudation rates for rapidly uplifting landscapes such as the Himalayas, the Southern Alps of New Zealand, and Taiwan. However, the role of deep-seated landslides in sediment flux from the moderate uplift, temperate maritime catchments that characterize many active margins is less well quantified. Using high resolution topography (lidar, photogrammetric), in-depth field analysis, and tephrochronology, I have estimated the 18,000 year sediment yield from terrestrial deep-seated landslides in the Waipaoa Sedimentary System, North Island New Zealand. This completes one of the first process-based millennial time-scale sediment budgets for this class of temperate maritime, active margin catchments which exhibit a globally significant discharge of sediment to the world‘s oceans. I apply fluvial and geomorphic modelling to reconstruct pre 18,000 cal. yr BP topography in 141 km^2 of detailed study areas and use the resulting volumetric estimate from 207 landslides to estimate deep-seated landslide sediment flux for the broader system. I find that 10.2 km^3 of deep-seated landslide-derived sediment with a multiplicative uncertainty of 1.9 km^3 (+9.2 km^3, -4.8 km^3) was delivered to terrestrial and marine sinks. This accounts for between 10 and 74% of the total mass of the terrestrial Waipaoa Sedimentary System budget of ca. 91,000 Mt (+37,000 Mt, -26,000 Mt). Combining the deep-seated landslides results with other studies of terrestrial sediment sources and terrestrial and shelf sinks, I find the estimated terrestrial source load ranges from 1.2 to 3.7 times larger than the mass of sediment sequestered in terrestrial and shelf depocentres. This implies that off-shelf transport of sediment is important in this system over the last 18,000 cal. yr BP, as it is today for anthropogenic reasons. Based on the sediment budget, the denudation rate for the terrestrial Waipaoa Sedimentary System of 0.8 mm yr^{-1} (+0.3 mm yr^{-1}, -0.2 mm yr^{-1}) is indistinguishable from the average terrestrial Waipaoa late Quaternary uplift rate indicating an approximate steady-state balance between denudation and uplift. In this analysis I have developed a quantitative understanding of the role of deep-seated landslides in an active margin catchment and used this understanding to explore

landscape and terrestrial source to marine sink sediment transfer dynamics.

3.2 Introduction

Catchment-wide sediment budgets can illuminate landscape processes controlling sediment generation and storage, sensitivity of different portions of the landscape to environmental change and the degree to which terrestrial changes can be tracked into offshore depocentres (e.g. Syvitski et al., 2005; Gomez et al., 2007; Covault et al., 2011). Recent studies quantifying potential sediment sources and sinks in the Waipaoa Sedimentary System (WSS) on the North Island East Coast (NIEC) of New Zealand (Fig. 3.1) have enabled a better understanding of the long term inputs and outputs to this globally significant (currently ca. 15.0 Mt yr^{-1}) sediment source (Foster and Carter, 1997; Orpin et al., 2006; Gomez et al., 2007; Marden et al., 2008; Gerber et al., 2010; Miller and Kuehl, 2010; Page and Lukovic, 2011; Marden et al., In prep.). However, the role in the sediment flux for one of the most obvious geomorphic processes in the WSS, deep-seated landslides, has to date been poorly quantified (Kuehl et al., 2006; Marden et al., 2008; Page and Lukovic, 2011). There is an emerging consensus that deep-seated landslides can account for a large proportion of the regional sediment yield for very high uplift landscapes such as the Himalayas, the Southern Alps of New Zealand, and Taiwan (e.g. Burbank et al., 1996; Hovius et al., 1997; Hewitt, 1998; Hovius et al., 2000; Korup et al., 2004; Korup, 2006), but the role of deep-seated landslides in the WSS remains to be quantified. This leads to one of the main objective for this study, to estimate sediment eroded by deep-seated landslides in the last ca. 18,000 cal. yr BP in the WSS.

Sediment discharge to the world's oceans is highest at active margins (e.g., Milliman and Farnsworth, 2011). Small upland catchments like the WSS are good sites to study sediment generation and transport from terrestrial source to marine sink because of their quick response to external forcing such as climate, tectonics, or anthropogenic modification (Milliman and Syvitski, 1992). Limited accommodation space for terrestrial sediment storage in these sedimentary systems facilitate the translation of upland fluctuations in sediment generation to marine depocentres relatively quickly, thus inviting a total source to sink or sediment budget approach to tracking sediment flux and landscape evolution over glacial - interglacial cycles. Ideally, information about the timing and magnitude of landscape modifying events propagate through a sedimentary system enabling terrestrial change to be explored by studies focusing on marine

depocentres. But the linkage between terrestrial sources and marine depocentres needs to be tested, in order to show that marine processes or sediment bypassing are not obscuring the record of terrestrial change. The upland, maritime temperate WSS offers the opportunity to test this linkage because of its manageable size, large sediment flux and quick response to external forcing (Wilmshurst et al., 1999; Gomez et al., 2007). Because of this potential to close sediment budgets and to connect landscape evolution to stratigraphy, the WSS was selected as part of the international, NSF supported, MARGINS Source-to-Sink initiative (Gomez et al., 2001; Kuehl et al., 2003, 2006; Carter et al., 2010).

In the terrestrial WSS (the source; Fig. 3.1) the change from the last glacial to the current interglacial climate at ca. 18,000 cal. yr BP was accompanied by a switch from river aggradation and relative landscape stability to river incision and increased landslide activity (Gage and Black, 1979; Berryman et al., 2000; Eden et al., 2001; Litchfield and Berryman, 2005; Marden et al., 2008, Marsaglia et al., 2010; Gomez and Livingston 2012; Marden et al., In prep.; Chapter 2). Offshore (the sink; Fig. 3.1) the exposed shelf was inundated by rising sea level (Gibb, 1986; Orpin et al., 2006; Gerber et al., 2010) with shorelines reaching their maximum inland extent at ca. 7,000 cal. yr BP (Brown, 1995; Wolinsky et al., 2010). Increased accommodation space due to sea level rise potentially led to high shelf depocentre trapping-efficiency (Carter et al., 2010; Gerber et al., 2010). However, without a more detailed long-term sediment budget for the WSS, it is difficult to know how tightly the terrestrial and marine portions of the WSS are coupled. Furthermore, without approaching closure of the catchment wide sediment budget, we do not know if it is possible to account for sediment when it crosses from the terrestrial system to a dispersive oceanic environment.

New high resolution topographic data sets (lidar and photogrammetry) combined with tephrochronology and field mapping have enabled the approximation of sediment flux from post 18,000 cal. yr BP deep-seated landslides in the WSS, allowing quantification of one of the outstanding large volume sediment sources in the WSS sediment budget. To accomplish this, I outline a methodology for reconstructing a significantly altered landscape and then explore the contributions of landslides to the wider WSS sediment budget. Finally, I discuss the implications of the sediment budget estimate on the dispersal of sediment within the WSS and the ability to track terrestrial landscape

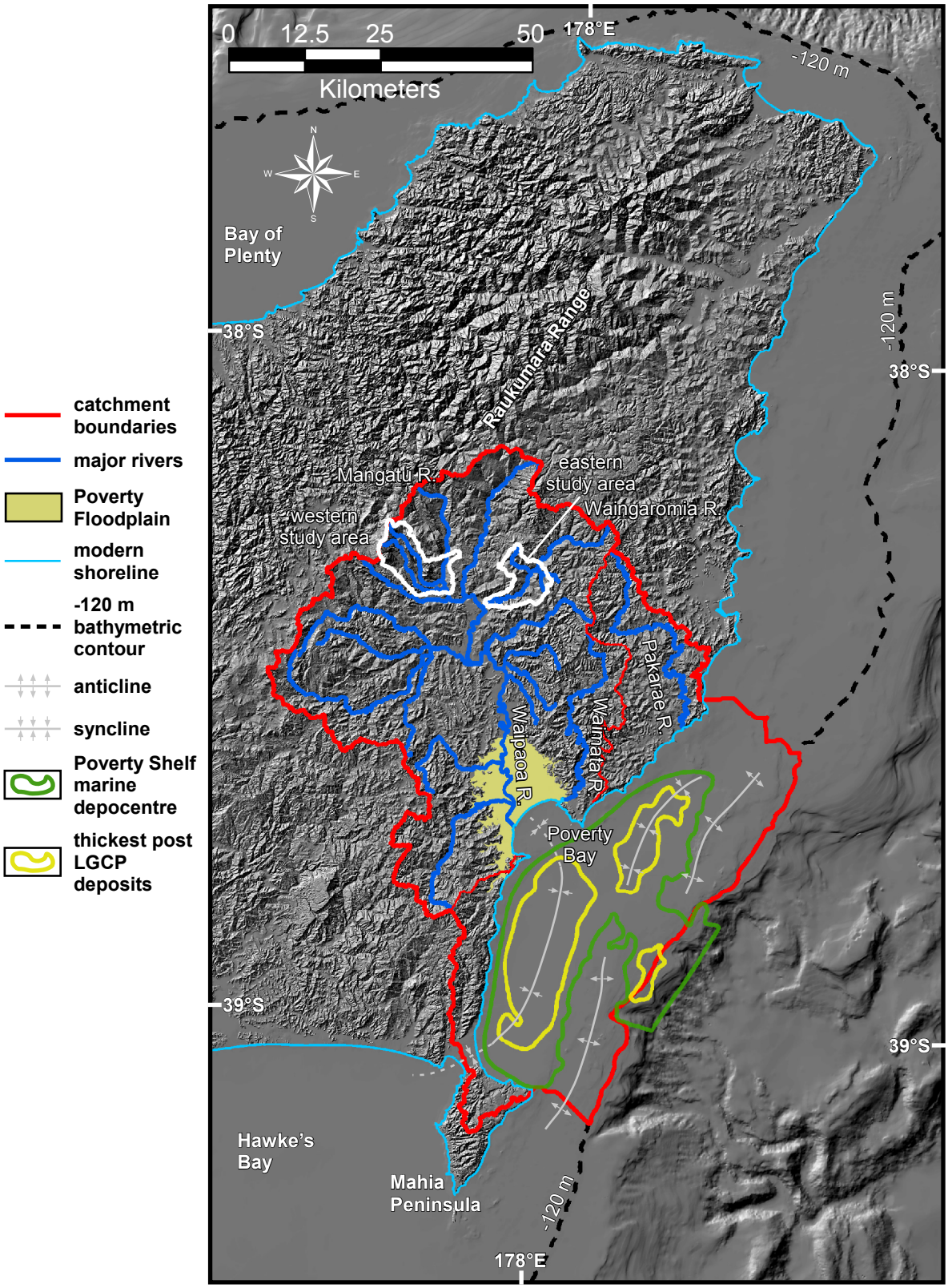

Figure 3.1. Regional map of the Waipaoa Sedimentary System showing the terrestrial sediment source and the terrestrial and marine depocentres. Also shown are major rivers and the two detailed study areas. The marine depocentres in this figure are modified from Gerber et al. (2010).

modification across the land-sea interface.

3.3 The Waipaoa Sedimentary System (WSS)

3.3.1 Regional geologic setting

The modern WSS stretches from the outer forearc (marine depocentres) of the Hikurangi subduction margin to the actively uplifting axial ranges of the North Island (Raukumara Range) (Fig. 2.1) and includes ca. 3200 km^2 of terrestrial landscape and ca. 1790 km^2 of marine environment (Fig. 3.1). The Waipaoa and Waimata river catchments drain ca. 2500 km^2 (ca. 78%) of the WSS with costal catchments, the Pakarae being the largest, draining the rest of the terrestrial setting. West of the Raukumara Range divide is the active Taupo Volcanic Zone (TVZ), one of the most active rhyolitic eruptive centres of the latest Pleistocene and Holocene (Smith et al., 2005) and the source for much of the tephra that helps constrain the age of landforms in the WSS (Fig. 2.1) (e.g. Berryman et al., 2000; Eden et al., 2001; Marden et al., 2008; Marden et al., In prep.; Chapter 2) In this tectonic regime active normal, thrust/reverse, and strike-slip faults have all been identified (e.g., Berryman et al., 2009; Litchfield et al., 2009). Many of these identified earthquake source structures could cause significant ground motions in the WSS (Modified Mercalli Intensity 8+) (Litchfield et al., 2009).

Regional-scale uplift of the Raukumara Range is driven by deep-seated subduction processes (plateau subduction, seamout subduction, tectonic erosion, and sediment underplating) (e.g. Walcott, 1987; Reyners et al., 1999; Upton et al., 2003; Litchfield et al., 2007). Local Quaternary uplift is not uniform across the catchment with parts of the lower catchment (southern Poverty Floodplain) undergoing subsidence and uplift at the headwaters approaching 4 mm yr^{-1} (Brown, 1995; Litchfield and Berryman, 2006). Apart from localised subsidence in Poverty Floodplain and Poverty Bay, the majority of the terrestrial system is probably experiencing uplift. There is evidence for coastal uplift exceeding 2 mm yr^{-1} both north and south of Poverty Bay with uplifted marine terraces observed on the north side of the Mahia Peninsula and around the Pakarae River mouth (Fig. 3.1) (Berryman et al. 1992; Berryman, 1993a,b; Wilson et al. 2006). Marine terraces are not preserved along most of the rest of the coastal foothills, but coastal uplift has been inferred for these areas (Fig. 3.1) (Gerber et al. 2010). Offshore, growing shelf edge anticlines and shelf synclines both reduce off-shelf sediment transport and provide

accommodation space (Fig. 3.1) (e.g. Lewis and Pettinga, 1993; Foster and Carter, 1997; Orpin et al., 2006; Gerber et al., 2010).

The exposed inner forearc sequence underlying most of the WSS is composed of imbricate-thrust Miocene-Pliocene marine mud and sandstones (Fig. 2.2) (Lewis and Pettinga, 1993; Mazengarb and Speden, 2000). Highly deformed allochthonous Cretaceous-Early Neogene marine mudstone, sandstone and limestones underlie about 12% of the modern terrestrial WSS, mostly in the northwest. Swelling smectite clays are present in the mudstones (Gage and Black, 1979; Pearce and Black, 1981; Pettinga and Bell, 1992; Lacoste et al., 2009), and even unweathered mudstone and sandstone outcrops exhibit low strength (uniaxial compressive and geological strength index) (Pettinga and Bell, 1992; Lacoste et al, 2009; Chapter 2). These tectonically crushed, compacted but poorly cemented, interbedded marine sediments of the NIEC forearc sequence are prone to widespread and deep-seated slope instability (Gage and Black, 1979; Pearce and Black, 1981; Pettinga and Bell, 1992; Page and Lukovic, 2011, Chapter 2).

The WSS has a maximum altitude of 1200 m. Mean altitude is ca. 300 m but only about 16% of the catchment is over 500 m. Relief is highest in the northwest of the catchment, approaching 600 m from valley floor to ridge top. Areas mapped as allochthonous marine sedimentary rocks, including limestones, correspond to the areas of highest relief (Mazengarb and Speden, 2000). Limestone ridges in this area exhibit the steepest slopes (up to 60°), while outcrops of Miocene melange, interpreted as diapiric, under-compacted shales, exhibit the lowest relief and gentlest slopes of any of the pre-Quaternary geologic units. Most of the rest of the catchment has maximum hillslope relief of ca. 300 m.

3.3.2 Climate

Modern climate in the WSS is temperate maritime with mean annual temperatures 12.5° to 15° C at the coast and lowlands, and 7.5° to 12.5° C in the uplands (Leathwick et al. 2002). Westerly winds shadow the Poverty Floodplain behind the Raukumara Range with mean annual precipitation less than 1000 mm at the Poverty Floodplain (Leathwick et al. 2002). Mean annual precipitation in mid-elevations is 1000 to 1500 mm and in the head waters 1500 to 2500 mm (Leathwick et al. 2002). High intensity rainstorms and

cyclones occur frequently, averaging about one every five years throughout the Holocene (Page et al., 2010) and do a significant amount of geomorphic work. This was well illustrated by the widespread landsliding, flooding and sedimentation following Cyclone Bola in 1988 (Page et al., 1994a, 1994b).

Broad paleoclimatic conditions in the WSS can be inferred from a number of paleoclimate studies using proxy data such as pollen assemblages, changes in sedimentation and stable isotope ratios from sites around the NIEC (e.g. Wilmshurst et al., 1999; Lowe et al., 1999; McGlone, 2001; Carter et al., 2002; Newnham and Lowe, 2000; Hajdas et al., 2006; Lorrey et al., 2008; Page et al., 2010, Orpin et al., 2010). Many of these high resolution paleoclimate records are summarized by Alloway et al. (2007), who produced a composite climate record for New Zealand. The Last Glacial Maximum is considered to be extended in New Zealand, beginning ca. 28,000 cal. yr BP and terminating at ca. 18,000 cal. yr BP, and is referred to as the Last Glacial Coldest Period (LGCP). The transition from the LGCP to Holocene interglacial conditions occurred from ca. 18,000 cal. yr BP to ca. 11,600 cal. yr BP and included a lateglacial climate reversal between ca. 13,500 and 11,600 cal. yr BP. The current Holocene interglacial period has had two phases of greatest warmth between ca. 11,600 and 10,800 cal. yr BP and from ca. 6,800 to 6,500 cal. yr BP (Alloway et al., 2007).

Climate change and the arrival of humans in New Zealand had significant effects on vegetation in the WSS, which also changed slope stability and sediment discharge (Gomez et al., 2007; Miller and Kuehl 2010; Chapter 2). Following the LGCP native mixed podocarp-angiosperm-beech forests expanded, reaching a pre lateglacial reversal maximum at ca. 15,500 cal. yr BP (Newnham and Lowe, 2000). However, the pre-lateglacial reversal ratio of lowland-montane podocarp pollen to upland grass pollen at an upland site (Kaipo Bog, Fig. 2.3) was still less than half that after ca. 11,600 cal. yr BP., indicating that full Holocene forest conditions were not reached until after this time. Human-induced vegetation change started with Polynesian (Maori) settlement in New Zealand around the 13th Century with fire used as a forest clearance tool (Wilmshurst et al., 2011; McWethy et al., 2010). Major deforestation by European settlers began in the mid 19th Century with wholesale conversion to pasture by the mid 20th Century (e.g. Pullar, 1962; Wilmshurst et al., 1999; Dymond et al., 1999).

3.4 Post LGCP sources of sediment

Likely sources of sediment from the terrestrial WSS are introduced here. These potential sources include: river incision, shallow landslides, overland flow, coastal erosion, and deep-seated landslides, the main subject of this chapter.

3.4.1 River incision

Following the Last Glacial Coldest Period (LGCP), rivers in the WSS, as elsewhere in New Zealand, switched from aggradation to incision (e.g. Berryman et al., 2000; Eden et al, 2001; Litchfield and Berryman, 2005; Gomez and Livingston, 2012; Chapter 2). Discrete disconnected-remnants of the LGCP aggradation terrace (T1) can be found up to 120 m above trunk and tributary channels as evidence of the magnitude of river incision (Berryman et al., 2000; Eden et al., 2001; Marden et al., 2008; Marden et al., In prep.). Three generations of older remnant aggradation terraces can be found above LGCP aggradation terrace (Berryman et al., 2000; Marden et al., 2008), but the LGCP terrace is by far the best preserved. In the lower WSS the T1 terrace has been buried under the Poverty Floodplain by more recent terrestrial aggradation and marine transgression (Fig. 3.1) (Berryman et al., 2000; Marden et al., 2008, Wolinsky et al., 2010). Fluvial deposits of the T1 terrace consist of 3 m to 20 m of sand, gravel, and cobble sized clasts covered by overbank silts and air-fall tephra. The thickness of the T1 gravel is generally less than 20% the total river incision (Marden et al., 2008). The age of T1 aggradation has been constrained by tephrochronology, beginning between the deposition of the Omataroa and the Kawakawa tephras, ca. 33,000 to 25,500 cal. yr BP and ceasing between the deposition of the Okareka and the Rerewhakaaitu tephras, ca. 22,000 to 18,000 cal. yr BP (Berryman et al., 2000; Eden et al., 2001; Litchfield and Berryman, 2005; Marden et al., 2008).

3.4.2 Deep-seated landslides

Deep-seated landslides (DSLS) are landslides that typically involve organic and inorganic soils (regolith) and varying amounts weathered or unweathered bedrock, often with a failure depth of more than about 3 m. These landslides are pervasive in the WSS (Gage and Black, 1979; Pearce and Black, 1981; Pettinga and Bell, 1992; Page and Lukovic, 2011, Chapter 2). Landslides are not limited to one mode of movement, and there are numerous examples of complex failure combining rotational, translational, and earthflow deep-seated mass movement. DSLS active since the LGCP can occupy up to

35% of the surface area (3D not planimetric) of WSS sub-catchments (Chapter 2). The vast majority of DSLS toe in streams, directly connecting them to the fluvial system and show a strongly coupled activity relationship with river incision (Page and Lukovic, 2011, Chapter 2). In Chapter 2, I argue that based on timing, valley geometry, and lack of structural control, many of the DSLS evident in the WSS were initiated by debuttressing due to river incision and triggered subsequently by climatic or seismic events.

3.4.3 Shallow landslides

Shallow landslides involving less than 3 m and typically less than 1 m of soils and weathered bedrock also are a major source of sediment to rivers in the modern WSS (Reid and Page, 2002). These landslides are usually triggered by high-intensity or long duration rainfall with single event rainfall-induced landsliding thresholds between 125 mm and 200 mm (Reid and Page, 2002). Large tropical storms can trigger significant shallow landsliding in the WSS as evidenced by the effect of Cyclone Bola (Page et al., 1999). Shallow landslide densities in the WSS during this 1 in 100 year event in 1988 were as high as 3.22 events per hectare (Page et al., 1999). Reid and Page (2002) estimated that about 15% of the annual suspended sediment yield of the modern Waipaoa is derived from shallow landslides, but the contribution during prehistoric times is less certain. The magnitude of shallow landsiding was certainly lower under primary forest cover than in the current pasture dominated WSS, but because there are not many large continuous areas of native forest left, it is difficult to estimate prehistoric shallow landslide rates. One potential estimate for reduction of shallow landsliding under canopy comes from Marden and Rowan (1994) who found that under exotic forests 8 years old or older, rates of shallow landsliding during Cyclone Bola were about 16 times lower than on pasture land. This broadly agrees with the effect of forest clearance from similar marine sedimentary terranes on shallow landslide rates from the Oregon Coast Range in the North American Cordillera (ca. 9 to 25 times increase) (Montgomery et al., 2000). Another estimate of the stabilizing effect of forests comes from NIEC lake sediment cores, showing that sedimentation after pasture conversion is 8 to 17 times higher than for primary forest (Page and Trustrum, 1997). However, this estimate does not specifically isolate the contribution from shallow landslides.

3.4.4 Other sources

Other major sources of sediment for the long term post LGCP sediment budget include

coastal erosion and overland flow. Historical coastal erosion rates in the WSS can be as high as 0.7 m yr^{-1} (Gibb, 1978). Holocene coastal erosion rates up to 0.5 m yr^{-1} have been estimated for Hawke's Bay (an area of similar geologic setting south of the WSS (Fig. 3.1) (Litchfield, 2008). Volumetric erosion estimates are less common because of variable coastal topography. However, volumetric rate estimates based on multi-temporal lidar on an Eocene-Miocene marine sediment dominated ca. 50 km stretch of coastline in southern California found that an average of 1.8 m^3 m^{-1} of sediment was eroded per year (Young and Ashford, 2006). Rates approaching these would translate to significant volumes of sediment in the WSS. The inferred coastal uplift outside of Poverty Floodplain (Brown, 1995; Gerber et al., 2010) and the lack of preserved marine terraces except for a few isolated localities south and north of the WSS (Berryman et al. 1992; Berryman, 1993a, b; Wilson et al. 2006) suggests that there has been coastal erosion and retreat since the sea level lowstand at the LGCP. The LGCP shoreline was approximately 25 km outboard of the current shoreline (Fig. 3.1), but it is difficult to reconstruct the topography when this part of the WSS was subaerial.

Page et al. (2004) estimated that overland flow was responsible for about 21% of the sediment budget from a small, pasture dominated NIEC catchment. Overland flow, including all types of surface water flow from high-frequency, low-magnitude sheetflow to low-frequency, high magnitude sheetflood (Hogg, 1982), is probably a less efficient erosive agent in primary forest conditions but could still deliver sediment to the fluvial system and to offshore depocentres over millennial time scales.

3.5 Study areas and geomorphic mapping

3.5.1 Study areas

Two representative study areas of contrasting lithology, structural setting, and relief were chosen to characterize the magnitude of deep-seated landsliding in the upper WSS. Within the limits of access and reasonable field size, these study areas were chosen as representative of the general hillslope processes in the WSS (Chapter 2). Detailed geological and geomorphic mapping combined with geomorphic age control and paleo-topographic reconstructions from these selected areas provided the main data sources for DSLS sediment budget estimations for the WSS.

The 57 km^2 eastern area is in the lower Waingaromia River catchment (Fig. 3.1), includes several complete tributary basins, and is predominantly underlain by Miocene-Pliocene marine mudstones. The 84 km^2 western area stretches from the lower Mangatu River to the catchment divide (Fig. 3.1), includes two large tributaries to the Mangatu River, and is underlain mostly by allochthonous Cretaceous-Early Neogene marine mudstones, sandstones, and limestones. Both representative areas have experienced significant post-LGCP river incision (25 m to 115 m), leaving terrace remnants stranded above the modern streams and knickpoints in the upper reaches of the tributaries (Crosby and Whipple, 2006; Marden et al., 2008).

3.5.2 Geomorphic mapping

Geomorphic mapping in the selected study areas was accomplished using a combination of field investigation, air photograph interpretation, and interpretation of high resolution topographic data. The high resolution topographic data sets used are: 1) Eastern area - 2.5 m vertical accuracy photogrammetric topography from predominantly clear ground (deforested) photography acquired in the late 1970's and early 1980's. Contours in this area were processed to a 5 m grid using ESRI ArcGIS® software; 2) Western area - sub-metre airborne lidar (light detection and ranging) topography was acquired during the 2010 Australasian autumn by NZ Aerial Mapping Limited. Funding for the lidar was provided by NSF MARGINS grant OCE-0841111 (Sediment production via landsliding). For this study, bare earth lidar return data was processed to a 2 m grid using free software tools available through the NSF Open Topography Portal (http://www.opentopography.org/). Field mapping of geomorphic features such as landslides, terraces and knickpoints complemented and verified mapping and stream profile analysis based on photography and high-resolution topography. A majority of the features mapped have been field verified (e.g., 60% of the mapped landslides) during field campaigns in 2009 and 2010. All features mapped were digitised into a geographic information system (GIS) (ESRI ArcGIS®) for analysis.

3.5.3 Results of geomorphic mapping

Two hundred and thirty-six deep-seated landslides that have been active since the end of the LGCP were geomorphologically mapped in the two study areas (Fig. 3.2). Hillslopes mobilized by landslide activity make up 35% of the surface area (3D not planimetric) of

the lower relief Miocene-Pliocene mudstone terrain of the eastern study area. The higher relief, older, limestone and mudstone-dominated western study area, in contrast, has only 13% of its surface area affected by post-LGCP landslides. Twenty-five T1 aggradation terrace remnants were mapped, many of which were originally identified by Marden et al., (2008). Fifty-eight non-lithologic post-LGCP river incision knickpoints were mapped and used to help define the T1 aggradation surface (Fig. 3.2). Non-lithologic knickpoints are located high up in the tributary system, which is in agreement with the findings reported by Crosby and Whipple (2006).

The mapping of the post-LGCP (18,000 cal. yr BP) DSLS in the study areas allows me to extract valuable information about the landslide inventory as a whole. Many authors have observed that the frequency distribution of landslide areas are heavy-tailed and that for large and medium-sized landslides, frequency distributions approximate a negative power-law function of landslide area (Van Den Eeckhaut et al., 2007 and references therein). This is true for the inventory of DSLS from the WSS study areas. Figure 3.3 shows the log-binned frequency density vs. area plot for DSLS inventory. The starting point of the power-law tail and the apparent rollover at smaller areas are artefacts of the incomplete inventory that includes no small landslides (Fig. 3.3). However, the approximate negative power-law tail has been shown to be robust, reflecting first order variations in slope stability thresholds for many different landscapes (Malamud et al., 2004 a, b, Van Den Eeckhaut et al., 2007; Korup et al., 2012). The scaling exponent ($-\beta$) of the non-cumulative power law tail for the inventory is estimated at 2.15 using a robust maximum likelihood fitting method (Clauset et al., 2009). Estimated β for eastern and western study areas individually are similar at 2.12 and 2.19, respectively, showing the fundamental nature of this parameter. The combined inventory β is slightly lower (flatter) than a worldwide average from other inventories ($\beta = 2.3$; Van Den Eeckhaut et al., 2007), and indicates that the landslide sediment budget for these areas are theoretically dominated by DSLS (Stark and Guzzetti, 2009). A comparison between the area frequency distributions of the detailed study areas and a larger (1026 landslides) air photo-based DSLS inventory for the Waipaoa and Waimata catchments (Page and Lukovic, 2011) is not appropriate because in that inventory individual landslides were not mapped in areas underlain by allochthonous geology, where practically the entire terrain is experiencing landslide activity. Excluding the areas where the largest landslides

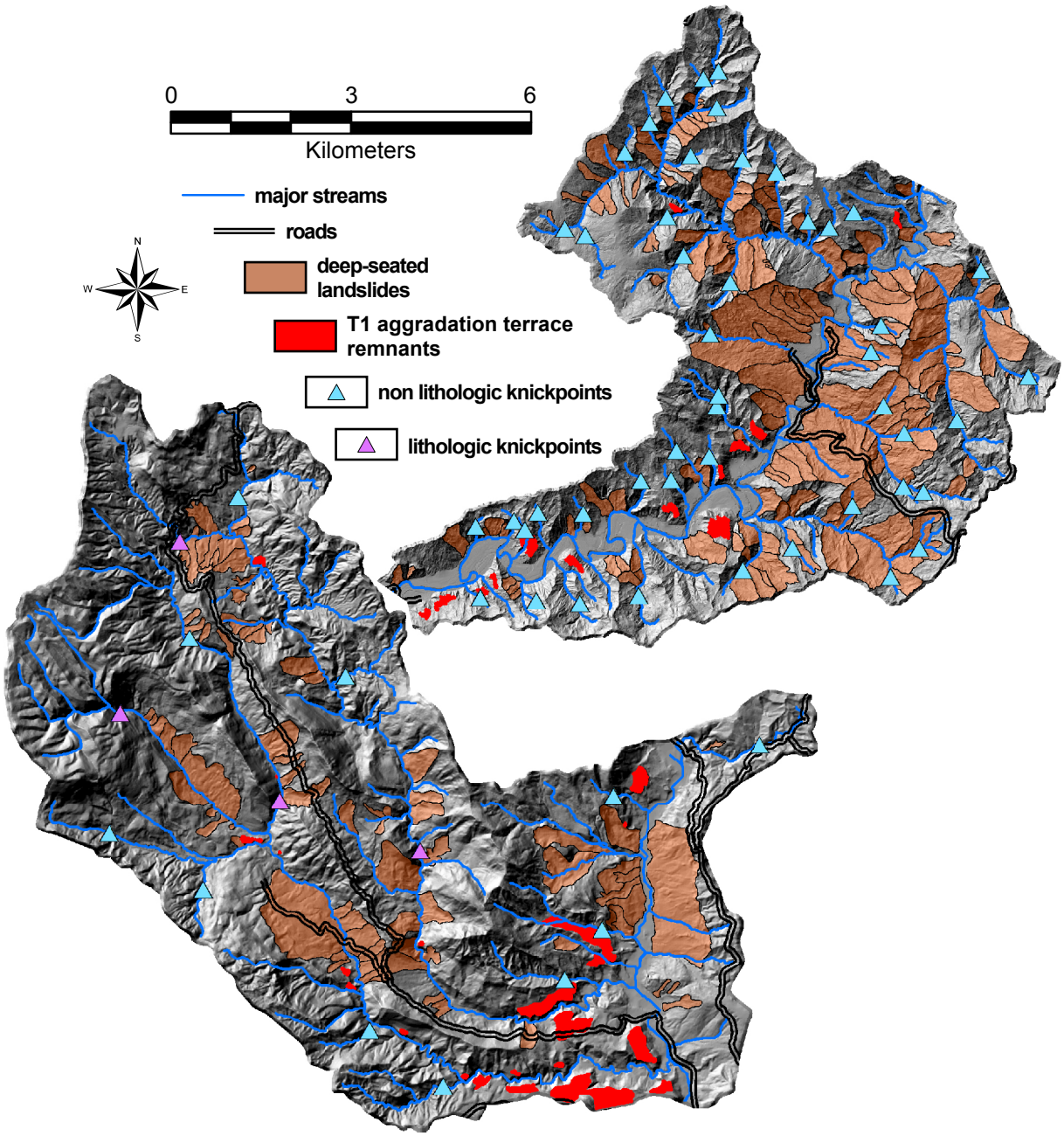

Figure 3.2. Results of the geomorphic mapping. Deep-seated landslides, T1 aggradation terrace remnants, and knickpoints in the two study areas.

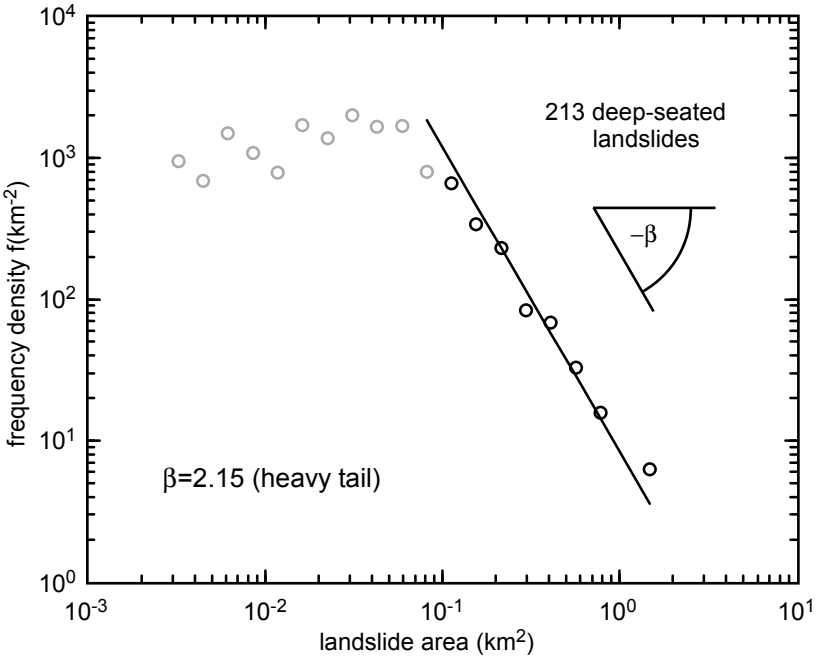

Figure 3.3. Log-binned frequency density vs. area plot for the deep-seated landslide inventory from the two WSS study sites. The scaling exponent (β) for the negative power-law tail is estimated at 2.15 (slope of the back line) using a robust maximum likelihood fitting method (Clauset et al., 2009). Heavy tailed distributions like this probably have landslide sediment budgets dominated by deep-seated landslides (Stark and Guzzetti, 2009).

are located from the landslide area dataset fundamentally change the frequency distribution.

3.6 Tephrochronology and age control

3.6.1 Age control methodology

Age control for landforms is important for the paleo-topographic reconstruction-based volumetric estimations so that the estimates reflect sediment removed from the terrestrial WSS since the end of the LGCP (ca. 18,000 cal. yr BP). First order age control for mapping only DSLS active since the LGCP is possible by mapping slides that crosscut the T1 LGCP aggradation surface (Marden et al., 2008). Very little datable organic material entrained in DSLS was found, with only three samples collected (one angiosperm and two podocarp logs). In the WSS, which lacks sufficient quartz for cosmogenic exposure ages and radiocarbon in landslide deposits, finer resolution age control for landslides and river terrace remnants is possible through tephrochronology. Detailed methodology for landform tephrochronology in the WSS is presented in Chapter 2. Table 2.1 lists the macroscopic tephras horizons used for landform tephrochronology in the WSS.

In general, the age of the oldest tephra on a landform is a minimum stabilization age for that landform (Lang et al., 1999). One hundred and seventy-three soil test pits were dug, and 64 sites were explored by soil auger across the two study areas for landform tephrochronology. Tephra for identification was collected from 80 test sites. Test pits and auger sites were generally located on the largest expanse of low slope ground available on a sampled landform, thus sampling sites with the best tephra preservation potential. Test pits samples were discrete, consisting of no more than 4 cm vertical of profile, while auger samples averaged no more than 10 cm of a soil profile. All of the sites have been logged and located by differential global positioning (DGPS).

Collected tephras were identified by electron probe microanalysis (EMPA), conducted on the JEOL JXA-8230 SuperProbe Electron Probe Microanalyser at Victoria University of Wellington. Basic procedures for sample preparation and EMPA follow Lowe (2011). Wavelength dispersive X-ray spectrometry was used for major oxide analysis of all samples. Multiple glass shards from each sample were analyzed with a defocused 20 μm diameter beam of 8.0 nA at 15 kV accelerating voltage (Chapter 2).

3.6.2 Landform tephrochronology results

Landform tephrochronology established the abandonment ages of prospective T1 terraces, helped to confirm that stable landforms have accumulated thick tephra cover and that the majority of the mapped landslides have been active since the end of the LGCP, ca. 18,000 cal. yr BP (Chapter 2).

Stable landforms such as terrace remnants, broad ridge tops, or uplands up-basin from knickpoints related to post-LGCP river incision (electron probe microanalysis results from 31 sites) are all overlain by thick tephra sequences, with basal tephras of Rerewhakaaitu (ca. 17,600 cal. yr BP) or older. These thick older tephra sequences can be stable even on steep slopes, with Rerewhakaaitu or older tephras observed on slopes ≥30°. Except for one sample identified as Waiohau Tephra (ca. 13,600 cal. yr BP), the Rerewhakaaitu Tephra (ca. 17,600 cal. yr BP) is the basal tephra coverbed on the rest of the prospective T1 terrace remnants analyzed.

Thick tephra sequences are not present on deep-seated landslides. The only exceptions

are small sections of intact translated blocks immediately below main head scarps. Field and EMPA assessment of 141 of the 236 mapped post-LGCP DSLS indicate that no tephra older than Rotoma (ca. 9500 cal. yr BP) is present on the body of these slides (Chapter 2). A full 70% of these landslides have accumulated only Taupo (ca. 1700 cal. yr BP) and Kaharoa (ca. 630 cal. yr BP), only Kaharoa, or no tephra cover (Chapter 2).

3.7 Volumetric reconstructions

3.7.1 Reconstruction methodology

I used a three-step approach to estimate the volume of material eroded by post-LGCP DSLS in the WSS: 1) in order to separate river incision sediment flux from landslide sediment flux, I reconstructed the T1 aggradation surface in the representative study areas; 2) pre-failure hillslopes for the mapped post-LGCP landslides were then reconstructed; and 3) methods were developed for scaling the representative study site volumetric estimates up for the entire terrestrial WSS.

3.7.2 Reconstructing the T1 surface

The volume of eroded material that post LGCP DSLS contributed to the WSS sediment budget overlaps with the volume of material eroded by river incision (Fig. 3.4a). The least complex way to account for this in the sediment budget estimate is to include any portion of a DSLS that is below the T1 aggradation surface in the volumetric estimate for river incision (Marden et al., 2008; Marden et al., In prep.). Likewise, the area under the T1 aggradation surface is excluded from the contributing area for other sediment sources (i.e. shallow landslides and overland flow).

In order to estimate the remaining (above T1) volumetric contribution of DSLS to the WSS sediment budget, it is crucial to develop a realistic model of the T1 surface. This is because the elevation at which this surface intersects with a landslide affects the volume of material attributed to that landslide (Fig. 3.4a and b). To model the T1 surface in the representative field areas, I mapped and field checked T1 aggradation terrace remnants and knickpoints and then interpolated between known T1 landscape markers using a realistic channel concavity developed from the slope-area relationship of T1 paleochannels.

The local slope of both detachment- and transport-limited channels generally scales as a

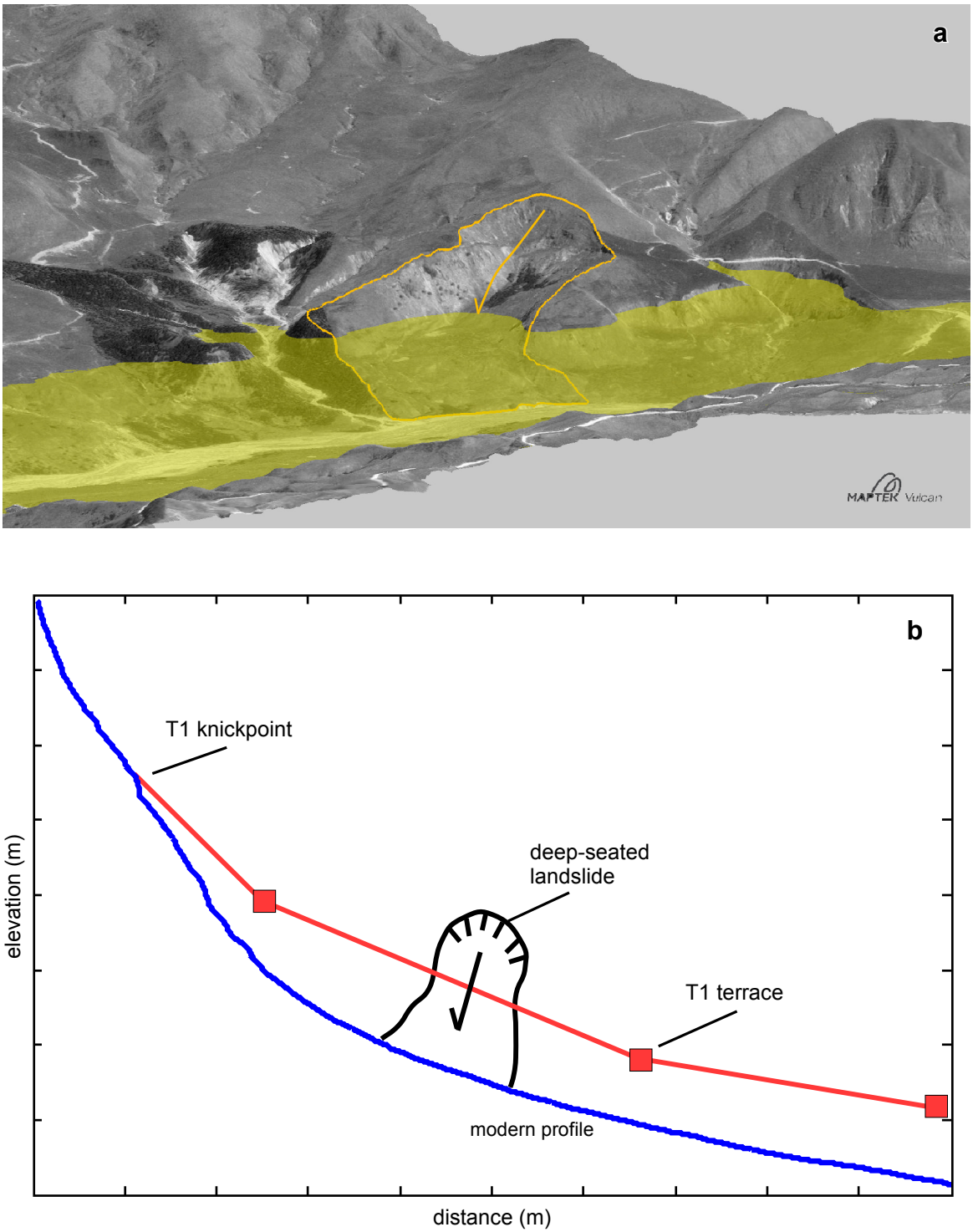

Figure 3.4. a) oblique view of aerial photography draped topography of a portion of the Mangatu River showing a large translational landslide (orange polygon) and the modelled T1 aggradation surface (yellow transparent surface). This illustrates that the volume of material that post LGCP DSLS contribute to the WSS sediment budget overlaps with the volume of material eroded by river incision. For this reason the DSLS sediment flux is calculated from the portion of the landslides that are above the T1 aggradation surface. b) Idealized stream profile view of a modern stream and the elevations of T1 terrace remnants and a T1 knickpoint with a DSLS cross-cutting the T1 surface and toeing in the stream. The method of reconstructing the T1 aggradation surface, whether by linear interpretation (shown) or by estimating a realistic concavity (described in the text) will influence the estimate of total sediment derived from DSLS.

power-law function of contributing drainage area (Wobus et al., 2006 and reference therein). This relationship can be represented by the equation:

(1) $$S = k_s A^{-\theta}$$

Where S is the local channel slope, A is the upstream drainage area, k_s is the channel steepness index, and θ is the channel concavity index.

Using this relationship, the upstream slope and the modern upstream drainage areas from non lithologic knickpoints and remnant T1 terraces, I was able to estimate T1 channel concavity (Fig. 3.5). For channels that have at least three T1 data points, I directly estimated concavity by regression. For the rest of the small channels in the representative study areas, I used an average regional T1 concavity of 1.05 derived from eight tributaries in the two study areas that either preserved multiple terrace remnants or pre T1 river incision stream profiles (Fig. 3.6). Modelled T1 elevation points every 10 m of horizontal stream distance were used to create a modelled T1 aggradation surface using the 3D software Maptek Vulcan® (Fig. 3.7)

3.7.3 Reconstructing the pre-failure hillslope

Pre-failure DSLS slope modelling relied on the modelled T1 aggradation surface, detailed mapping of the scarps, and landform geochronology which separates older intact surfaces from landslides. By modelling the T1 aggradation surface, the paleovalley floor or base of the pre-failure slope was estimated. Profiles (linear interpolation) were then drawn between the T1 aggradation surface and the landslide head scarps to represent the most likely pre-failure hillslope profile (Fig. 3.8a). A best fit surface was constructed through the 3D landslide outline polygon and the slope profiles using 4th order polynomial regression (Fig. 3.8b). This was found to fit the natural curvature of intact slopes better than lower order regressions. When the T1 to head scarp profiles did not provide enough constraint for the regression, the pre-failure surface was further refined by limited contouring between landslide scarps and profiles using the curvature of the surrounding intact slopes as a guide.

Profiles, contours, and regression surfaces were all created using Maptek Vulcan®

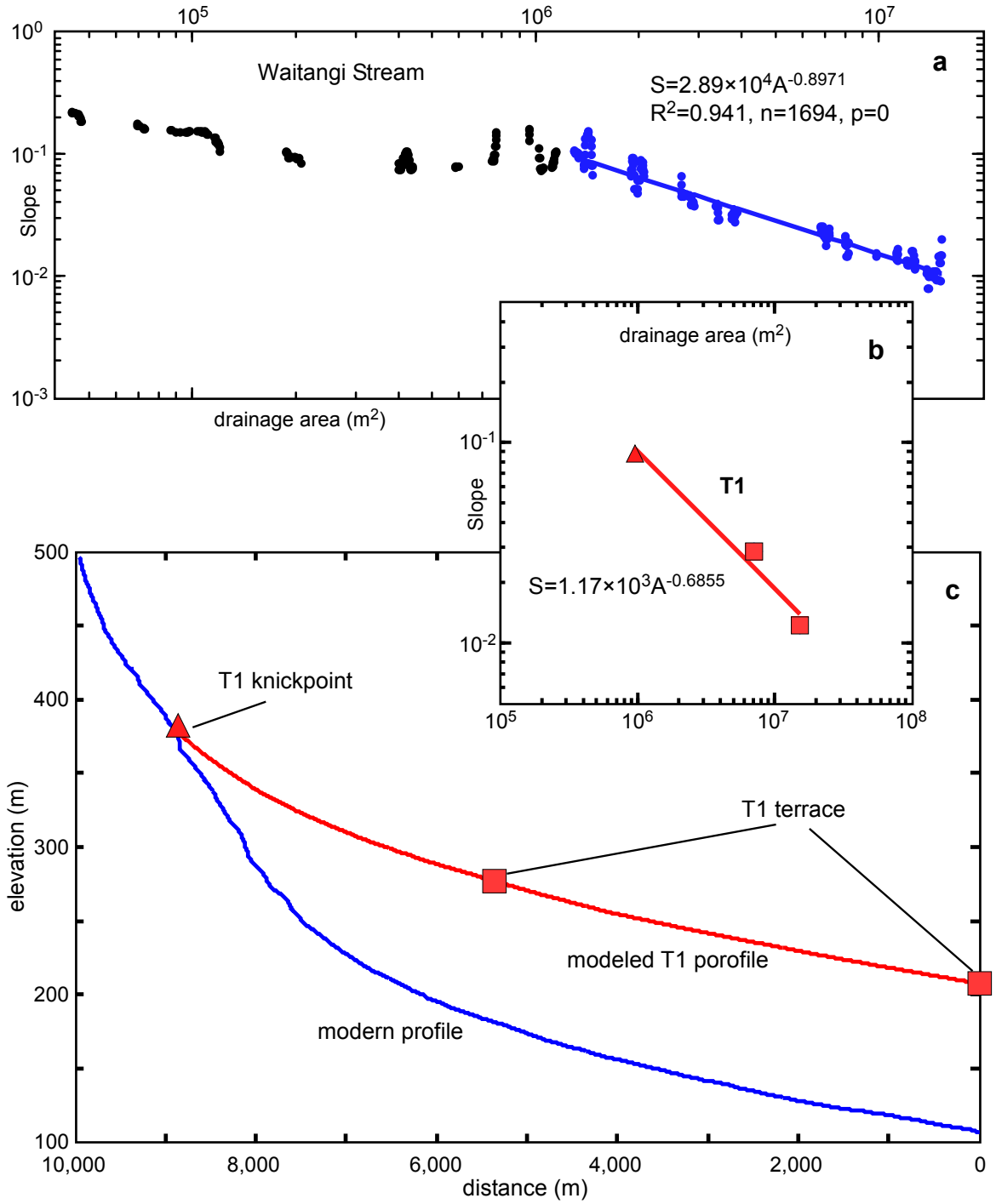

Figure 3.5. a) Slope-area plot of the modern Waitangi Stream (Fig. 3.6) in the eastern study area. Both slope and drainage area are derived from lidar topography following methods outlined in Wobus et al. (2006). The slope-area regression is estimated at areas below the threshold area above which fluvial scaling is not present and debris flow processes may dominate (Wobus et al., 2006) b) Slope-area regression for the T1 aggradation remnants remaining above the Waitangi Stream. The scaling exponent, concavity, is slightly lower than modern in this case. c) Stream profile plot showing the modelled T1 aggradation profile for Waitangi Stream using the empirical realistic concavity estimate from the regression.

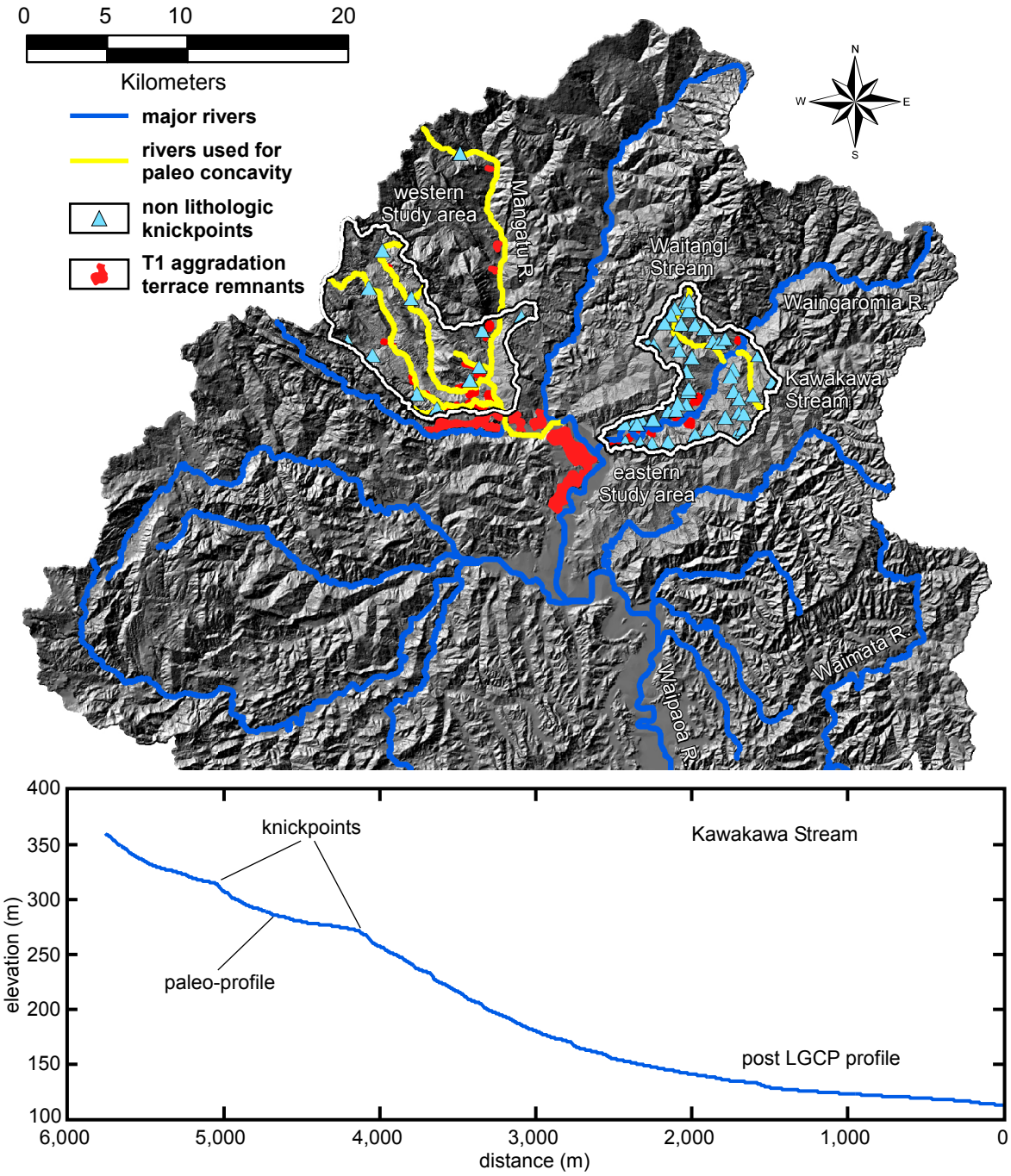

Figure 3.6. Map of the upper Waipaoa catchment showing major tributaries used to estimate an average regional concavity for T1 paleochannels. T1 concavity is estimated from regressions of terrace and knickpoint slope-area plots and from sections of streams that exhibit a relict concavity above a T1 knickpoint, such as in the Kawakawa Stream as show in the stream profile plot.

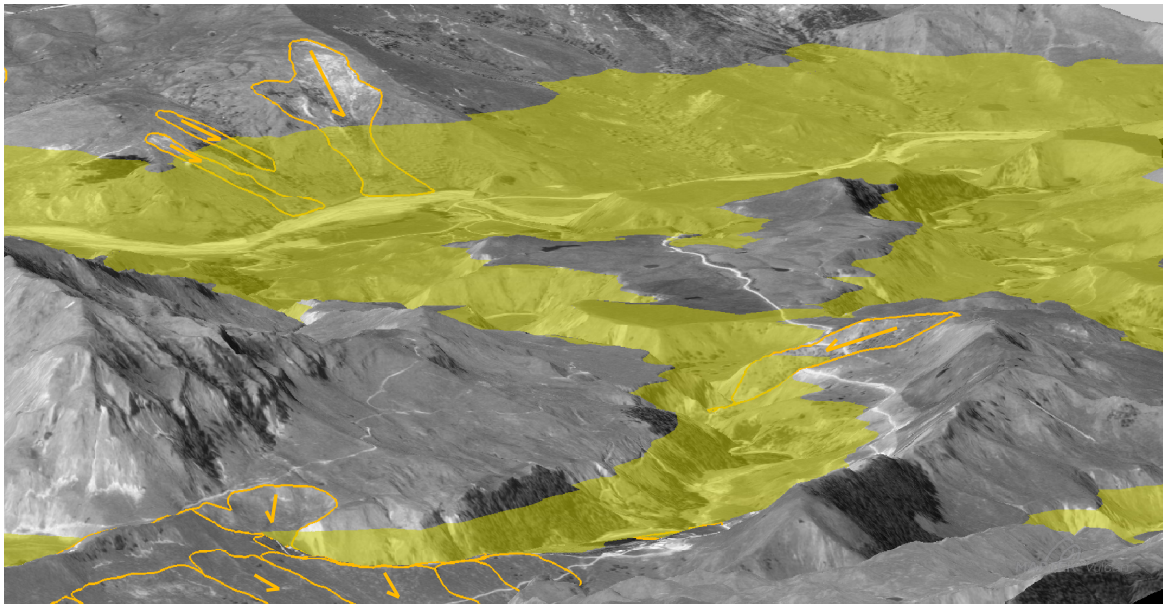

Figure 3.7. Oblique view of aerial photography draped topography of a portion of the Mangatu River and two of its large tributaries showing DSLS (orange polygons) and the modelled T1 aggradation surface (yellow transparent surface). This is an example of the stream profile modeling techniques described in the text.

software. The volume difference between the best fit regression surface (pre-failure slope) and the modern surface was then calculated. The volume of any part of the landslide deposit that is above this modelled pre-failure slope, such as convex deposits near the toe, was subtracted from the total volume. This resulted in a volumetric estimate of the amount of DSLS-derived material that is missing from the hillslope and presumed to have been delivered to the fluvial system.

3.7.4 Scaling to the entire WSS

To scale the DSLS-derived sediment volumetric estimates up from the representative study areas to an estimate of sediment delivered from DSLS in the terrestrial WSS, I used three methods: 1) scaling-up sediment yields from the study areas; 2) volume-area relationships applied to a catchment wide DSLS inventory; and 3) estimating a landslide magnitude scale.

The first method assumes that the study areas are truly representative and simply applies the 18,000 cal. yr BP volumetric sediment yield for the study areas to the DSLS susceptible area of the terrestrial WSS. I define this susceptible area as the 2504.5 km^2 of the Waipaoa, Waimata, and Pakarae river catchments and the southern coastal

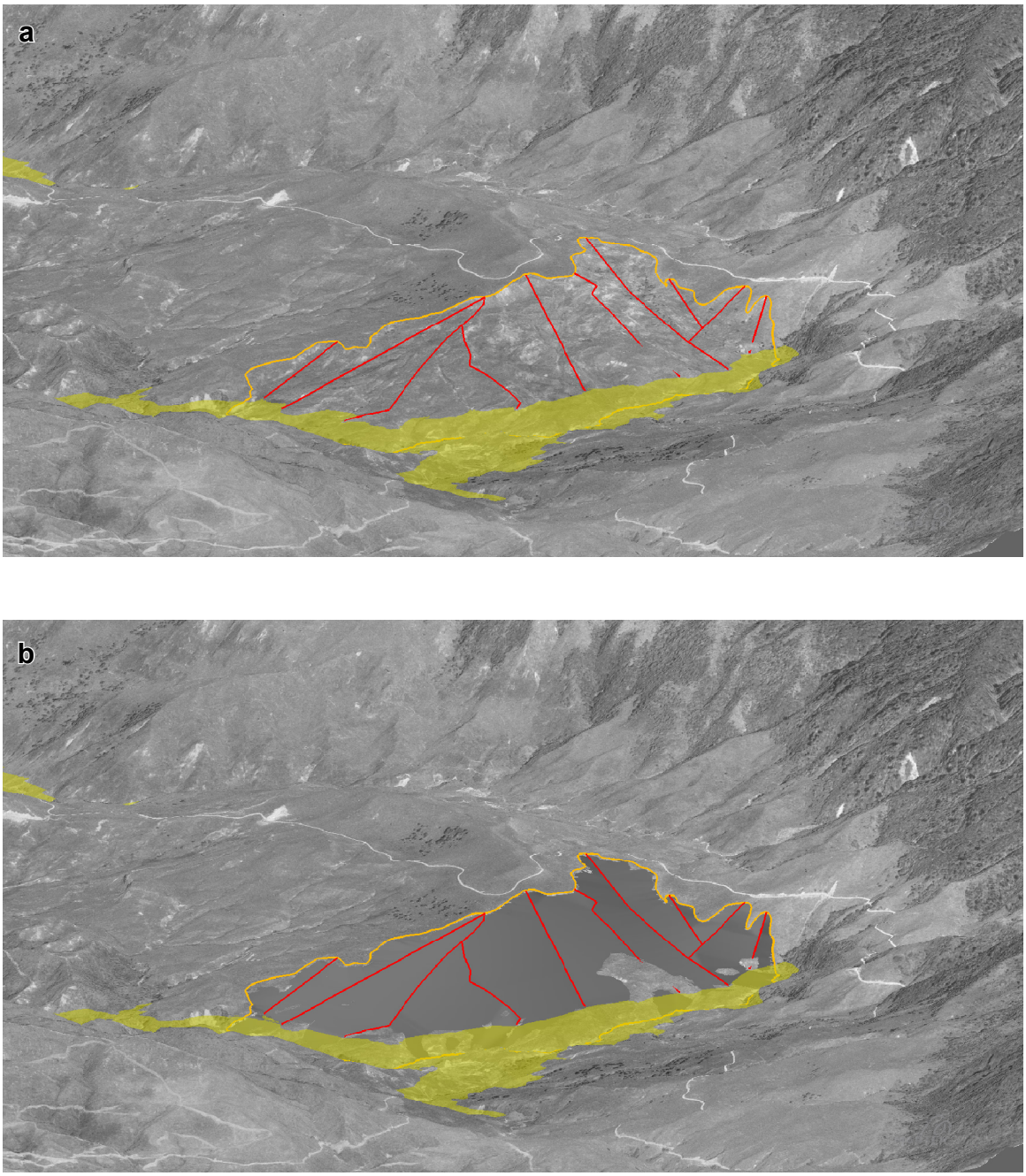

Figure 3.8. Oblique view of aerial photography draped topography of a portion the headwaters of a major tributary to the Mangatu River showing a deep-seated landslide (orange polygon) and the modelled T1 aggradation surface (yellow transparent surface). a) Detailed mapping of the scarp and extent of the landslide and profiles connecting the scarp to the modelled T1 surface (red lines) are used to model the prefailure surface of this landslide. b) A 4th order polynomial regression through the extent and profiles that models the prefailure surface (dark grey shading). Portions of the modern topography showing through the modelled surface represent landslide material in storage and are subtracted from the estimate of missing volume under the modelled surface to derive an estimate of volume above the T1 aggradation surface delivered to the stream and missing from the hillslope. In this case this is ca. 3,855,000 m^3.

catchments (Fig. 3.1) outside of the areas under the modelled T1 aggradation surface (Marden et al., 2008; Marden et al., In prep.) and coastal flats ≤ 5º slope (Poverty Floodplain, the Pakarae River flats, and the Mahia Peninsula neck).

I also estimated DSLS sediment output from the terrestrial WSS by developing two landslide volume-area relationships, one for the complete mapped landslide areas and the other for portions of the DSLS that are above the T1 aggradation surface. Many authors have found that landslide volume (V_L) scales as a positive power-law function with landslide area (A_L) (Guzzetti et al. 2009; Larsen et al. 2010 and references therein):

(2) $$V_L = \alpha A_L^{\gamma}$$

Where γ and α are the scaling exponent and intercept, respectively. The volume-area scaling relationship results presented below are estimated from n = 1000 bootstrap estimates based on randomly iterated samples of 50% of the reconstructed pre-failure hillslope landslide area and volume datasets. This method of volume-area regression yields a realistic estimate for distributions of scaling exponents and intercepts and eliminates any systematic bias when applying least squares regressions to log-transformed data.

These volume-area scaling relationships are then used to estimate the volume of all the DSLS mapped by Page and Lukovic (2011) in the Waipaoa and Waimata catchments outside of the study areas, where the more detailed DSLS inventory is used (Fig. 3.9). This inventory does not have any absolute age control but is considered to capture events younger than the LGCP (ca. 18,000 cal. yr BP) (Page and Lukovic, 2011). The volume delivered from the areas mapped by Page and Lukovic (2011) as landslide terrain (120 km^2) (Fig. 3.9), instead of individual landslides, was estimated by averaging landslide depth based on valley floor to ridge top landslides from the detailed study areas. The total volumetric sediment yield based on the Waipaoa and Waimata catchments DSLS inventory was then scaled-up to the entire WSS.

Both the representative sediment yield and broader DSLS inventory volume-area scaling methods are likely to produce minimum volumetric estimates over the 18,000 year

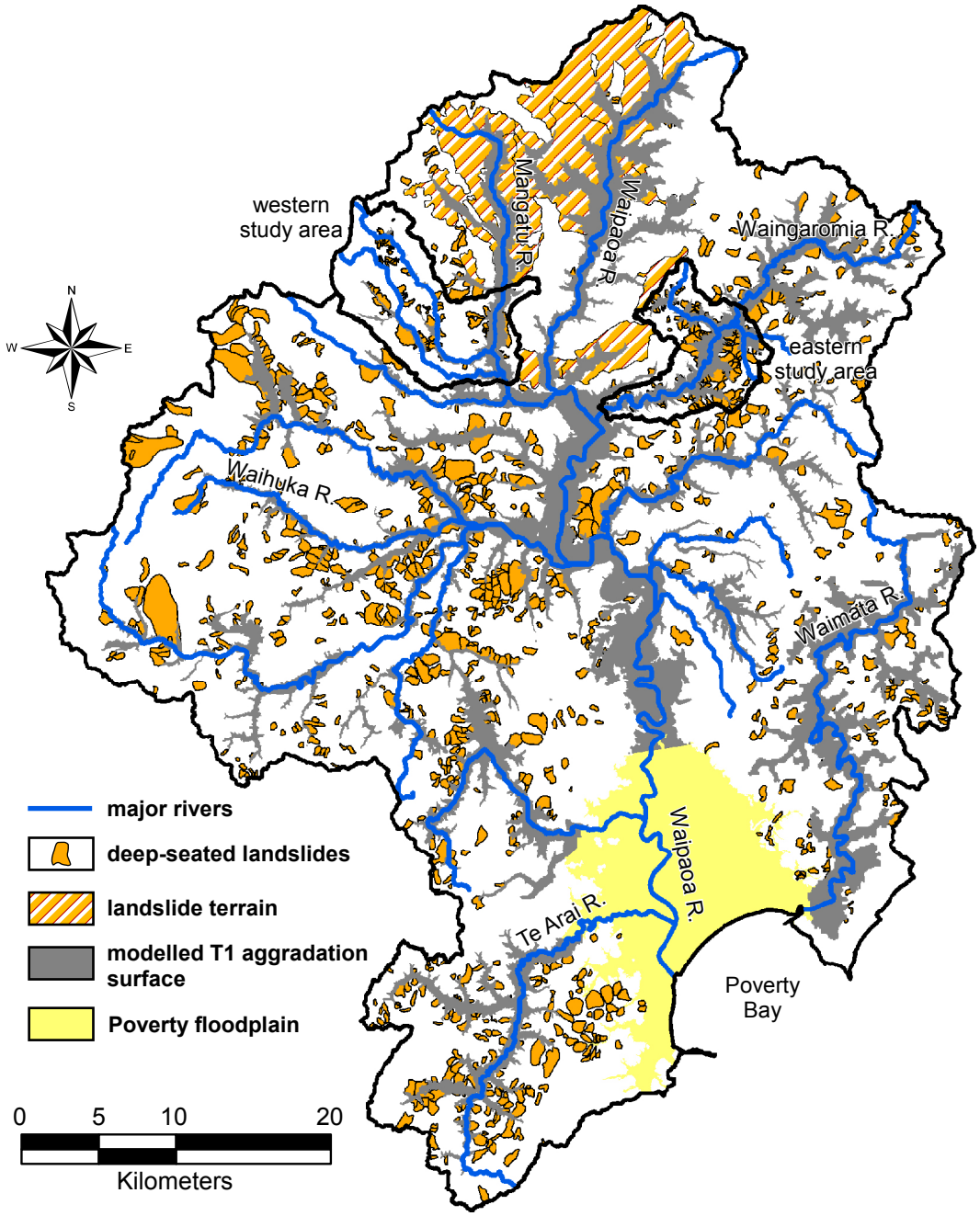

Figure 3.9. Combined DSLS inventory for the Waipaoa and Waimata catchments. Deep-seated landslides mapped outside of the western and eastern study areas are from Page and Lukovic, 2011. Landslide terrain was mapped by Page and Lukovic (2011) in areas where it was is difficult to differentiate individual landslide features.

record. This is because errors of omission (older landslides not being recognized) are probably the largest single source of uncertainty. A more detailed analysis of uncertainty is presented in sections 3.9 and 3.10.

Finally, I used methodology developed by Malamud et al. (2004 a, b) to estimate the total landslide numbers and total volume of an expected landslide inventory based on the properties of the area frequency distribution of a partial landslide inventory. This method uses empirical landslide area data from three substantially complete and substantially different landslide inventories to define a landslide magnitude scale and estimate the magnitude for incomplete inventories, such as the DSLS inventory from the study areas. The landslide magnitude scale, as defined by Malamud et al. (2004 a, b), is related to total numbers of landslides (shallow and DSLS):

(3) $$m_L = \log_{10}(N_{LT})$$

Where m_L is the landslide magnitude and N_{LT} is the total number of landslides. Landslide magnitude can be estimated by comparing the area frequency distribution of partial inventories to a proposed general N_{LT}-dependent landslide frequency distribution (Malamud et al., 2004 a, b; Van Den Eeckhaut et al., 2007). A total volumetric estimate is possible by converting the frequency distribution derived theoretical mean landslide area to volume and multiplying by the number of landslides. Malamud et al. (2004a) use the volume-area relationship developed by Hovius et al., (1997) ($\gamma = 1.5$ and $\alpha = 0.05$) to derive a N_{LT} dependent average volume ($\overline{V}_L$)

(4) $$\overline{V}_L = 7.30\times10^{-6}\, N_{LT}^{0.1222}$$

3.7.5 Results of the volumetric reconstructions

Figure 3.10 shows the reconstructed T1 aggradation surface using an estimated realistic concavity for the paleo channels. The T1 surface occupies 21.06 km^2 of the eastern study area (57 km^2). Using this, post-T1 (18,000 cal. yr BP) river incision in the eastern area is calculated at 1.02 km^3. The T1 surface occupies 15.62 km^2 of the western area (84 km^2) and results in a calculation of 0.61 km^3 of post-T1 river incision. Together this is just under 10% of the volume of river incision reported by Marden et al. (In prep.) for the

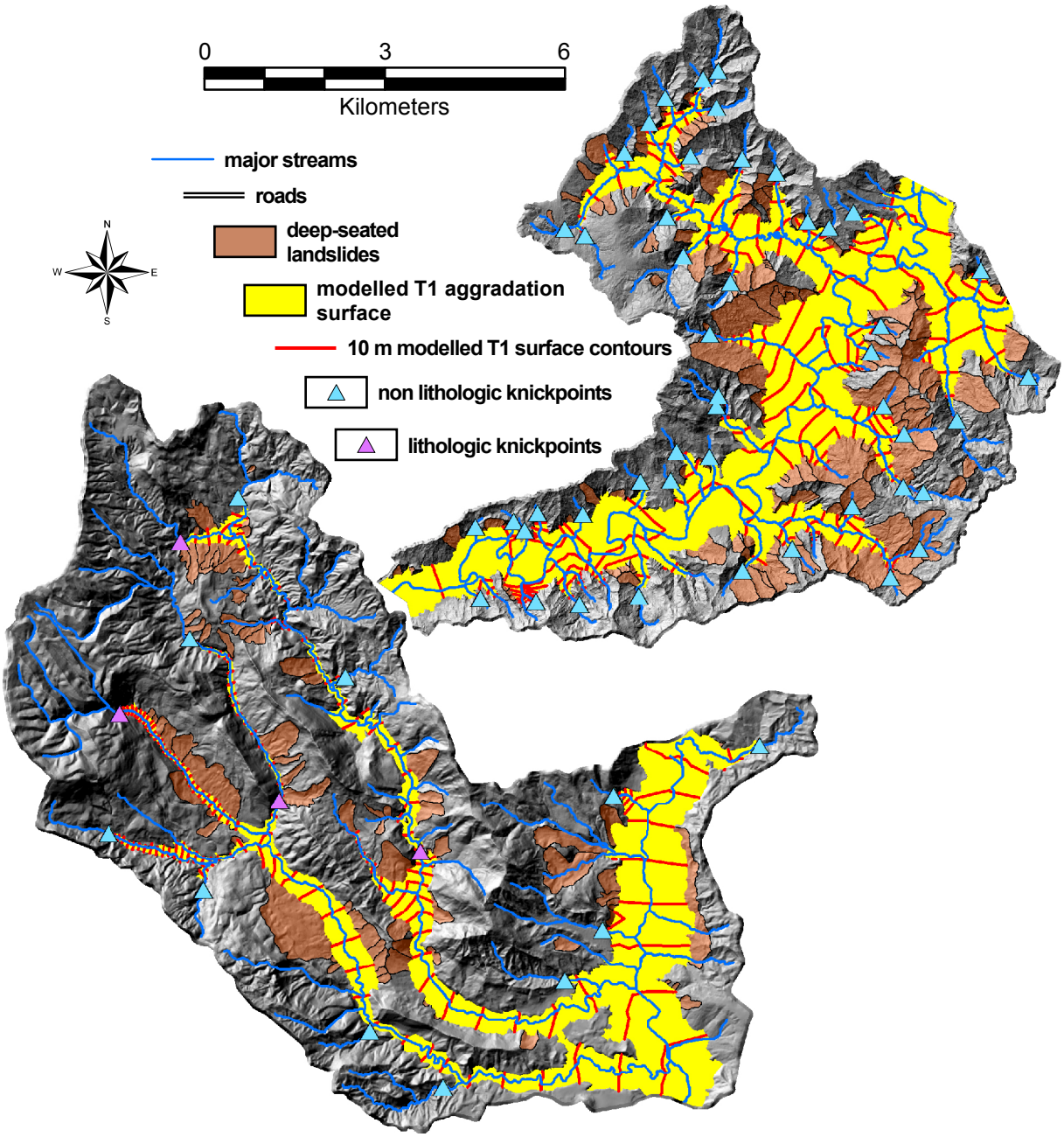

Figure 3.10. Results of the T1 aggradation surface reconstruction. Modelled T1 surface shown in yellow with 10 m contours in red.

entire Waipaoa and Waimata catchments (ca. 2500 km^2).

Reconstructions of non-nested DSLS for the combined areas yielded a total sediment volume of 0.38 km^3 (377,659,137 m^3) that is missing from the system and presumed delivered to the fluvial network. Two hundred and seven DSLS are partially or entirely above the T1 aggradation surface, and it is these scarp and translational portions of the landslide features that have delivered the majority (80%) of the sediment volume at 0.30 km^3 (300,892,396 m^3).

The landslide volume-area relationship for the complete mapped landslides and the portions of the DSLS that are above the T1 aggradation surface are shown in Fig. 3.11 a and b respectively. The scaling relationship for the landslides taken as whole features is:

(5) $$V_L = 0.0104 \times A_L^{1.554}$$

with $\log\alpha = -1.983 \pm 0.3$ with units $m^{(3-2\gamma)}$ and $\gamma = 1.554 \pm 0.062$ (Fig. 3.11a). The volume-area scaling relationship for the portions of the DSLS that are above the T1 aggradation surface is:

(6) $$V_L = 0.0694 \times A_L^{1.437}$$

with $\log\alpha = -1.159 \pm 0.310$ $m^{(3-2\gamma)}$ and $\gamma = 1.437 \pm 0.065$ (Fig. 3.11b).

Both scaling relationships are similar to that reported by Hovius et al. (1997) (Fig 3.11 - green line), Guzzetti et al. (2009) (Fig 3.11 - blue line), and Larsen et al. (2010). There is more scatter in the data of the second relationship for landslide portions above the T1 aggradation surface. This is because not all DSLS extend from valley floor to ridge top, which makes the area of a landslide above the T1 surface partially dependent on its location in the landscape.

The volumetric DSLS sediment yield from the combined study areas for the area above the T1 aggradation surface (104 km^2) is 1.608×10^{-7} $km^3\ km^{-2}\ yr^{-1}$ over the 18,000 year study period. When scaled-up to the entire terrestrial WSS (2504.5 km^2), this equates to

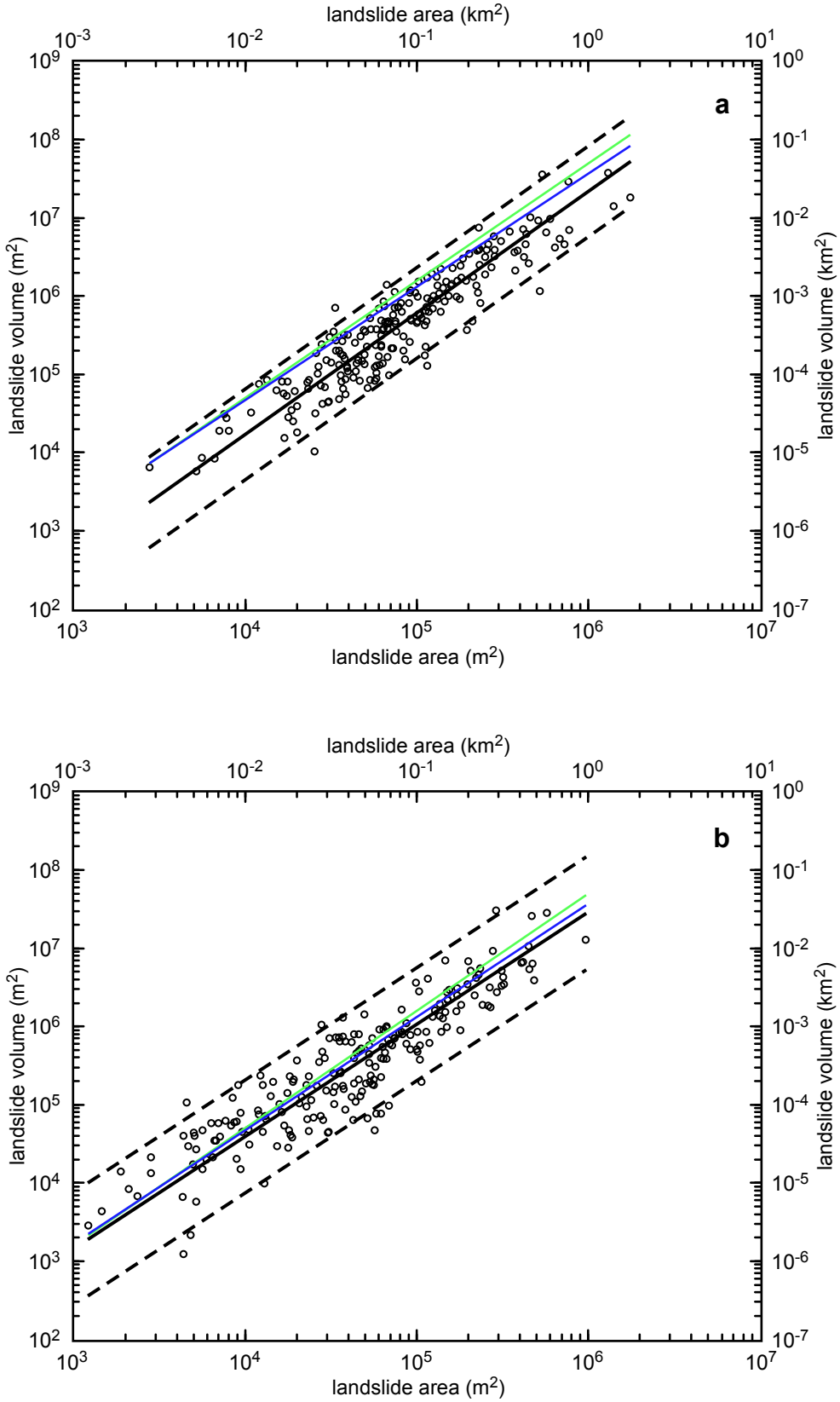

Figure 3.11. Volume-area scaling relationships for DSLS mapped in the detailed study areas (a) and those portions of landslides above the T1 aggradation surface (b). Black lines are regressions described in the text with dashed lines as 95% confidence intervals. The green line is the volume-area scaling from Hovius et al., (1997), and the blue line is the scaling regression from Guzzetti et al., (2009).

7.25 km^3 of sediment delivered to terrestrial and marine sinks from DSLS.

This estimate is within the range of the volumetric estimate derived from the volume-area relationships applied to the air photo based Waipaoa and Waimata DSLS inventory (Page and Lukovic, 2011) (Fig. 3.9). For landslides that intersect the T1 aggradation surface, scaling parameters from regression 6 were used to estimate the volumes of landslides above this surface, for landslides that do not intersect the T1 surface, scaling parameters from regression 5 were used. To simulate some of the inherent uncertainties of such an extrapolation, I used a Monte Carlo simulation of n = 10,000 runs with scaling parameter values randomly drawn from the volume-area relationships (5 and 6) assuming a normal distribution for γ and a lognormal distribution for α. Total landslide volume is obtained by applying this scaling randomised relationship to a given dataset. Figure 3.12 shows the results of some of these simulations applied to different datasets. Approximate median and asymmetric uncertainty approximating 68.2% (σ) of the data about the median are used to describe these positively skewed results (Limpert et al., 2001).

Using this method it is estimated that 10.2 km^3 of sediment with a multiplicative uncertainty of 1.9 km^3 (+9.2 km^3, -4.8 km^3) was delivered to terrestrial and marine sinks from DSLS. The asymmetric uncertainty is a product of three-dimensional results (volume) of a population of landslides and is propagated through the rest of source to sink estimates.

As a final check on these estimates, I used the general landslide frequency distribution developed by Malamud et al. (2004 a, b) from empirical data to estimate the m_L and total volume for 18,000 years of landslide activity in the combined study areas (Fig. 3.13). Then, I scaled this volume up to the entire WSS by deriving a volumetric landslide sediment yield. The m_L for the combined areas is 4.8 ± 0.2 (Fig. 3.13). Equation 3 estimates the total number of landslides (shallow and DSLS) (N_{LT}) that my inventory would contain if it were substantially complete at 63,096 with a multiplicative uncertainty of 1.7 (+44,167, -31,981). Total volume over 18,000 years scaled-up to the entire contributing WSS using equations 3 and 4 (Malamud et al. 2004 a, b.) is 31.7 km^3 with a multiplicative uncertainty of 1.7 km^3 (+22.1 km^3, -13.1 km^3).

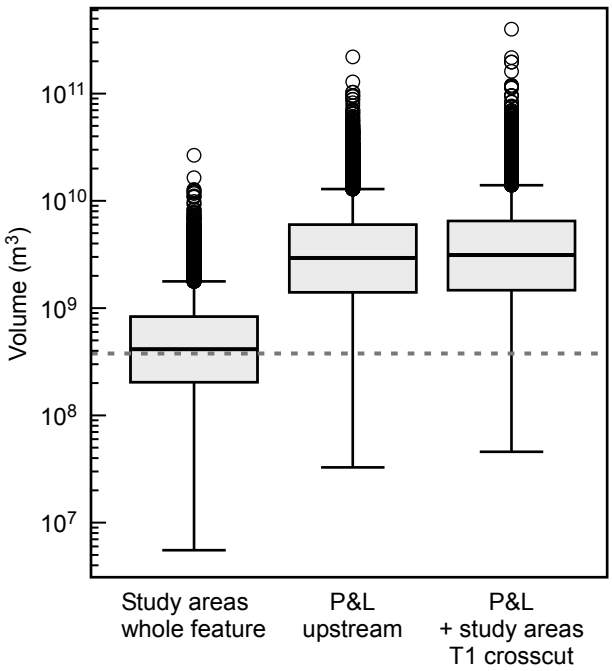

Figure 3.12. Box and whisker plots of the results of Monte Carlo simulations of volume-area scaling applied to total DSLS volumes for selected landslide inventories. Grey dashed line is the sum of the reconstructed topography modelled volumes of whole feature DSLS from the study areas (3.77×10^8 m^3). The box on the left (1) is the volume-area estimated total volume for the whole feature DSLS from the study areas using equation 5. The median of the estimate is 4.14×10^8 m^3, showing good agreement with the empirical data. The middle box (2) is the total volume estimate for the whole feature DSLS from the Page and Lukovic (2011) inventory that are upstream from areas of major river incision, also using equation 5. The box on the right (3) is the volume estimate for all the portions of landslides that are above the T1 aggradation surface from landslides that are crosscut by the modelled T1 surface from the detailed study areas and the Page and Lukovic (2011) inventory. This estimate uses equation 6. Boxes 2 and 3 plus the estimate from areas mapped as landslide terrain yield the total area scaled landslide volume of 10.2 km^3.

3.8 Conversion to mass

To compare terrestrial erosion and sediment storage with marine sediment storage in a source-to-sink context, an estimation of the density of eroded rock material and sediments in storage is required. This is particularly important because terrestrial bedrock materials can be up to three times more dense than the marine product of terrestrial erosion (Orpin et al., 2006). Furthermore, to draw a meaningful comparison between the terrestrial and marine volumes or masses, it is essential that the estimates be compatible, i.e. dry bulk density.

For the mud-dominated sediment stored offshore in the Poverty shelf and slope basins since the last glacial sea-level lowstand, Orpin et al. (2006) estimated a dry bulk density of 852 Mt km^{-3} (Mt km^{-3} = kg m^{-3}). This estimate is based on a model of exponential

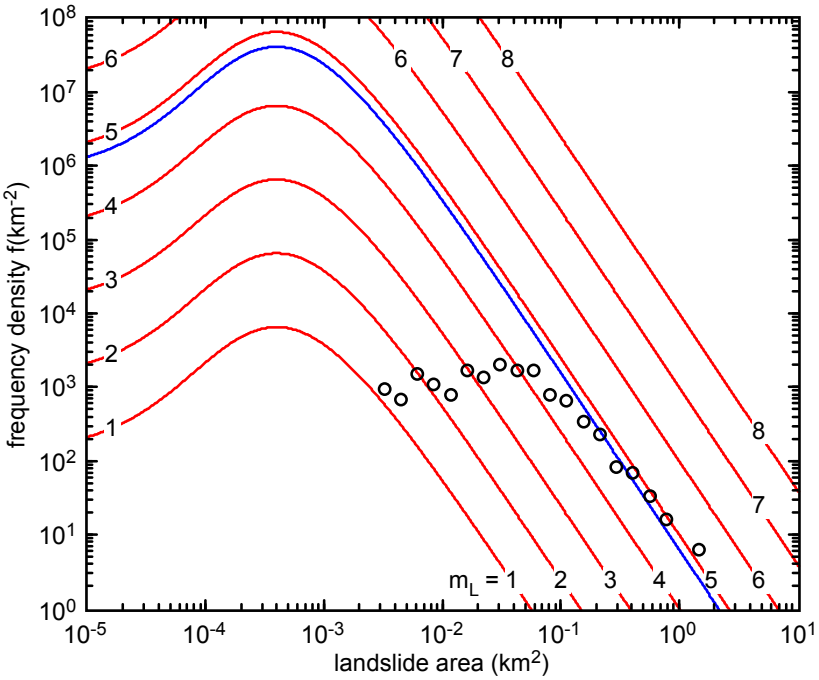

Figure 3.13. Log-binned DSLS frequency density vs. area for the two WSS study sites (black circles) plotted against the landslide magnitudes m_L = 1, 2,....,8 proposed by Malamud et al., (2004 a, b). The blue general frequency density curve equates to a m_L = 4.8.

decrease in porosity with depth (Sclater and Christie, 1980) guided by down-core physical properties from sediment cores collected off the northeast coast of New Zealand (Barnes et al., 1991; Carter et al., 1999; Carter et al., 2002). The model assumes an initial surface porosity of ca. 70%, which is based on measurements immediately below the water-sediment interface from around the region (Orpin et al., 2006). Porosity measurements from three piston cores of the top ca. 20 m of sediment from the WSS shelf depocentres indicate that porosity is only close to 70% in the top metre of sediment and varies down core from 60% to 50% (Gerber et al., 2010), which is somewhat lower than would be predicted by the exponential model employed by Orpin et al. (2006), even when taking in to account some slight compaction of the retrieved cores. Considering that the marine depocentres are bowl-shaped with more area in the upper horizons (Orpin et al., 2006; Gerber et al., 2010) and assuming a grain density of 2650 Mt km^{-3} with porosities ranging from 55%-65%, I calculate an average marine depocentre dry bulk density of 1060 ± 130 Mt km^{-3}.

Density estimates for terrestrial bedrock and sediments are problematic because of a lack of porosity or bulk density measurements in terrestrial depocentres, like Poverty

Floodplain, and the heterogeneity of geologic units over large areas. It is, however, necessary to estimate the density of rock material eroded if any sediment budget comparison between terrestrial source and marine sink is possible. Fortunately, there are sources of density data for rock and soil units available (Whiteford and Lumb, 1975; Preston and Crozier, 1999).

For bedrock units in the WSS, I made use of a catalogue of physical properties of rock (Whiteford and Lumb, 1975). This catalogue contains density measurements (dry, wet and grain) of different rock samples collected throughout New Zealand. To estimate dry density for bedrock units in the Waipaoa, I selected 332 rock samples found within the WSS catchment or around the Raukumara Peninsula no more than 60 km from the WSS. All of the samples are located by Sheet and Grid reference accurate to about 100 m. About 60% of these samples were identified by lithology. For the samples not identified by lithology, I assigned a lithology by matching reported collection locations with the currently available geologic map (Mazengarb and Speden, 2000). The dry density average and standard deviation for different lithologies was calculated from these samples. Data are sparse for some lithologies, but there is sufficient measurements on the mudstone and sandstone units that make up over 75% of the exposed bedrock lithologies in the WSS (Fig. 2.2) (mudstone n = 43 and sandstone n = 147). The mudstone dry density measurements exhibited the largest variation of all the major lithologies, and the standard deviation of dry density measurements from mudstone (190 Mt km^{-3}) is used as an uncertainty estimate for the all of the derivative dry density measurements.

The lithologic average dry density measurements were incorporated into a GIS of the available geologic mapping enabling an area-weighted average bedrock dry density estimate for any area in the WSS. The area-weighted average bedrock density for the WSS is 2580 ± 190 Mt km^{-3}. The area-weighted average bedrock density for the area that has experienced significant river incision since the LGCP (area under the modelled T1 aggradation surface) is also 2580 ± 190 Mt km^{-3}.

The density for material eroded by both shallow and deep-seated landslides was estimated by assuming DSLS were eroding mostly (90%) bedrock material and shallow landslides were eroding mostly (90%) soil materials. Soil densities for the tephric NIEC

soils from 15 Hawke's Bay sites range from 890 to 1600 Mt km^{-3} with an average of 1240 Mt km^{-3} and a standard deviation of 190 Mt km^{-3} (Preston and Crozier, 1999). Using the average bedrock density for the WSS and the average soil density, material removed by DSLS has a density estimate of 2450 ± 190 Mt km^{-3}, and material removed by shallow landslide processes has a density estimate of 1370 ± 190 Mt km^{-3}. Material removed by coastal erosion is also assumed to be mostly bedrock with a density estimate the same as for DSLS.

The T1 aggradation gravels that have been eroded by river incision are composed of mudstone and sandstone clasts that reflect the geology of the terrestrial WSS (Marsaglia et al., 2010). The thickness of gravel above bedrock strath ranges from up to 20 m in main stems to as little as 3 m in smaller tributaries. Regardless of the thickness, aggradation deposits composed of sand, gravel, and cobble sized clasts, D_{50} 34 ± 6 mm (Marsaglia et al., 2010), are generally less than 20% of the total river incision. The dry density of these deposits can be estimated by assuming an average clast density of 2580 ± 190 Mt km^{-3} (same as the average catchment bedrock density) and a porosity of ca. 20% for an average dry density of 2060 ± 190 Mt km^{-3}. While acknowledging the statistical limitations of the median grain size - porosity relationship (Frings et al., 2011), the porosity of ca. 20% is consistent with empirical predictors based on median grain size (Wu and Wang, 2006). Since the aggradation deposits are generally less than 20% of the total river incision and the remaining ca. 80% is bedrock, average dry density of materials eroded by river incision is ca 2480 ± 190 Mt km^{-3}.

In the absence of a direct measurement of the dry density of sediments sequestered under the Poverty Floodplain, and considering that these deposits are mostly silts (Brown, 1995; Wolinsky et al., 2010), I estimate a density based on two samples from Late Pleistocene silts from the Bay of Plenty with an average dry bulk density of ca. 1500 Mt km^{-3} ($\sigma \sim 160$ Mt km^{-3}) (Whitford and Lumb, 1975). This is consistent with a theoretical estimate made by Wolinsky et al. (2010). The dry bulk density of surficial overbank silts have been measured at 1300 Mt km^{-3} (Gomez et al., 1999) and are empirically predicted to be the same (Wu and Wang, 2006). Taking into account compaction of the, in places, over 100 m thick deposits comprising the Poverty Floodplain (Brown 1995; Wolinsky et al., 2010) I suggest that a dry density of ~1500 ± 160 Mt km^{-3} is a reasonable estimate.

A summary of dry density estimates for Waipaoa and Waimata source materials and the sediments sequestered under the Poverty Bay Floodplain is given in Table 3.1.

Terrestrial Waipaoa sediment source or sink	Dry Density Estimate (Mt km^{-3})	±
Entire watershed	2450	190
Waipaoa bedrock	2580	190
Deep-seated landslides	2450	190
Coastal erosion	2450	190
Shallow landslides	1370	190
Overland flow	1240	190
Bedrock eroded by post LGCP incision	2580	190
T1 terrace gravels	2060	190
Material eroded by post LGCP incision	2480	190
Poverty Floodplain	1500	160

Table 3.1. Dry density estimates for Waipaoa and Waimata source materials and the sediments sequestered under the Poverty Floodplain.

3.9 Sediment budget

Having estimated the DSLS volumetric sediment load and dry density, it is now possible to put these estimates in the context of the overall WSS sediment budget (Table 3.2, Fig. 3.14). In this analysis I specifically estimate sediment load delivered from DSLS separately from load from shallow landslides. This is because there is good evidence that volume-area scaling factors (α and γ) are different for shallow, soil-based landslides than for DSLS (Larsen et al., 2010), shallow landslide material has a different density than DSLS material, and because modern shallow landslide sediment yield for the Waipaoa catchment has been previously estimated (Reid and Page, 2002; Page and Lukovic, 2011). Estimates for volumes of terrestrial sediment sources other than DSLS and for terrestrial and marine sediment sinks come from a variety of published sources (Reid and Page, 2002; Page et al., 2004; Young and Ashford, 2006; Orpin et al., 2006; Marden et al., 2008; Gerber et al., 2010; Page and Lukovic, 2011) and are explained below. Uncertainty estimates presented in Table 3.2 generally reflect error derived from statistical methods and do not represent an estimate of the unquantifiable sources of uncertainty for any given estimation method.

	Process	Volume (km^3)	±	Dry Bulk Density Estimate	±	Mass (Mt)	±	Reference
Source	Deep-seated landslides	10.2	+9.2 -4.8	2450	190	25039	+22623 -11798	This study
	Coastal erosion	5.4	0.9	2450	190	13230	3231	Young and Ashford, 2006
	Shallow landslides	6.4	1.5	1370	190	8768	3271	Reid and Page, 2002; Page and Lukovic, 2011
	Overland flow	1.8	0.4	1240	190	2232	838	Page et al., 2004
	Channel incision	16.7	2.5	2480	190	41416	6976	Marden et al., 2012
					Total	90685	+36939 -26114	
Sink	Floodplain deposition	6.6	2.0	1500	160	9900	4026	Marden et al., 2008
	Marine shelf	33.0	2.0	1060	130	34980	6410	Gerber et al., 2010
					Total	44880	10436	

Table 3.2. The ca. 18,000 cal. yr BP process based sediment budget for the Waipaoa Sedimentary System. All volume units are km^3, all mass units are Mt and all density units are Mt km^{-3}.

3.9.1 Deep-seated landslides

My preferred estimate for the DSLS total volume is 10.2 km^3 (+9.2 km^3, -4.8 km^3) calculated from the derived volume-area relationships (equations 5 and 6) applied to the WSS air photo DSLS inventory (Page and Lukovic, 2011). This is because it is the most direct measurement of known landslides in the WSS. This estimate does overlap with the sediment load extrapolation from the two representative study areas (7.25 km^3), which provides a degree of confidence in both estimates that are largely based on different populations of DSLS.

Both estimates are likely to be underestimates because over the 18,000 year post-LGCP period of interest, evidence of some DSLS will have been lost, and any degradation of scarps would lead to lower volumetric estimates. There is, however, a small possibility that some landslides in the two study areas that form the main dataset initiated before the end of the LGCP, leading to an overestimate of the scarp-based volumetric reconstructions. I find this unlikely as a majority of the DSLS studied are linked to post LGCP river incision (Chapter 2), but the landform tephrochronology does leave this as a possibility. Another indication of the degree of underestimation is the frequency distribution-based estimate of N_{LT}. Using this method I estimate that 63,096 (+44,167, -31,981) shallow and DSLS would have been active in the two study areas since the LGCP and even considering large numbers of shallow landslides, this is considerably more than the 236 DSLS mapped. This N_{LT} estimate for a small portion of the WSS is also considerably more than the air photo-based inventory for the entire Waipaoa and Waimata catchments (1026 DSLS) (Page and Lukovic, 2011).

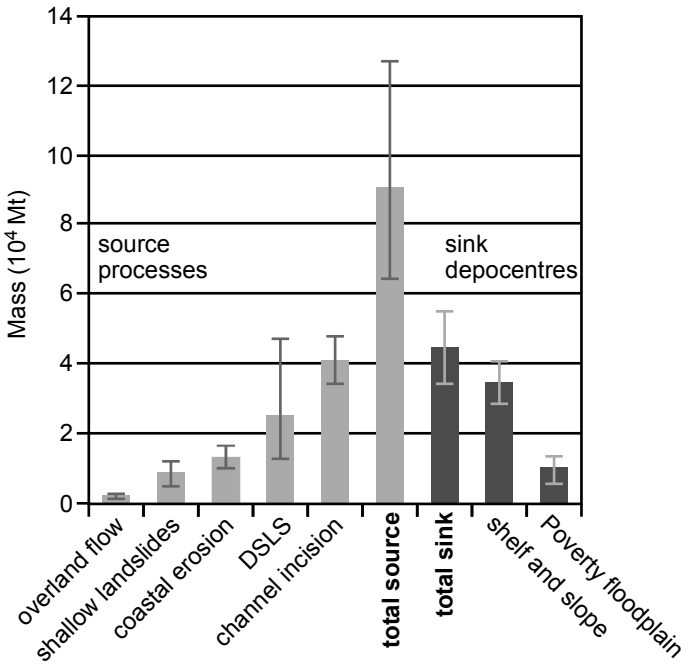

Figure 3.14. Bar graph with uncertainty estimates showing the ca. 18,000 cal. yr BP process based sediment budget for the Waipaoa Sedimentary System. Light grey bars are terrestrial sources and dark grey bars are terrestrial and marine depocentres.

I can use the landslide frequency distribution-derived volumetric estimate (Malamud et al., 2004 a, b) of 31.7 km^3 (+22.1 km^3, -13.1 km^3) as a check on the more direct measurements. This estimate is also in broad agreement considering that the fact that the landslide frequency distribution-derived estimate includes all landslides (shallow and DSLS) and does not differentiate between above and below T1 surface sediment delivery. I do not incorporate this frequency distribution volumetric estimate into the overall WSS sediment budget because of its strong dependence on estimates of volume-area power law scaling constants and exponents, α and γ, respectively. Changing these factors by small margins significantly changes the relationship between $\overline{V}_L$ and N_{LT} and can have a large impact on total landslide volume estimates (Larsen et al., 2010; Korup et al., 2012). For example, if the volume-area relationship developed by Guzzetti et al. (2009) from worldwide landslides is used instead of the Hovius et al., (1997) relationship (Fig. 3.11), the estimated $\overline{V}_L$ is consistently higher, which when integrated over thousands of landslides (N_{LT}) significantly alters volumetric estimates (Fig. 3.15). In addition, it appears that the power law scaling constants and exponents are distinct for populations of DSLS and shallow soil-based landslides (Larsen et al., 2010), suggesting that the different landslide processes should be treated separately when estimating volumes.

3.9.2 Shallow landslides

The volumetric contribution of shallow landslides to the WSS is based on work by Reid and Page (2002), Marden and Rowan (1994), Page and Trustrum, (1997), and Page and Lukovic (2011). The basic methodology is outlined in Page and Lukovic (2011) and uses the modern Waipaoa shallow landslide sediment yield (Reid and Page, 2002) as a base estimate. I then scale this estimate up to the contributing terrestrial WSS (in this case, also excluding the area of mapped DSLS) and apply a fern-scrub and full forest reduction in rates of shallow landsliding to rates generated from areas currently in pasture. The rate reduction used is 5 times (fern-scrub) for the period 18,000 to 13,000, and 15 times for the full forest conditions between 13,000 and today (Marden and Rowan, 1994, Page and Trustrum, 1997). I estimate that 6.4 ± 1.5 km^3 has been delivered to terrestrial and marine depocentres by shallow landslide processes. The uncertainty estimate on this volume is carried over from the original sediment yield estimate of $2.6 \times 10^6 \pm 0.6$ t yr^{-1} (Reid and Page, 2002).

3.9.3 River incision and other sources

The total volume from post-LGCP river incision from the Waipaoa and Waimata River catchments has been estimated to be 16.7 km^3 (Table 3.2) (Marden et al., 2008; Marden et al., In prep.). This estimate was based on reconstructing the LGCP T1 aggradation surface from extensive T1 terrace remnant mapping and a linear interpretation between remnants. While the linear interpretation between terraces of the T1 stream profiles was not sufficient for reconstructions in the detailed study areas, this method is considered appropriate for the large area of the Waipaoa and Waimata catchments. An estimated uncertainty of about 15% is based on a comparison between the volumetric results from the detailed study areas for my T1 reconstructions and the Waipaoa catchment-wide reconstruction (Marden et al., In prep.). The estimated 16.7 ± 2.5 km^3 of river incision derived sediment is also likely to be an underestimate because the other costal catchments of the WSS, notably the Pakarae (Fig. 3.1), are not included. The Waimata River catchment is ca. 230 km^2 which is about the same size as the Pakarae catchment (245 km^2) and Marden et al. (2008) estimated that river incision accounted for ca. 2.6 km^3 of sediment from this catchment. However, there have been no detailed studies of river incision in the Pakarae or other costal catchments, so I use the 16.7 ± 2.5 km^3 calculation and acknowledging the likely underestimate.

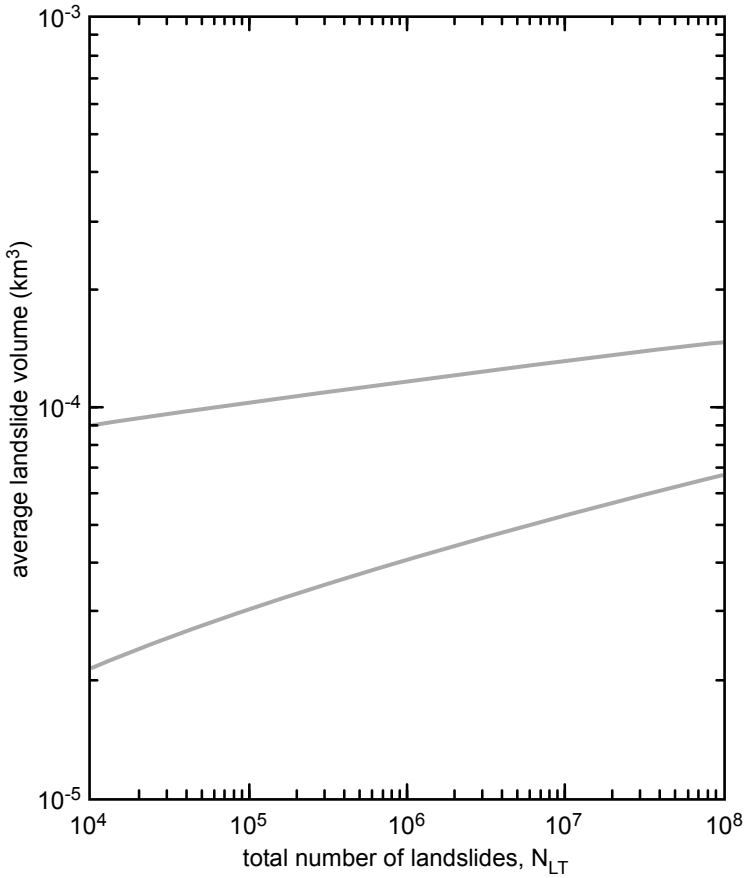

Figure 3.15. The dependence of the average landslide volume ($\overline{V}_L$) on the total number of landslides after Malamud et al. (2004a). The upper and lower curves show the difference in changing the scaling exponent in the volume-area relationship by only 0.05. The upper curve uses the volume-area scaling from Guzzetti et al. (2009), and the lower curve uses volume-area scaling from Hovius et al. (1997) which was employed by Malamud et al. (2004 a&b). Small differences in the volume-area scaling factors can lead to large differences in the estimated average landslide volume, which when integrated over thousands of landslides, can lead to very large differences in total volume estimates.

The volume of sediment mobilized by overland flow was estimated by scaling up the overland flow yield estimate for the modern Lake Tutira catchment (Page et al., 2004) (Fig. 2.3) to the WSS and applying a 50% reduction to account for native forest ground cover. This estimate is 1.8 ± 0.4 km^3 (Table 3.2). The uncertainty estimate for overland flow is based on the 20% reported uncertainty from Page et al. (2004). There are no real measurements of actual overland flow yield under the native forest cover and my estimation here is little more than a rough approximation.

To assess coastal erosion the 1.8 $m^3\ m^{-1}yr^{-1}$ lidar based southern California (Young and Ashford, 2006) modern volumetric coastal erosion estimate was scaled-up for the WSS. This estimate of coastal erosion was undertaken on a coastline of similar lithology to the

WSS and is a volumetric estimate rather than the more common linear estimate of coastal erosion. Reported uncertainty for this study was 16%, and this has been carried through my 5.4 ± 0.9 km^3 estimate (Table 3.2). Statistical uncertainty aside, there is a large degree of uncertainty in this estimate primarily because I have no way of estimating the average length or relief of the WSS shoreline over the last 18,000 cal. yr BP. I suspect that this estimate is also an underestimate because even though the southern California coastal rock types are similar to the WSS, the average relief on the modern WSS shoreline is more than two times greater, exposing larger volumes of material to coastal processes. Also, linear rates of Holocene coastal erosion estimated for portions of Hawke's Bay (Litchfield, 2008) appear to be up to an order of magnitude higher than what my volumetric estimate would predict.

3.9.4 Terrestrial and marine sinks

The Poverty Floodplain is the most significant terrestrial sediment sink (Brown 1995; Marden et al., 2008; Wolinsky et al., 2010). A volumetric estimate for the post-18,000 cal. yr BP sediment in storage under the floodplain is based on an extensive dataset of water bore logs (compiled in Brown 1995 and Wolinsky et al., 2010) and estimated at 6.6 km^3 (Table 3.2, Fig. 3.14) (Marden et al., 2008). I estimate a 30% uncertainty in the volumetric estimate based on uncertainty in interpolation between water bores and extrapolation to the deepest part of the basin (Wolinsky et al., 2010).

The largest sink for the WSS are the shelf and outer shelf depocentres (Fig. 3.1). There a post-LGCP transgressive sequence has been imaged by 3.5 kHz seismic profiles (Orpin et al., 2006) and over 1800 km of high-resolution chirp seismic lines using a 30 ms frequency sweep from 0.5 to 7.2 kHz (Gerber et al., 2010). Interpretations of the depth to the LGCP erosion surface vary depending on the datasets used and how extensively gas obscures reflectors in this seismic data. (Orpin et al., 2006; Gerber et al., 2010). I adopt the larger depocentre model presented by Gerber et al. (2010) for my sediment budget because it is based on the higher resolution chirp seismic data. Assuming that the average seismic velocity for the post-LGCP sediment is between 1500 and 1700 m s^{-1}, the volume stored in the shelf depocentres is 33.0 ± 2.0 km^3 (Table 3.2, Fig. 3.14) (Thomas Gerber, personal communication, 2012).

3.10 Discussion

Deep-seated landslides active since the LGCP (18,000 cal. yr BP) are a significant source of sediment in the WSS over the 18,000 year study period. Based on my estimates DSLS account for between 10 to 74% of the total mass of the WSS sediment budget of ca. 91,000 Mt (+37,000 Mt, -26,000 Mt) (Table 3.2, Fig. 3.14). This equates to a DSLS sediment yield of between 294 to 1,057 t km^{-2} yr^{-1} out of the total terrestrial yield of between 1,431 to 2,830 t km^{-2} yr^{-1}. I acknowledge that this is a broad first order estimate but, as I have attempted to show, both statistical uncertainty and potential errors of omission when identifying erosional geomorphic features over long time periods reduce my ability to precisely quantify their impact.

Even with the large reported statistical uncertainty I am reasonably confident that at least 25,000 Mt of sediment from DSLS activity has been delivered to terrestrial and marine depocentres since the LGCP. This is because the statistical uncertainty is asymmetric and positively skewed, and the most likely source of uncertainty in accounting for 18,000 years of DSLS activity is from omission, which would tend to lower my estimates. The argument that errors of omission reduce my sediment load estimate is strengthened by the representative landslide magnitude scale of 4.8 ± 0.2 (Fig. 3.13) and the derived 63,096 (+44,167, -31,981) total number of landslides (N_{LT}) from the two detailed study areas. Even though the estimated N_{LT} includes both shallow and DSLS, this estimate clearly suggests that I have not captured all the DSLS activity over 18,000 years in my inventory of 236 landslides.

The denudation rate calculated from the sediment budget (Table 3.2, Fig. 3.14) for the contributing area of the terrestrial WSS is 0.8 mm yr^{-1} (+0.3, -0.2 mm yr^{-1}). This is well within the range of calculated denudation rates for small temperate tectonically active catchments (e.g. Montgomery and Brandon, 2002; Von Blanckenburg, 2005; Covault et al., 2011, Norton et al., 2011; Mackey and Roering, 2011). The denudation rate is also close to the average terrestrial WSS late Quaternary uplift rate of for the middle reaches of the catchment (0.5 to 1.1 mm yr^{-1}) estimated by Berryman et al. (2000). In catchments experiencing transport-limited denudation, rates of uplift and denudation have no specific reason to balance. However, in Chapter 2 I argue that the post LGCP WSS is experiencing detachment-limited denudation with threshold hillslopes adjusting to

continued river incision through deep-seated bedrock landsliding. In this case, denudation across an actively uplifting terrain is controlled by rates of channel incision directly coupled to rates of uplift modulated by climate cycles and the expectation is that long term basin averaged denudation rates reflect long term uplift rates (e.g. Montgomery and Brandon, 2002; Binnie et al., 2007). I also find that there is balance between area normalized rates of incision and area normalized rates of bedrock DSLS. Channel incision in the last 18,000 years, over the area affected by incision, is eroding at 2.0 ± 0.3 mm yr^{-1} while bedrock deep-seated landsliding, over the area of known landslides, is eroding at 2.2 mm yr^{-1} (+1.9, -1.0 mm yr^{-1}). This suggests an approximate steady-state landscape characterized by threshold hillslopes that are strongly coupled to river incision and uplift.

The estimated terrestrial source sediment load ranges from 1.2 to 3.7 times larger than the sediment sequestered in terrestrial and shelf depocentres. In the broadest of terms, the WSS sediment budget does not show orders of magnitude imbalances. However, the largest source of uncertainty for the estimated source load comes from the DSLS estimate (Fig. 3.14), which I suggest is likely to be an underestimate rather than an overestimate. In addition, I find it more likely that there are other unquantified sources of sediment contributing to the terrestrial and shelf depocentres (such as river incision in the Pakarae catchment) than that these depocentres have been significantly underestimated. Because of this I suggest that over the last ca. 18,000 cal. yr BP a significant amount of sediment has bypassed the Poverty Floodplain and shelf depocentres.

In the modern deforested WSS only 3.6 ± 0.9 Mt yr^{-1} (ca. 25%) of the current total 15.0 ± 6.7 Mt yr^{-1} Waipaoa River sediment load is retained in the shelf depocentres (Hicks et al., 2000; Hicks et al., 2004; Miller and Kuehl, 2010). This low modern shelf depocentre trapping efficiency is contrasted with estimates of high Holocene trapping efficiency. Estimates of the amount of sediment deposited in the shelf depocentres between 5,500 to 200 cal. yr BP are very close to the running mean modelled paleo-Waipaoa River suspended sediment load of 2.3 ± 4.5 Mt yr^{-1} from 3,000 to 700 cal. yr BP (Kettner et al., 2007; Gerber et al., 2010). Because of the agreement between these estimates, it has been suggested that that the shelf depocentres had a high tapping efficiency during at least the

late Holocene (Gerber et al., 2010, Carter et al., 2010). Accepting these estimates and using my post-LGCP sediment budget (Table 3.2, Fig. 3.14), I estimate that the load delivered from the terrestrial WSS was 6.2 Mt yr^{-1} (+3.0, -2.1 Mt yr^{-1}) between ca. 18,000 and 5,500 cal. yr BP. This implies that if the current load to the shelf of 3.6 ± 0.9 Mt yr^{-1} represents some threshold over which sediment is dispersed off the shelf, as implied by Gerber et al. (2010), then potentially about half of the latest Pleistocene and early Holocene sediment load would have bypassed the shelf depocentres. It is further likely that a large percentage of this load was delivered to the marine environment during the period of most significant river incision and landslide activity between ca. 13,500 to 8,000 cal. yr BP (Gomez and Livingston, 2012, Marden et al., In prep.; Chapter 2). It is possible that during this time period very large amounts of sediment were being dispersed off-shelf, like in the modern WSS.

This argument brings into focus a central question about Source-to-Sink studies: can marine depocentres reliably record the magnitude of change the terrestrial system experiences due to climate, tectonic or paired forcing? In the WSS, it appears that sediment bypassing of the shelf depocentres is highest when the signal of landscape change is greatest (modern deforestation, latest Pleistocene and early Holocene river incision and landsliding). This suggests that the marine sediment record may understate large perturbations in terrestrial landscape evolution.

3.11 Summary and conclusions

To produce quantitative estimates of the role of DSLS in a moderate relief, moderate uplift, temperate maritime active margin sedimentary system, I have applied fluvial and geomorphic modelling to reconstruct pre ca. 18,000 cal. yr BP topography in 141 km^2 of detailed study area. Then I developed methods for estimating landslide volumes and used the resulting volume-area scaling relationships to estimate sediment flux related to DSLS for the broader system. Finally, I have included the estimates of the role of DSLS in the WSS in context of the sediment budget for the whole system.

By estimating the 18,000 year sediment flux sourced from terrestrial deep-seated landslides in the Waipaoa Sedimentary System, I have derived one of the first process-based long term sediment budgets for a class of temperate maritime active margin

catchments that exhibit a globally significant discharge of sediment to the world‘s oceans (Milliman and Syvitski, 1992; Milliman and Farnsworth, 2011). The sediment budget shows that DSLS are responsible for between 10 to 74% of the total mass of sediment delivered to terrestrial and marine depocentres. This equates to a DSLS sediment yield of between 294 to 1,057 t km^{-2} yr^{-1} out of the total terrestrial yield of between 1,431 to 2,830 t km^{-2} yr^{-1}. Within the limits of my budget, DSLS and post LGCP channel incision account for over 70% of the sediment exported from the system, showing quantitatively that these processes that are significant drivers of long term landscape evolution are also major sources of sediment generation.

The apparent post LGCP denudation rate for the contributing area of the WSS is 0.8 mm yr^{-1} (+0.3, -0.2 mm yr^{-1}). This is indistinguishable from the average terrestrial WSS late Quaternary uplift rate for the middle reaches of the catchment (0.5 to 1.1 mm yr^{-1}) estimated from Late Pleistocene aggradation terraces by Berryman et al. (2000) and suggests an approximate steady-state balance between denudation and uplift over glacial-interglacial cycles in this part of the Hikurangi subduction margin.

The estimated terrestrial source sediment load ranges from 1.2 to 3.7 times larger than the sediment sequestered in terrestrial and shelf depocentres. Despite the uncertainties involved, I suggest that over the last ca. 18,000 cal. yr BP a significant amount of sediment has bypassed the Poverty Floodplain and shelf depocentres. This bypassing may have been at a maximum between ca. 13,500 to 8,000 cal. yr BP when the largest terrestrial changes in landscape morphology were occurring (Gomez and Livingston, 2012, Marden et al., In prep.; Chapter 2), potentially obscuring this record of terrestrial change in the shelf depocentres.

Chapter 4: Stream profile analysis and uplift in the Waipaoa and Waimata catchments

4.1 Introduction and background

The terrestrial portion of the Waipaoa Sedimentary System (WSS) straddles the actively uplifting inner forearc and axial ranges of the Hikurangi subduction margin (Fig. 2.1). Over glacial-interglacial cycles tectonic uplift of the inner subduction margin is the driver for erosion rates in this system, i.e. long-term balance between uplift and erosion (e.g. Burbank et al., 1996, Montgomery, 2001; Pazzaglia and Brandon, 2001; Litchfield and Berryman, 2006; Binnie et al., 2007; Larsen and Montgomery, 2012). However, long-term (millennial) uplift rates are difficult to estimate and may be spatially variable across active areas of mountain building. In this chapter, I examine previous estimates for tectonic uplift across the terrestrial WSS and apply stream profile analysis in the Waipaoa and Waimata catchments of the WSS to identify patterns of differential uplift across the terrestrial part of the WSS.

Uplift of the Raukumara Range is primarily occurring on a regional scale, driven by deep-seated subduction processes including: oceanic plateau subduction, seamount subduction, tectonic erosion and sediment underplating (Walcott, 1987; Reyners et al., 1999; Upton et al., 2003; Litchfield et al., 2007; Clark et al., 2010). Quaternary uplift is non-uniform across the terrestrial WSS with parts of the lower Waipaoa catchment (southern Poverty Bay Floodplain) undergoing tectonic subsidence, while uplift of the headwaters approaches 4 mm yr^{-1} (Ota et al., 1991, 1992; Brown, 1995; Berryman et al., 2000; Litchfield and Berryman, 2006). North of the subsiding parts of Poverty Bay Floodplain, Holocene uplift of the coastal terrestrial WSS is driven by offshore reverse faults (Ota et al., 1991; Litchfield et al., 2010; Clark et al., 2010) and is constrained by uplifted marine terraces at the Pakarae River mouth at 3.2 ± 0.8 mm yr^{-1}(Wilson et al., 2006).

Uplift rates for the upper Waipaoa catchment have been estimated by comparing the elevations of two generations of fluvial aggradation terraces, T3 and T1, that are correlated to high $\delta^{18}O$ cool Marine Isotope Stages 4 and 2 and with periods of glacial advance in the South Island (Berryman et al., 2000; Litchfield and Berryman 2005;

Litchfield and Berryman 2006). The T3 and T1 surfaces are dated at ca. 55,000 and 18,000 cal. yr BP, respectively, using tephrochronology techniques (Litchfield and Berryman, 2005). Berryman et al. (2000) and Litchfield and Berryman (2006) assumed that the current difference in elevation between these two terrace surfaces is due to tectonic uplift and estimated late Pleistocene uplift rates for the upper middle Waipaoa catchment at between 1 and 2 mm yr^{-1}. Incorporating results from other Raukumara Peninsula catchments, there appears to be a strong gradient of increasing uplift from approximately ca. 1 mm yr^{-1} in the middle of the Waipaoa catchment to 4 mm yr^{-1} in the headwaters (Litchfield and Berryman, 2006). Geological uplift rates (over the last 5 million years) calculated from Neogene mudstones in the eastern upper Waipaoa catchment loosely agree with the geomorphic uplift estimates at 0.7 mm yr^{-1} (Litchfield and Berryman, 2006).

River incision rates in the upper Waipaoa catchment during the Latest Pleistocene (ca. 18,000 cal. yr BP) to the present are much higher than uplift rates calculated between aggradation terraces T3 and T1, and range from 2 to 7 mm yr^{-1} (Litchfield and Berryman, 2006). These incision rates overestimate bedrock incision because they are calculated between the elevation of the T1 aggradation terrace and the modern stream channel including the T1 aggradation deposits, instead of between the T1 strath and the modern stream channel. Litchfield and Berryman (2006) suggest that the difference between uplift rates and Latest Pleistocene to Holocene river incision rates may reflect either periods of relative tectonic quiescence in the Late Pleistocene or that uplift rates have increased.

4.2 Methods

To investigate uplift patterns in the Waipaoa and Waimata river catchments, I compiled field measurements of elevation differences between terrace pairs and completed stream profile analysis of the Waimata River and 19 major tributaries of the mainstem Waipaoa River. By comparing drainage basin area-normalized steepness indices of these major tributaries, spatial patterns of river steepness can be analyzed. I also estimated drainage basin area weighted average tributary Latest Pleistocene to Holocene river incision to compare with the results from the steepness analysis.

Two sets of newly mapped T3 and T1 aggradation terraces were analyzed in the Mangapapa tributary (Figs. 2.2, 4.3), and four sites of T1 bedrock strath to modern stream channel were analyzed across the detailed study areas (Fig. 2.2). The T3 aggradation terrace was identified by cover stratigraphy, aided by the identification of several tephra cover beds through electron probe microanalysis (EMPA). The basal tephra of the cover sequence for this terrace is interpreted to be the Rotoehu tephra (ca. 55,000 cal. yr BP) (Fig. 4.1) (Berryman et al., 2000; Newnham et al., 2004; Litchfield and Berryman, 2005). The T1 terraces are all dated by tephrochronology (see Chapter 2), and elevation measurements for T3 and T1 terraces, T1 bedrock strath, and modern stream channels are all determined by Differential Global Positioning System (DGPS).

Potential tectonic uplift rates (and uncertainties) between the T3 and T1 terraces were calculated following a modified version of the method used by Berryman et al. (2000). The major modification to this method is the use of probable bedrock strath age rather than the age of the cessation of aggradation to calculate uplift rates. Central to the concept of using pairs of fluvial terraces to calculate uplift is that rock incision keeps pace with uplift (e.g. Pazzaglia and Brandon, 2001). This assumption may be correct when rivers are eroding bedrock by either incision or valley widening but cannot be the case when rivers are aggrading and are decoupled from bedrock (e.g. Bull, 1991; Pazzaglia and Brandon, 2001; DeVecchio et al., 2012). Thus, the time period over which a strath terrace is uplifted is from the time the river stops cutting the strath to when the river returns to dynamic equilibrium with uplift. In this case, the valley widening episode (strath cutting) is considered the most likely time of equilibrium between climate, uplift, and incision. This relationship makes the time period between the estimated strath ages of the T3 and T1 terraces the most appropriate one over which to calculate potential tectonic uplift rates. Because of lack of exposure, the vertical measurement between T3 and T1 terraces is made between terrace surfaces. This relies on the assumption that the aggradation and cover thickness covering the T3 and T1 strath surfaces are similar and largely cancel each other out. Elevation uncertainty of over 8 m incorporated into the uncertainty estimate (Berryman et al., 2000) reflects this assumption.

Estimated bedrock strath ages for T3 and T1 come from tephrochronology and previously published optically stimulated luminescence (OSL) ages. T1 aggradation started between the deposition of the Omataroa and the Kawakawa tephras (Berryman et

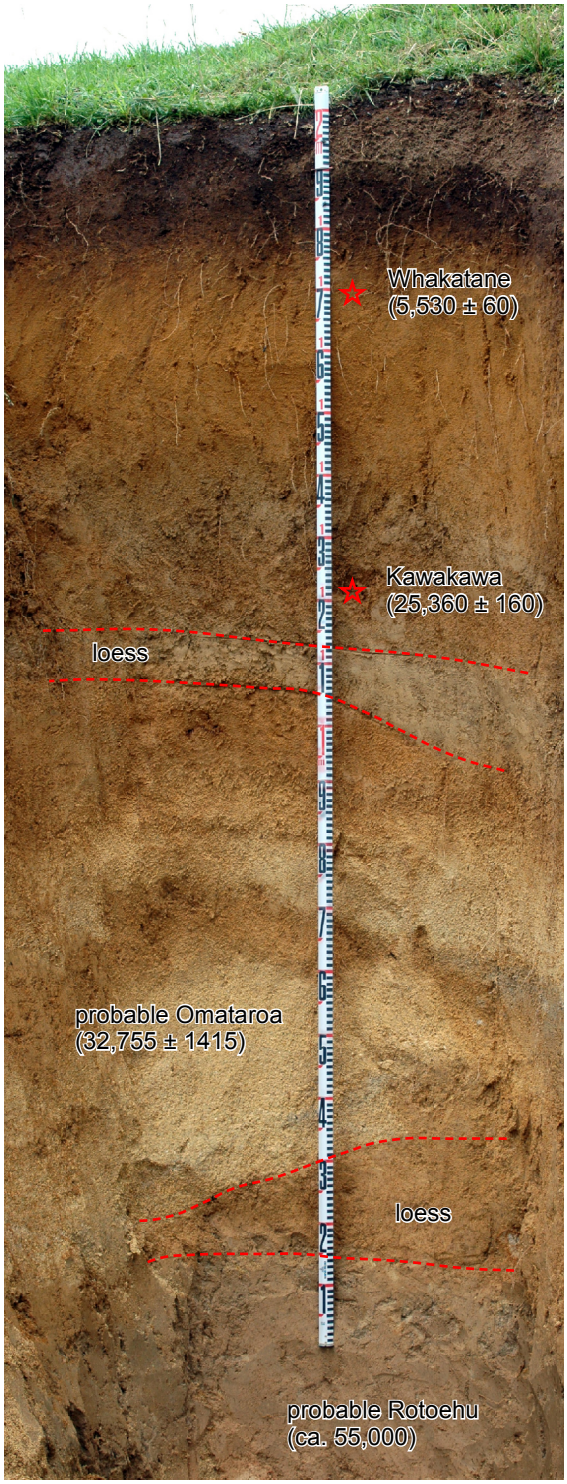

Figure 4.1. Cover stratigraphy on one of the T3 terrace remnants along the Mangapapa stream. The rod length is 2 m. Stars indicate locations and results of EMPA glass chemistry tephra identification. Mid-point and 2σ uncertainty tephra ages are calibrated from C^{14} dates on proximal deposits (Newnham et al., 2004; Smith et al., 2005; Lowe et al., 2008; Vandergoes et al., 2013). The stratigraphy at this location closely agrees with the cover stratigraphy of other East Coast, North Island T3 aggradation terraces (Litchfield and Berryman, 2005).

al. 2000; Litchfield and Berryman 2005; Marden et al., 2008), dated at 32,755 ± 1415 cal. yr BP and 25,360 ± 160 cal. yr BP, respectively (Smith et al., 2005; Lowe et al., 2008; Vandergoes et al., 2013). Because the Kawakawa tephra is found in the basal units of the T1 aggradation gravels and the widespread Omataroa tephra has never been observed in the gravels, the age of the Omataroa is taken as the maximum age for the beginning of aggradation and is a reasonable age for the T1 strath. A minimum age for the T3 strath

can be inferred from the oldest OSL date in T3 aggradation gravels to be 75,300 ± 5,500 cal. yr BP (Litchfield and Rieser, 2005). Bedrock river incision rates were calculated using the age of the Omataroa tephra (32,755 ± 1415 cal. yr BP) as the age of the T1 strath and the DGPS determined elevations. Figure 4.2 shows examples of the T1 gravels resting on the T1 bedrock strath for two of the incision-rate estimation sites.

Stream profile analysis of the effect of uplift on the Waimata River and 19 major tributaries of the mainstem Waipaoa River uses the long-recognized power law scaling relationship between drainage area and slope (e.g. Leopold and Miller, 1956) and takes advantage of the drainage area-normalized channel steepness index, k_s (equation 1, Chapter 3) (Wobus et al., 2006 and references therein). For streams that are in equilibrium with climate and uplift, the steepness index (k_s) is roughly proportional to the ratio of uplift to erodibility (e.g. Snyder et al., 2000; Kirby and Whipple, 2001; Wobus et al., 2006). For this reason the steepness index, normalized for concavity, is a good proxy for uplift.

Slope-area and longitudinal profile data were extracted from a 15 m digital elevation model (Columbus et al., 2011), using methods outlined by Wobus et al. (2006). Critical thresholds for fluvial process-dominated slope-area scaling were determined graphically (Wobus et al., 2006). Four streams that exhibited extreme convexities (knickpoints) in their profiles below the critical thresholds were removed from further analysis (coloured yellow in Fig. 4.3). Channel steepness index (k_s) and concavity (θ) were determined by linear regression for each stream, and a common concavity for all the analyzed streams was determined using the statistical program SMATR, that is based on methods outlined in Warton et al. (2006). Normalized channel steepness (k_{sn}) was then estimated by regression using the common calculated concavity (Wobus et al., 2006).

Estimates of drainage basin area-weighted average tributary Latest Pleistocene to Holocene river incision used mapped T1 aggradation terraces and 15 m digital topography to estimate river incision in the major tributaries (Columbus et al., 2011; Marden et al., In prep.). Incision at any given mapped T1 terrace remnant was calculated as the difference between the elevation of the T1 aggradation terrace surface and the elevation of the modern river. Since the modelled T1 aggradation surface declines in

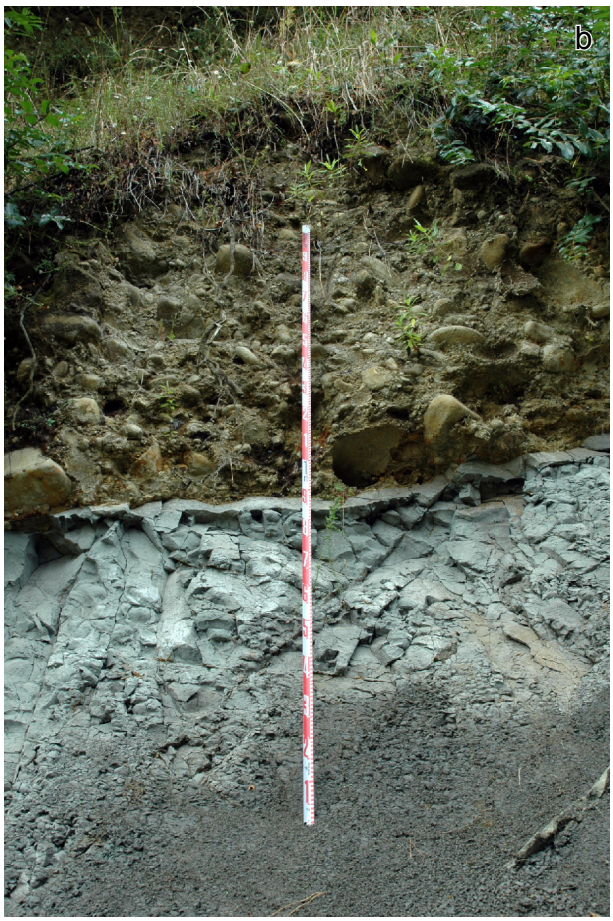

Figure 4.2. T1 bedrock strath in the Waingaromia catchment stranded between 89 m and 96 m above modern streams. a) T1 strath, aggradation gravels, and cover sequence above the Waitangi Stream. The aggradation gravels and cover sequence are ca. 8 m thick at this location. b) T1 strath and some aggradation gravels above the Waingaromia River. The rod length is 2 m. The aggradation gravels and cover sequence are ca. 22 m thick at this location.

elevation relative to the modern channel at low drainage areas (see Chapter 3, Marden et al., 2008; Marden et al., In prep.), a contributing drainage basin area-weighted average river incision was calculated from the T1 aggradation terrace remnants in each tributary. The contributing drainage basin area is a proxy for discharge and assumes that higher discharge streams have more power to incise. This weighted incision estimate is useful for comparing to the k_{sn} data, but considering that river incision may be discharge threshold-limited rather than simply correlated (Crosby and Whipple, 2006) and that many other factors may influence river incision, such as bedrock lithology, the weighted incision estimate should not be considered a predictive measure of actual incision at any tributary. Uncertainties in this weighted average are reported at the one sigma range.

4.3 Results

Uplift rate estimates from two Mangapapa stream T3-T1 terrace pairs are 0.5 ± 0.3 mm yr^{-1} and 0.6 ± 0.3 mm yr^{-1}, respectively (Fig. 4.3). These rates are similar to rates from T3-T1 terrace pairs identified by Berryman et al. (2000), which have been recalculated using the strath ages to 0.7 ± 0.3mm yr^{-1} and 0.9 ± 0.3 mm yr^{-1} (Fig. 4.3). T1 strath to modern stream channel weighted bedrock incision rates range from 0.4 ± 0.3 mm yr^{-1} in the headwaters of the Mangamaia stream (contributing drainage basin area ca. 8.2 km^2) to 2.9 ± 0.9 mm yr^{-1} in the Waingaromia River (contributing drainage basin area ca. 135.1 km^2) (Figs. 4.2b, 4.3).

Longitudinal and slope-area profiles for 16 of the 20 analyzed tributaries exhibited profiles without major convexities suggesting at least dynamic equilibrium with current climate and tectonic uplift (e.g. Bull, 1991). The common concavity index (θ) determined for these 16 tributaries is 0.75 (Fig. 4.4), which is relatively high compared to the typical range of 0.35-0.65 (Wobus et al., 2006) but not outside the range estimated for other channels (Sklar and Dietrich, 1998). Spatial patterns of normalized channel steepness (k_{sn}) were analyzed by separating relatively high k_{sn} tributaries from relatively low k_{sn} tributaries and plotting the results on a map of the Waipaoa and Waimata catchments (Fig. 4.3). The only clear pattern is that channels with their headwaters in the Raukumara Range have higher steepness indices than channels with their headwaters in the coastal or middle catchment foothills (Fig. 4.3). The significance of the shift in k_{sn} between the two groups, high and low, was tested using a Wald statistical test (Warton et

Figure 4.3. See next page for caption.

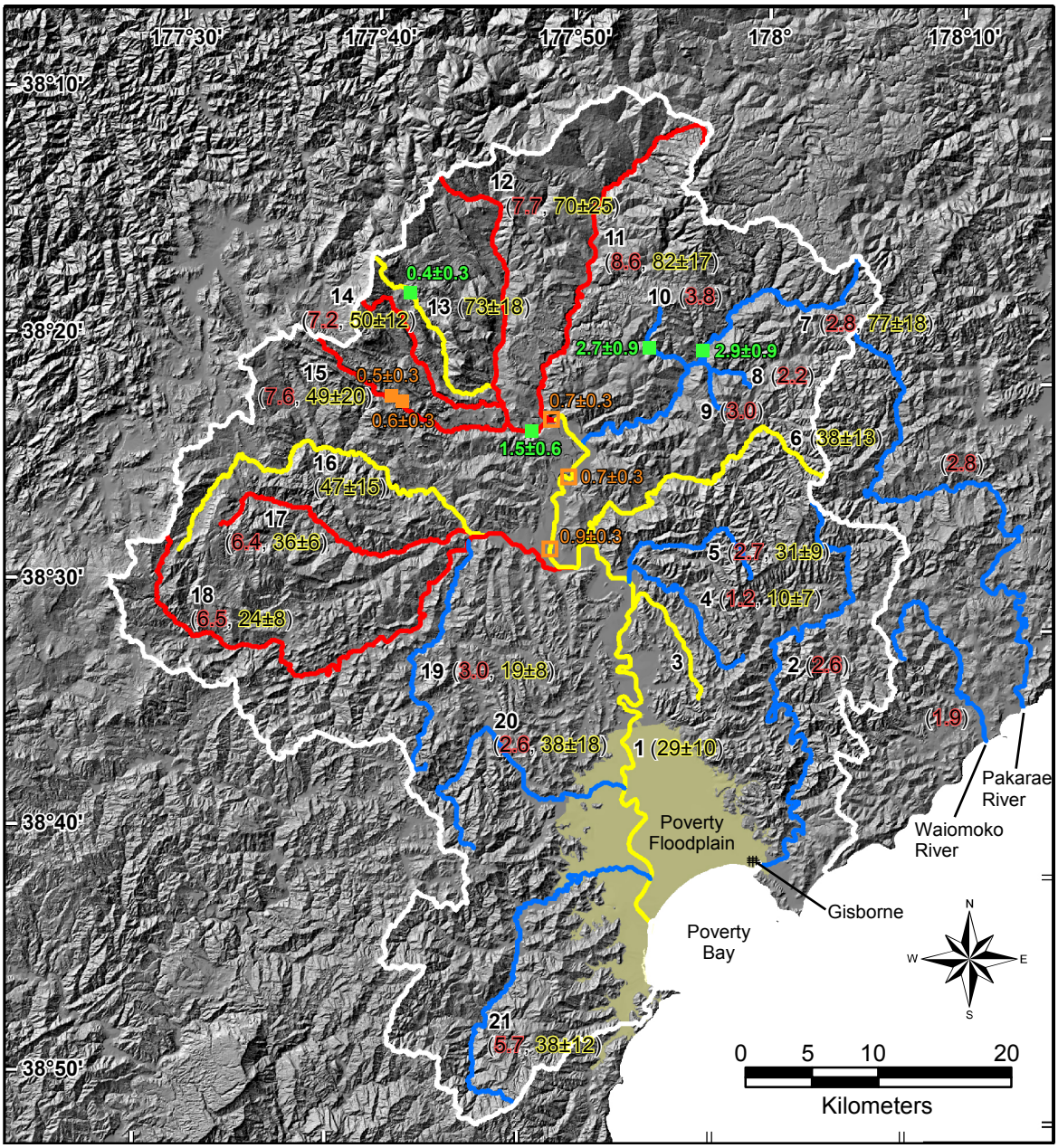

Major rivers and streams

1) Waipaoa
2) Waimata
3) Ngakoroa
4) Urutaranga
5) Mangaoai
6) Waihora
7) Waingaromia
8) Kawakawa E.
9) Kawakawa
10) Waitangi
11) Upper Waipaoa
12) Mangatu
13) Mangamaia
14) Mangapapa
15) Urukokomuka
16) Waikahu
17) Waihuka
18) Wharekopae
19) Totangi
20) Waikakariki
21) Te Arai

low k_{sn} tributaries

high k_{sn} tributaries

tributaries not analyzed

1.5±0.6 **T1 strath to modern river incision rates (mm yr^{-1})**

0.6±0.3 **potential tectonic uplift rates between T3 and T1 terraces(mm yr^{-1})**

0.7±0.3 **recalculated T3 to T1 uplift rates from Berryman et al. (2000) (mm yr^{-1})**

19 (3.0, 19±8)

river number — **k_{sn}×10^3** — **weighted average tributary incision (m)**

Figure 4.3. Results of stream profile analysis in the Waipaoa and Waimata catchments (white catchment boundary). Tributaries in blue exhibit low normalized steepness indices (k_{sn}) (low uplift) and tributaries in red exhibit high k_{sn} (high uplift). With the exception of the main-stem Waipaoa River, yellow tributaries have significant knickpoints located in their middle reaches and do not have long stretches of similar concavity. The main-stem Waipaoa River was not included in the analysis because it is transport-limited rather than largely detachment-limited like many of the other tributaries. Normalized steepness indices are also provided for the coastal Waimoko and Pakarae rivers. These two rivers are outside the main area of analysis and have not been the subject of previous terrace mapping efforts.

al., 2006) and found to be highly significant. The ratio of k_{sn}(high)/ k_{sn}(low) in the WSS is 2.6 which is considerably higher than the ratio of 1.8 measured in the King Range of northern California across a change of independently estimated tectonic uplift that ranges from ca. 0.5 mm yr^{-1} to 4 mm yr^{-1} (Snyder et al., 2000; Wobus et al., 2006).

The high k_{sn} tributaries contain the highest drainage basin area-weighted average post-T1 incision, with the exception of the Waigaromia catchment which has experienced very high incision (Fig. 4.3). The weighted-average river incision ranges from 10 ± 7 m to 82 ± 17 m. High uncertainties reflect that many local factors such as lithology and/or discharge thresholds may affect river incision at different points in a channel even in those tributaries that exhibit relatively smooth concave longitudinal profiles.

4.5 Discussion and conclusions

Stream profile analysis suggests that tectonic uplift in the tributaries that are draining the Raukumara Peninsula is significantly higher than in the foothill tributaries, if changes in erodibility across the Waipaoa and Waimata catchments are assumed to be small (e.g. Kirby and Whipple, 2001; Wobus, et al., 2006). This analysis does not illuminate the nature of the transition between zones of low and high uplift, but work by Litchfield and Berryman (2006), Litchfield et al. (2007), and Clark et al. (2010) indicates that it is likely to be somewhat distributed rather than discrete. Stream profile analysis further does not quantify the various rates of uplift as independent non-geomorphic estimates of uplift are not available for most of the two catchments.

High k_{sn} tributaries roughly spatially correlate with high incision tributaries, but there is a large degree of variability of incision at any given location. The varying rates of incision at any specific terrace pair or T1 to modern location may be due to local factors including rock resistance, sediment load and discharge. In addition, the Waingaromia

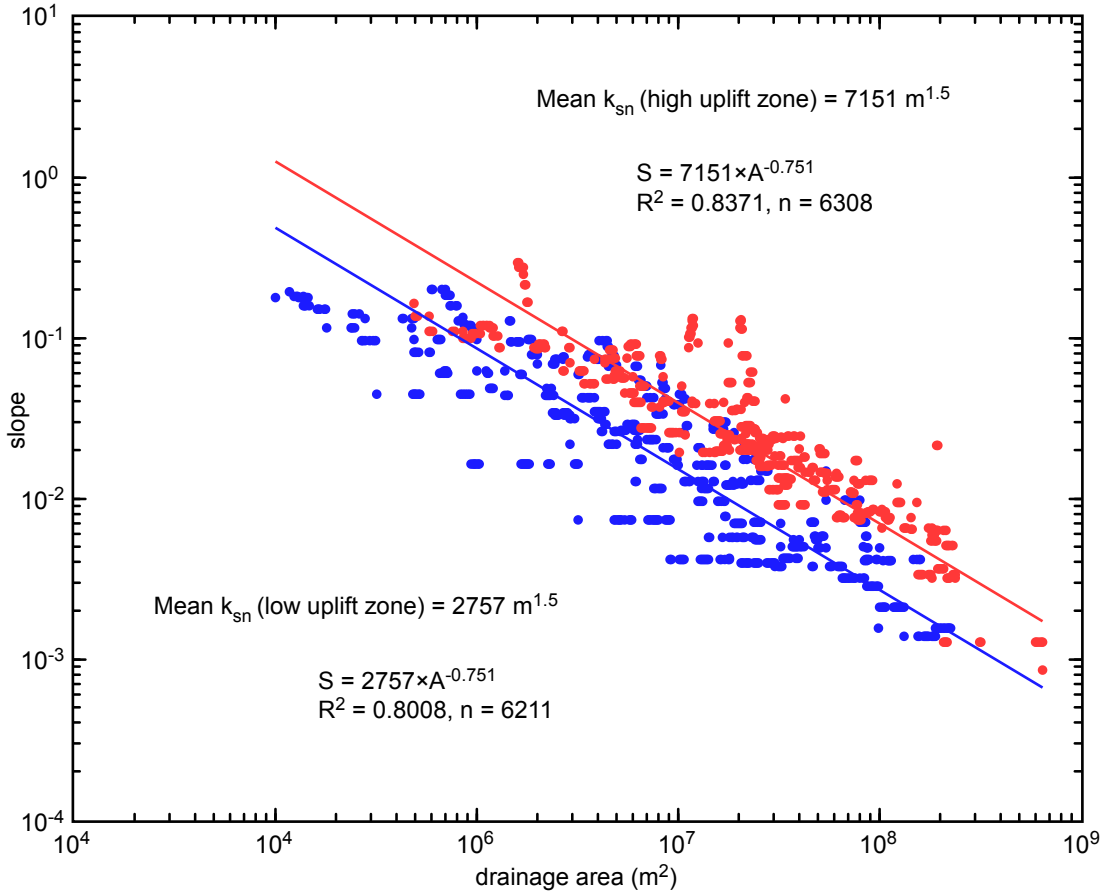

Figure 4.4. Slope-area plot for all the analysed tributaries, limited to areas below the individual tributary critical threshold for fluvial process-dominated slope-area scaling. Red points are from tributaries draining the Raukumara Peninsula and blue points are from the other foothill tributaries (see Fig. 4.3). Both data sets have a highly probable common slope (concavity, θ) and come from populations with statistically different channel steepness (k_{sn}). k_{sn} for channels with common concavity of 0.751 have units of $m^{1.5}$.

catchment exhibits high incision at relatively low normalized steepness (Fig. 4.3). This may be a result of lower rock-mass strength and thus higher erodibility in the Waingaromia catchment at similar drainage areas to the upper Waipaoa and Mangtu rivers. Higher erodibility would lead to lower k_{sn} but higher incision rates. However, other than being the largest analyzed tributary catchment underlain dominantly by Miocene to Pliocene mudstones, there does not appear to be anything unique about the geology of Waingaromia River (Fig. 2.2) (Mazengarb and Speden, 2000).

The incision variability highlights one of the problems of using fluvial systems to quantify tectonic uplift without other independent measurements. Central to the concept of using pairs of fluvial terraces to calculate uplift is that rock incision keeps pace with uplift (e.g. Pazzaglia and Brandon, 2001); however, other factors influence this dynamic

equilibrium including but not limited to: discharge, sediment supply (climate) and erodibility (lithology) (e.g. Bull, 1991; Snyder et al., 2000, 2003, Wobus et al., 2006). Most of the streams analyzed show relatively smooth concave longitudinal profiles suggesting that they are not experiencing significant transient disequilibrium. However, a dynamic equilibrium where stream incision keeps pace with uplift does not necessarily mean that the rate of stream incision equals the rate of uplift, only that streams have a strong tendency to incise toward the base level of erosion (Bull, 1991). Whether streams attain their ultimate base level of erosion depends on the erodibility of their channels and the time over which climatic conditions favour channel incision. This may help explain why there is an apparent several-fold difference between the uplift rates calculated from T3-T1 terrace pairs and T1 to modern river incision rates. As shown by proxy through global sea level curves, the climate during the current interglacial is different than the climate during the warm stadials when the T3 and T1 straths were being cut (e.g. Shackleton, 1987; Rohling et al., 1998; Siddall, et al., 2007; Rohling et al., 2009). Eustatic sea level today is higher than it has been any time in the last ca. 125,000 cal. yr BP indicating different climatic condition than at ca. 75,000 and 33,000 cal. yr BP (approximate T3 and T1 strath ages, respectively). Tectonic uplift rates might have remained largely uniform since ca. 75,000 cal. yr BP, but the efficiency of river incision may be higher under current climatic conditions.

Stream profile analysis of the Waipaoa and Waimata catchments of the terrestrial WSS is consistent with higher tectonic uplift in the upper Waipaoa than much of the rest of the system. Profile analysis combined with analysis of river incision between the cutting of T3-T1 strath, and modern channels indicates that although rates of river incision track rates of tectonic uplift, other factors such as erodibility and climate may obscure a direct equivalence relationship. Without other independent estimates, quantification of tectonic uplift rates across the terrestrial WSS remains problematic. However, based on the available geomorphic evidence, uplift rates are likely to be between 1 and 4 mm yr^{-1} (Berryman et al., 2000, Litchfield and Berryman 2006) with highest rates confined to an area of about a third of the entire WSS in the northwestern Waipaoa catchment.

Chapter 5: Conclusions

Two hundred and thirty-six deep-seated landslides that have been active at various times since the end of the Last Glacial Coldest Period (LGCP) (ca. 18,000 cal. yr BP) have been identified in 141 km^2 of representative upper Waipaoa catchment study area. Depending on the underlying geology, landslides make up between 13% and 35% of the surface area of these areas. Landslide aspect is not closely linked with bedding structure; dip-slope landslides are approximately randomly correlated to underlying geologic structure with only ca. 25% of landslides with proximal bedrock attitude measurements considered dip-slope landslides. Further, deep-seated bedrock landslides are spatially and temporally correlated with post LGCP river incision. I conclude that slopes underlain by low strength and highly sheared bedrock were debuttressed by river incision and as hillslopes reached threshold gradients, they responded by gravitational collapse. These deep-seated bedrock landslides may have been triggered by intense or long duration precipitation events or by large earthquakes, but the underlying causes for the widespread landsliding are river incision and low bedrock mass strength.

Landform tephrochronology indicates that widespread slope instability did not initiate until after the deposition of the ca. 13,600 cal. yr BP Waiohau tephra. Tephrochronology and geomorphic mapping results further indicate that rapid incision and debuttressing appears to have occurred almost synchronously throughout in the upper WSS (i.e., from the headwaters to the mainstem). Within the limits of the tephrochronology, there is good agreement between the timing of hillslope debuttressing and other independent terrace-based degradation estimates of the timing of most rapid river incision after the LGCP (Berryman et al., 2010; Marden et al., in prep).

My conceptual model shows how hillslopes in the WSS responded to climate and vegetation change during the last glacial-interglacial transition. Widespread deep-seated landsliding caused by slope oversteepening and debuttressing resulted from climate-modulated, uplift-driven river incision. These post-LGCP deep-seated landslides shaped the modern morphology of the WSS to the extent that even interfluves were, in places, shifted and lowered. Through this work I have shown how climate and tectonic uplift

have shaped hillslope morphology.

To produce quantitative estimates of the role of deep-seated landslide in the Waipaoa Sedimentary System fluvial and geomorphic modelling was used to reconstruct pre ca. 18,000 cal. yr BP topography, and I developed methods for estimating landslide volumes. By estimating the 18,000 year sediment flux sourced from terrestrial deep-seated landslides, I have completed one of the first process-based long term sediment budgets for a class of temperate maritime active margin catchments that exhibit a globally significant discharge of sediment to the world's oceans (Milliman and Syvitski, 1992; Milliman and Farnsworth, 2011). My sediment budget shows that deep-seated landslides are responsible for between 10 to 74% of the total mass of sediment delivered to terrestrial and marine depocentres. This equates to a deep-seated landslide sediment yield of between 294 to 1,057 t km^{-2} yr^{-1} out of the total terrestrial yield of between 1,431 to 2,830 t km^{-2} yr^{-1}. Within the limits of the budget, deep-seated landslides and post-LGCP channel incision account for over 70% of the sediment eroded from the system, showing quantitatively that these processes that are significant drivers of long term landscape evolution are also major sources of sediment generation.

The estimated terrestrial source sediment load ranges from 1.2 to 3.7 times larger than the sediment sequestered in terrestrial and shelf depocentres. Despite the uncertainties involved, I suggest that over the last ca. 18,000 cal. yr BP a significant amount of sediment has bypassed the Poverty Floodplain and shelf depocentres. This bypassing may have been at a maximum between ca. 13,500 to 8,000 cal. yr BP when the largest terrestrial changes in landscape morphology were occurring (Gomez and Livingston, 2012, Marden et al., In prep.) potentially obscuring this record of terrestrial change in the shelf depocentres.

The post-LGCP denudation rate for the contributing area of the terrestrial WSS derived from the sediment budget is 0.8 mm yr^{-1} (+0.3, -0.2 mm yr^{-1}). This is indistinguishable from the average late Quaternary uplift rate for the middle reaches of the terrestrial system (0.5 to 1.1 mm yr^{-1}) estimated from Late Pleistocene aggradation terraces by Berryman et al. (2000). This match in rates suggests an approximate steady-state balance between denudation and uplift over glacial-interglacial cycles is occurring in this part of

the Hikurangi subduction margin.

Stream profile analysis of the Waipaoa and Waimata catchments of the terrestrial WSS is consistent with higher tectonic uplift in the upper Waipaoa than much of the rest of the system. Profile analysis combined with analysis of river incision indicates that although rates of river incision track rates of tectonic uplift, other factors such as erodibility and climate may obscure a direct equivalence relationship. Without other independent estimates, quantification of tectonic uplift rates across the terrestrial WSS remains problematic. However, analysis indicates that the highest rates of uplift are confined to an area of about a third of the entire WSS in the northwestern Waipaoa catchment.

In this study I have used high resolution topographic data sets combined with field mapping and landform tephrochronology to show that bedrock landsliding is coupled to river incision and by proxy, to changing climate in uplifting terrains. I have also used geomorphic data to explore differential uplift across an active margin sedimentary system. And finally, estimated that deep-seated landsliding can account for a significant portion of the long-term sediment budget in a typical temperate maritime active margin catchment.

Bibliography

Alloway B.V., Lowe D.J., Barrell D.J.A., Newnham, R.M., Almond P.C., Augustinus P.C., Bertler N.A.N., Carter, L.C., Litchfield N., McGlone M.S., Shulmeister J., Vandergoes M.J., Williams P.W. and NZ-INTIMATE Members, 2007. Towards a climate event stratigraphy for New Zealand over the past 30,000 years. Journal of Quaternary Science 22: 9-35.

Augustinus, P., D'Costa, D., Deng. Y., Hagg, J. and Shane, P., 2011. A multi-proxy record of changing environments from ca. 30000 to 9000 cal. yr BP: Onepoto maar paleolake, Auckland, New Zealand. Journal of Quaternary Science 26, (4) 389-401.

Bakker, L., Lowe, D. J. and Jongmans, A. G., 1996. A micromorphological study of pedogenic processes in an evolutionary soil sequence formed on late quaternary rhyolitic tephra deposits, North Island, New Zealand. Quaternary International, 34-36, 249-261.

Barnes, P. M., Cheung, K. C., Smits, A. P., Almagor, G., Read, S. A. L., Barker, P. R. and Froggatt, P., 1991. Geotechnical analysis of the Kidnappers slide, upper continental slope, New Zealand. Marine Geochronology 10, 159-188.

Berryman, K. R., Ota, Y. and Hull, A. G., 1992. Holocene evolution of an estuary on a tectonically rising coast; the Pakarae River locality, Eastern North Island, New Zealand. Sedimentary Geology 80(3-4), 151-165.

Berryman, K., 1993a. Age, height, and deformation of Holocene marine terraces at Mahia Peninsula, Hikurangi subduction margin, New Zealand. Tectonics 12 (6), 1347-1364.

Berryman, K., 1993b. Distribution, age, and deformation of Late Pleistocene marine terraces at Mahia Peninsula, Hikurangi subduction margin, New Zealand. Tectonics 12 (6), 1365-1379.

Berryman, K., Marden, M., Eden, D., Mazengarb, C., Ota, Y. and Moriya, I., 2000. Tectonic and paleoclimatic significance of Quaternary river terraces of the Waipaoa River, east coast, North Island, New Zealand. New Zealand Journal of Geology and Geophysics 43, 229-245.

Berryman, K., Marden, M., Palmer, A.and Litchfield, N., 2009. Holocene rupture of the Repongaere fault, Gisborne: Implications for Raukumara Peninsula deformation and impact on the Waipaoa sedimentary system. New Zealand Journal of Geology and Geophysics 52(4), 335-347.

Berryman, K., Marden, M., Palmer, A., Wilson, K., Mazengarb, C. and Litchfield, N., 2010. The post-glacial downcutting history in the Waihuka tributary of Waipaoa River, Gisborne district: implications for tectonics and landscape evolution in the Hikurangi subduction margin, New Zealand. Marine Geology 270(1-4), 55-7.

Bibliography

Binnie, S. A., Phillips, W. M., Summerfield, M. A. and Fifield, L. K., 2007. Tectonic uplift, threshold hillslopes, and denudation rates in a developing mountain range. Geology 35(8), 743-746.

Brown, L.J., 1995. Holocene shoreline depositional processes at Poverty Bay, a tectonically active area, northeastern North Island, New Zealand. Quaternary International 26, 21-33.

Bull, W. B., 1991. Geomorphic responses to climatic change. New York, NY, United States of America: Oxford Univ. Press, New York, NY, 326 p.

Burbank, D. W., Leland, J., Fielding, E., Anderson, R. S., Brozovic, N., Reid, M. R. and Duncan, C., 1996. Bedrock incision, rock uplift and threshold hillslopes in the northwestern Himalayas. Nature (London) 379(6565), 505-510.

Carter, R. M., McCave, I. N., Richter, C. and Carter, L., Shipboard Party, 1999. Leg 181 summary: southwest Pacific paleoceanography. In: Proceedings of the Ocean Drilling Program, Initial Reports, vol. 181 including original data from ODP Janus web database <www-odp.tamu.edu/publications/181_IR/181ir.htmS>.

Carter, L., Manighetti, B., Elliot, M., Trustrum, N. and Gomez, B., 2002. Source, sea level and circulation effects on the sediment flux to the deep ocean over the past 15 ka off eastern New Zealand. Global and Planetary Change 33, 339-355.

Carter, L., Orpin, A.R. and Kuehl, S.A., 2010. From mountain source to ocean sink - the passage of sediment across an active margin, Waipaoa Sedimentary System, New Zealand. Marine Geology 270(1-4), 1-10.

Clark, K., Berryman, K., Litchfield, N., Cochran , U. and Little, T. 2010. Evaluating the coastal deformation mechanisms of the Raukumara Peninsula, northern Hikurangi subduction margin, New Zealand and insights into forearc uplift processes. New Zealand Journal of Geology and Geophysics 53(4), 341-358.

Clauset, A., Shalizi, C. R. and Newman, M. E. J., 2009. Power-law distributions in empirical data. Society for Industrial and Applied Mathematics Review 51(4), 661.

Columbus, J., Sirguey, P. and Tenzer, R., 2011. A free fully assessed 15 metre digital elevation model for New Zealand. Survey Quarterly 66, 16-19.

Covault, J. A., Romans, B. W., Graham, S. A., Fildani, A. and Hilley, G. E., 2011. Terrestrial source to deep-sea sink sediment budgets at high and low sea levels: Insights from tectonically active southern California. Geology 39(7), 619-622.

Crosby, B. and Whipple, K ., 2006. Knickpoint initiation and distribution within fluvial networks: 236 waterfalls in the Waipaoa River, North Island, New Zealand. Geomorphology 82, 16-38.

DeVecchio, D. E., Heermance, R. V., Fuchs, M. and Owen, L. A., 2012. Climate-controlled landscape evolution in the Western Transverse Ranges, California; insights from Quaternary geochronology of the Saugus Formation and strath terrace flights. Lithosphere 4, (2), 110-130.

Drost, F., Renwick J., Bhaskaran B., Oliver H. and McGregor J., 2007. A simulation of New Zealand's climate during the Last Glacial Maximum. Quaternary Science Reviews 26 (19-21), 2505-2525.

Dymond, J.R., Jessen, M.R. and Lovell, L.R., 1999. Computer simulation of shallow landsliding in New Zealand hill country. International Journal of Applied Earth Observation and Geoinformation 1,122-131.

Eden, D.N., Palmer, A.S., Cronin, S.J., Marden, M. and Berryman, K.R., 2001. Dating the culmination of river aggradation at the end of the last glaciation using distal tephra compositions, eastern North Island, New Zealand. Geomorphology 38, 133-151.

Foster, G. and Carter, L., 1997. Mud sedimentation on the continental shelf at an accretionary margin; Poverty Bay, New Zealand. New Zealand Journal of Geology and Geophysics 40(2), 157-173.

Frings, R. M., Schüttrumpf, H. and Vollmer, S., 2011. Verification of porosity predictors for fluvial sand-gravel deposits. Water Resources Research 47, 15p.

Gage M. and Black, R. D., 1979. Slope stability and geological investigations at Mangatu State Forest, New Zealand Forest Service, Forest Research Institute Technical Paper No. 66, 47p.

Gerber, T.P., Pratson, L.F., Kuehl, S.A., Walsh, J.P., Alexander, C. and Palmer, A., 2010. The influence of sea level and tectonics on Late Pleistocene through Holocene sediment storage along the high-sediment supply Waipaoa continental shelf. Marine Geology 270 (1-4), 139-159

Gibb, J.G., 1978. Rates of coastal erosion and accretion in New Zealand. New Zealand Journal of Marine and Freshwater Research 12, 429-456.

Gibb, J., 1986. A New Zealand regional Holocene eustatic sea-level curve and its application to determination of vertical tectonic movements. Royal Society of New Zealand Bulletin 24, 377-395

Gomez, B., Eden, D. N., Hicks, D. M., Trustrum, N. A., Peacock, D. H. and Wilmshurst, J., 1999. Contribution of floodplain sequestration to the sediment budget of the Waipaoa River, New Zealand. Geological Society Special Publications, 163, 69-88.

Gomez, B., Fulthorpe, C., Carter, L., Berryman, K., Browne, G., Green, M., Hicks, M. and Trustrum, N., 2001. Continental margin sedimentation to be studied in New Zealand, EOS, Transactions, American Geophysical Union 82 (14), 161-167.

Gomez, B., Carter, L. and Trustrum, N. A., 2007. A 2400 yr record of natural events and anthropogenic impacts in intercorrelated terrestrial and marine sediment cores; Waipaoa sedimentary system, New Zealand. Geological Society of America Bulletin 119(11-12), 1415-1432.

Gomez, B. and Livingston, D. M., 2012. The river it goes right on: Post-glacial landscape evolution in the upper Waipaoa River basin, eastern North Island, New Zealand. Geomorphology (159-160), 73-83.

Griffiths, G.A., 1982. Spatial and temporal variability in suspended sediment yields of North Island basins, New Zealand. Water Resources Bulletin 18, 575 -584.

Guthrie-Smith, H.G., 1969. Tutira: The Story of a New Zealand Sheep Station: Wellington, A.H. and A.W. Reed., 464 p.

Guzzetti, F., Ardizzone, F., Cardinali, M., Rossi, M. and Valigi, D., 2009. Landslide volumes and landslide mobilization rates in Umbria, central Italy. Earth and Planetary Science Letters 279(3-4), 222-229.

Hajdas, I., Lowe, D. J., Newnham, R. M. and Bonani, G., 2006. Timing of the late-glacial climate reversal in the Southern Hemisphere using high-resolution radiocarbon chronology for Kaipo Bog, New Zealand. Quaternary Research, 65(2), 340-345.

Healy, J., Vucetich, C. G. and Pullar, W. A., 1964. Stratigraphy and chronology of late Quaternary volcanic ash in Taupo, Rotorua, and Gisborne districts. Bulletin - New Zealand Geological Survey. 88p.

Hewitt, K., 1998. Catastrophic landslides and their effects on the upper Indus streams, Karakoram Himalaya, northern Pakistan. Geomorphology 26(1-3), 47-80.

Hicks, D. M., Hill, J., and Shankar, U., 1996. Variation of suspended sediment yields around New Zealand: The relative importance of rainfall and geology, IAHS Publications 236, 149-156.

Hicks, D. M., Gomez, B. and Trustrum, N. A., 2000. Erosion thresholds and suspended sediment yields, Waipaoa River basin, New Zealand. Water Resources Research 36(4), 1129-1142.

Hicks, D. M., Gomez, B. and Trustrum, N. A., 2004. Event suspended sediment characteristics and the generation of hyperpycnal plumes at river mouths; east coast continental margin, North Island, New Zealand. Journal of Geology 112(4), 471-485

Hoek, E., and Brown, E. T., 1997. Practical estimates of rock mass strength. International Journal of Rock Mechanics and Mining Sciences 34 (8), 1165-1186.

Hogg, S. E. (1982). Sheetfloods, sheetwash, sheetflow, or...? Earth-Science Reviews 18(1), 59-76.

Hovius, N., Stark, C. P. and Allen, P. A., 1997. Sediment flux from a mountain belt derived by landslide mapping. Geology 25(3), 231-234.

Hovius, N., Stark, C. P., Chu, H.and Lin, J., 2000. Supply and removal of sediment in a landslide-dominated mountain belt; central range, Taiwan. Journal of Geology 108(1), 73-89.

Jarosewich, E., Nelen, J. A., Norberg, J. A., 1980. Reference samples for electron microprobe analysis. Geostandards Newsletter. 4, 44p.

Jochum, K. P., Stoll, B., Herwig, K., Willbold, M., Hofmann, A. W., Amini, M., Aarburg, S., Abouchami, W., Hellebrand, E., Mocek, B., Raczek, I., Stracke, A., Alard, O., Bouman, C., Becker, S., Duecking, M., Braetz, H., Klemd, R., de Bruin, D., Canil, D., Cornell, D., de Hoog, C., Dalpe, C., Danyushevsky, L., Eisenhauer, A., Gao, Y., Snow, J. E., Groschopf, N., Guenther, D., Latkoczy, C., Guillong, M., Hauri, E. H., Hoefer, H. E., Lahaye, Y., Horz, K., Jacob, D. E., Kasemann, S. A., Kent, A. J. R., Ludwig, T., Zack, T., Mason, P. R. D., Meixner, A., Rosner, M., Misawa, K., Nash, B. P., Pfaender, J., Premo, W. R., Sun, W. D., Tiepolo, M., Vannucci, R., Vennemann, T., Wayne, D. and Woodhead, J. D., 2006. MPI-DING reference glasses for in situ microanalysis; new reference values for element concentrations and isotope ratios. Geochemistry, Geophysics, Geosystems - G3, 7(2), 44.

Kettner, A. J., Gomez, B. and Syvitski, J. P. M., 2007. Modeling suspended sediment discharge from the Waipaoa River system, New Zealand; the last 3000 years. Water Resources Research 43(7), W07411

Kirby, E. and Whipple, K., 2001. Quantifying differential rock-uplift rates via stream profile analysis. Geology, 29(5), 415-418.

Korup, O., McSaveney, M. J. and Davies, T. R. H., 2004. Sediment generation and delivery from large historic landslides in the Southern Alps, New Zealand. Geomorphology 61(1-2), 189-207.

Korup, O., 2006. Effects of large deep-seated landslides on hillslope morphology, western Southern Alps, New Zealand. Journal of Geophysical Research 111, 18.

Korup, O., Gorum, T. and Hayakawa, Y., 2012. Without power? Landslide inventories in the face of climate change. Earth Surface Processes and Landforms 37(1), 92-99.

Kuehl, S., Carter, L., Gomez, B. and Trustrum, N., 2003. Holistic approach offers potential to quantify mass fluxes across continental margins. EOS, Transactions, American Geophysical Union, vol. 84 (38), 379-388.

Kuehl, S., Alexander, C., Carter, L., Gerald, L., Gerber, T., Harris, C., McNinch, J., Orpin, A., Pratson, L., Syvitski, J. and Walsh, J.P., 2006. Understanding sediment transfer from land to ocean. EOS, Transactions, American Geophysical Union 87 (29) 281.

Lacoste, A., Lonke, L., Chanier, F., Bailleul, J., Vendeville, B. C. and Mahieux, G., 2009. Morphology and structure of a landslide complex in an active margin setting: The Waitawhiti complex, North Island, New Zealand. Geomorphology 109, 184-196.

Lang, A., Moya, J., Corominas, J., Schrott, L. and Dikau, R., 1999. Classic and new dating methods for assessing the temporal occurrence of mass movements. Geomorphology 30(1-2), 33-52.

Larsen, I. J., Montgomery, D. R. and Korup, O., 2010. Landslide erosion controlled by hillslope material. Nature Geoscience 3(4), 247-251.

Larsen, I. J. and Montgomery, D. R., 2012. Landslide erosion coupled to tectonics and river incision. Nature Geoscience advance online publication, http://dx.doi.org/10.1038/ngeo1479.

Leathwick, J. R., Wilson, G. and Stephens, R. T. T., 2002. Climate Surfaces for New Zealand. Landcare Research Contract Report LC9798/126.

Leopold, L. B. and Miller, J. P., 1956. Ephemeral streams - hydraulic factors and their relation to the drainage net. U.S.Geological Survey Professional Paper 262-A, 37 pp.

Lewis, K. B., and Pettinga, J. R., 1993. The emerging imbricate frontal wedge of the Hikurangi Margin, in Sedimentary Basins of the World ,vol. 2, South Pacific Sedimentary Basins, edited by P. B . Ballance, 225-250, Elsevier, New York.

Limpert, E., Stahel, W. A. and Abbt, M., 2001. Log-normal distributions across the sciences- keys and clues. Bio-Science 51, 341-352.

Litchfield, N. and Berryman, K., 2005. Correlation of fluvial terraces within the Hikurangi Margin, New Zealand: implications for climate and baselevel controls. Geomorphology 68, 291-313.

Litchfield, N. J., and Rieser, U., 2005. Optically stimulated luminescence age constraints for fluvial aggradation terraces and loess in the eastern North Island, New Zealand. New Zealand Journal of Geology and Geophysics, 48(4), 581-589.

Litchfield, N. J. and Berryman, K. R., 2006. Relations between postglacial fluvial incision rates and uplift rates in the North Island, New Zealand. Journal of Geophysical Research 111. F02007.

Litchfield, N., Ellis, S., Berryman, K. and Nicol, A., 2007. Insights into subduction-related uplift along the Hikurangi Margin, New Zealand, using numerical modeling. Journal of Geophysical Research 112, F02021.

Litchfield, N. J., 2008. Using fluvial terraces to determine holocene coastal erosion and late pleistocene uplift rates; an example from northwestern Hawke's Bay, New Zealand. Geomorphology 99(1-4), 369-386.

Litchfield, N., Berryman, K., Brackley, H., Carter, L., Marden, M., Page, M., and Trustrum, N., 2008. The Waipaoa Sedimentary System: research review and future directions. IAHS Publication, 325.

Litchfield, N. J., Smith, W. D. and Berryman, K. R., 2009. Return times for high levels of ground shaking (≥ MM7) in the Waipaoa and Waitaki River catchments, GNS Science Report 2009/03. 94p.

Litchfield, N., Wilson, K., Berryman, K., and Wallace, L., 2010. Coastal uplift mechanisms at Pakarae River mouth; constraints from a combined Holocene fluvial and marine terrace dataset. Marine Geology, 270(1-4), 72-83.

Lorrey, A., Williams, P., Salinger, J., Martin, T., Palmer, J., Fowler, A., Zhao, J-X and Neil, H., 2008. Speleothem stable isotope records interpreted within a multi-proxy framework and implications for New Zealand palaeoclimate reconstruction. Quaternary International 187, 52-75.

Lowe, D., Newnham, R. and Ward, C., 1999. Stratigraphy and chronology of a 15 ka sequence of multi-sourced silicic tephras in a montane peat bog, eastern North Island, New Zealand. New Zealand Journal of Geology and Geophysics 42, 565-579.

Lowe, D., Shane, P., Alloway, B. and Newnham, R., 2008. Fingerprints and age models for widespread New Zealand tephra marker beds erupted since 30,000 years ago: a framework for NZ-INTIMATE. Quaternary Science Reviews 27, 95-126.

Lowe, D., 2011. Tephrochronology and its application: A review. Quaternary Geochronology 6, 107-153.

Mackey, B. H. and Roering, J. J., 2011. Sediment yield, spatial characteristics, and the long-term evolution of active earthflows determined from airborne LiDAR and historical aerial photographs, Eel River, California. Bulletin of the Geological Society of America 123(7-8).

Malamud, B. D, Turcotte, D. L., Guzzetti, F. and Reichenbach, P., 2004a. Landslide inventories and their statistical properties. Earth Surface Processes and Landforms 26, 687-711.

Malamud, B. D, Turcotte, D. L., Guzzetti, F. and Reichenbach, P., 2004b. Landslides, earthquakes and erosion . Earth and Planetary Science Letters 229, 45-59.

Marden, M. and Rowan, D., 1994. Protective value of vegetation on Tertiary terrain before and during Cyclone Bola, East Coast, North Island, New Zealand. New Zealand Journal of Forestry Science 23, 255-263.

Marden, M., Mazengarb, C., Palmer, A., Berryman, K. and Rowan, D., 2008. Last glacial aggradation and postglacial sediment production from the non-glacial Waipaoa and Waimata catchments, Hikurangi Margin, North Island, New Zealand. Geomorphology 99, 404-419.

Marden, M., Betts, H., Palmer, A., Tayor, R. and Bilderback, E., In prep. Post-Last Glacial Maximum channel incision and sediment flux history of the non-glacial Waipaoa River, North Island, New Zealand.

Marsaglia, K. M., DeVaughn, A. M., James, D.E. and Marden, M., 2010. Provenance of fluvial terrace sediments within the Waipaoa sedimentary system and their importance to New Zealand source-to-sink studies. Marine Geology 270, 84-93.

Mazengarb, C. and Speden, I.G., 2000. Geology of the Raukumara Area. Institute of Geological and Nuclear Sciences 1:250,000 geological map 6. 1 sheet and 60pp. Institute of Geological and Nuclear Sciences Ltd., Lower Hutt, New Zealand.

McGlone, M. S., 2001. A late Quaternary pollen record from marine core P69, southeastern North Island, New Zealand. New Zealand Journal of Geology and Geophysics 44, 69-77.

McGlone, M.S., 2002. A Holocene and latest Pleistocene pollen record from Lake Poukawa, Hawke‘s Bay, New Zealand. Global and Planetary Change 33, 283-299.

McGlone, M. S., Turney, C. S. M. and Wilmshurst J. M., 2005. Otamangakau (Tongariro) and Durham Road (Taranaki) and the climatic interpretation of the Late-Glacial central North Island vegetation record. In Proceedings of 2005 NZ-INTIMATE Meeting, GNS Rafter Laboratory, Lower Hutt, July 4-5 2005, Alloway, B.V. and Shulmeister, J. (eds). Institute of Geological and Nuclear Sciences, Science Report, SR 2005/18,13.

McWethy, D. B., Whitlock, C., Wilmshurst, J. M., McGlone, M. S., Fromont, M., Li, X., Dieffenbacher-Krall, A., Hobbs, W.O., Fritz, S.C. and Cook, E.R., 2010. Rapid landscape transformation in south island, New Zealand, following initial Polynesian settlement. Proceedings of the National Academy of Sciences of the United States of America 107(50), 21343-21348.

Miller, A. J. and Kuehl, S. A., 2010. Shelf sedimentation on a tectonically active margin; a modern sediment budget for poverty continental shelf, New Zealand. Marine Geology 270(1-4), 175-187.

Milliman, J. D. and Farnsworth, K. L., 2011. River Discharge to the Coastal Ocean : A Global Synthesis. Cambridge University Press. 394 p.

Milliman, J. D. and Syvitski J. P. M., 1992. Geomorphic/tectonic controls of sediment discharge to the ocean: The importance of small mountainous rivers. The Journal of Geology 100 (5), 525-544.

Montgomery, Schmidt, K. M., Greenberg, H. M. and Dietrich, W. E., 2000. Forest clearing and regional landsliding. Geology 28(4), 311-314.

Montgomery, D. R., 2001. Slope distributions, threshold hillslopes, and steady-state topography. American Journal of Science, 301(4-5), 432-454.

Montgomery, D. R. and Brandon, M. T., 2002. Topographic controls on erosion rates in tectonically active mountain ranges. Earth and Planetary Science Letters 201(3-4), 481-489.

Neef, G. and Bottrill, R. S., 1992. The Cenozoic geology of the Gisborne area (1:50,000 metric sheet Y18AB) North Island, New Zealand, New Zealand Journal of Geology and Geophysics 35, 4, 515-531.

Newnham, R. M. and Lowe, D. J., 2000. Fine-resolution record of late-glacial climate reversal from New Zealand. Geology 28, 759-762.

Newnham, R.M., Lowe, D.J., Green, J.D., Turner, G.M., Harper, M.A., McGlone, M.S., Stout, S.L., Horie, S. and Froggatt, P.C. 2004, A discontinuous ca. 80 ka record of late Quaternary environmental change from Lake Omapere, Northland, New Zealand, Palaeogeography, Palaeoclimatology, Palaeoecology, 207 (1-2),165-198.

Niemann, J. D., Gasparini, N. M., Tucker, G. E., and Bras, R. L., 2001. A quantitative evaluation of Playfair's law and its use in testing long-term stream erosion models. Earth Surface Processes and Landforms, 26(12), 1317-1332.

Norton, K. P., von Blanckenburg, F., DiBiase, R., Schlunegger, F.and Kubik, P. W., 2011. Cosmogenic super(10)be-derived denudation rates of the eastern and southern European Alps. International Journal of Earth Sciences 100(5), 1163-1179.

Orpin, A. R., Alexander, C., Carter L., Kuehl and S., Walsh, J. P., 2006. Temporal and spatial complexity in post-glacial sedimentation on the tectonically active, Poverty Bay continental margin of New Zealand. Continental Shelf Research 26, 2205-2224.

Orpin, A. R., Carter, L., Page, M. J., Cochran, U. A., Trustrum, N. A., Gomez, B., Palmer, A. S., Mildenhall, D. C., Rogers, K. M., Brackley, H. L. and Northcote, L., 2010. Holocene sedimentary record from Lake Tutira: A template for upland watershed erosion proximal to the Waipaoa Sedimentary System, northeastern New Zealand. Marine Geology 270, 11-29.

Ota, Y., Hull, A. G. and Berryman, K. R., 1991. Coseismic uplift of Holocene marine terraces in the Pakarae river area, eastern North Island, New Zealand. Quaternary Research, 35(3), 331-346.

Ota, Y., Hull, A. G., Iso, N., Ikeda, Y., Moriya, I. and Yoshikawa, T., 1992. Holocene marine terraces on the northeast coast of North Island, New Zealand, and their tectonic significance. New Zealand Journal of Geology and Geophysics, 35(3), 273-288.

Page, M. J., Trustrum, N. A. and DeRose, R. C., 1994a. A high resolution record of storm-induced erosion from lake sediments, New Zealand. Journal of Paleolimnology 11, 333-348.

Page, M. J., Trustrum, N. A. and Dymond, J., 1994b. Sediment budget to assess the geomorphic effect of cyclonic storm, New Zealand. Geomorphology 9, 169-188.

Page, M. J. and Trustrum, N. A., 1997. A late Holocene lake sediment record of the erosion response to land use change in a steepland catchment, New Zealand. Zietschrift für Geomorphology N.F. 41, 369-392.

Page, M. J., Reid, L. M. and Lynn, I. H., 1999. Sediment production from Cyclone Bola landslides, Waipaoa catchment. Journal of Hydrology (NZ) 38, 2, 289-308.

Page, M.J., Trustrum, N.A., Brackley, H.L. and Baisden, W.T. 2004. Erosion-related soil carbon fluxes in a pastoral steepland catchment, New Zealand. Agriculture, Ecosystems and Environment 103:561-579.

Page, M. J., Trustrum, N. A., Orpin, A. R., Carter, L., Gomez, B., Cochran, U. A., Mildenhall, D. C., Rogers, K. M., Brackley, H. L., Palmer, A. S. and Northcote, L., 2010. Storm frequency and magnitude in response to Holocene climate variability, Lake Tutira, North-Eastern New Zealand. Marine Geology 270, 30-44.

Page, M. J. and Lukovic, B., 2011. An inventory of deep-seated landslides in the Waipaoa and Waimata catchments. GNS Science Report 2011/08. 74 p.

Pazzaglia, F. J. and Brandon, M. T., 2001. A fluvial record of long-term steady-state uplift and erosion across the Cascadia forearc high, western Washington state. American Journal of Science, 301(4-5), 385-431.

Pearce, A. J. and Black, R., D., 1981. Erosion and sediment transport in Pacific rim steeplands. IAHS Publication 132, 95-121.

Pettinga, J. R. and Bell, D. H., 1992. Engineering geological assessment of slope instability for rural land-use, Hawke‘s Bay, New Zealand.- in: Bell, D.H. (ed.): Landslides - Proceedings of the Sixth International Symposium, Christchurch, 10-14 February 1992, Rotterdam, A.A. Balkema, Vol. 2(3), 1467-1480.

Preston N. J. and Crozier M. J., 1999. Resistance to shallow landslide failure through root-derived cohesion in East Coast hill country soils, North Island, New Zealand. Earth Surface Processes and Landforms 24, 665-675.

Pullar, W. A., 1962. Soils and agriculture of Gisborne plains. Soil Bureau Bulletin (New Zealand, Department of Scientific and Industrial Research).Wellington. 89 pp.

Reid, L. M. and Page, M. J., 2002. Magnitude and frequency of landsliding in a large New Zealand catchment. Geomorphology 49(1-2), 71-88.

Reyners, M., Eberhart-Phillips, D. and Stuart, G., 1999. A three-dimensional image of shallow subduction; crust structure of the Raukumara Peninsula, New Zealand. Geophysical Journal International, 137(3), 873-890.

Rohling, E. J., Fenton, M., Jorissen, F. J., Bertrand, P., Ganssen, G., and Caulet, J. P., 1998. Magnitudes of sea-level lowstands of the past 500,000 years. Nature (London), 394(6689), 162-165.

Rohling, E. J., Grant, K., Bolshaw, M., Roberts, A. P., Siddall, M., Hemleben, C., and Kucera, M., 2009. Antarctic temperature and global sea level closely coupled over the past five glacial cycles. Nature Geoscience, 2(7), 500-504.

Sandiford A., Newnham R., Alloway B. V. and Ogden, J., 2003. A 28000-7600 cal yr BP pollen record of vegetation and climate change from Pukaki Crater, northern New Zealand. Palaeogeography, Palaeoclimatology, Palaeoecology 201, 235-247.

Schmidt, K. M. and Montgomery, D. R., 1995. Limits to relief. Science, 270(5236), 617-620.

Sclater, J.G. and Christie, P.A.F., 1980. Continental stretching; explanation of post-Mid-Cretaceous subsidence of central North Sea basin. AAPG Bulletin, 64 (5), 781-782.

Shackleton, N. J., 1987. Oxygen isotopes, ice volume and sea level. Quaternary Science Reviews, 6 (3-4), 183-190.

Shane, P. A. R., Smith, V. C., Lowe, D. J. and Nairn, I. A., 2003. Reidentification of ca. 15,700 cal yr BP tephra bed at Kaipo Bog, eastern North Island: implications for dispersal of Rotorua and Puketarata tephra beds. New Zealand Journal of Geology and Geophysics 46, 591-596.

Shulmeister, J., Goodwin, I., Renwick, J., Harle, K., Armand, L., McGlone, M. S., Cook, E., Dodson, J., Hesse, P.P., Mayewski, P. and Curran, M.. 2004. The Southern Hemisphere westerlies in the Australasian sector over the last glacial cycle: a synthesis. Quaternary International 118-119, 23-53.

Siddall, M., Chappell, J., abd Potter, E. K., 2007. Eustatic sea level during past interglacials. Developments in Quaternary Science, 7, 75-92.

Sklar, L. and Dietrich, W. E., 1998. River longitudinal profiles and bedrock incision models; stream power and the influence of sediment supply. Geophysical Monograph, 107, 237-260.

Smith, V., Shane, P. and Nairn, I., 2005. Trends in rhyolite geochemistry, mineralogy, and magma storage during the last 50 kyr at Okataina and Taupo volcanic centres, Taupo volcanic zone, New Zealand. Journal of Volcanology and Geothermal Research 148, 372-406.

Smith, V. C., Shane, P. A. R., Nairn, I. A. and Williams, C. M., 2006. Geochemistry and magmatic properties of eruption episodes from Haroharo linear vent zone, Okataina Volcanic Centre, New Zealand, during the last 10 kyr. Bulletin of Volcanology 69, 57-88.

Snyder, N. P., Whipple, K. X., Tucker, G. E. and Merritts, D. J., 2000. Landscape response to tectonic forcing: Digital elevation model analysis of stream profiles in the Mendocino triple junction region, Northern California. Bulletin of the Geological Society of America, 112(8), 1250-1263.

Snyder, N. P., Whipple, K. X., Tucker, G. E. and Merritts, D. J., 2003. Channel response to tectonic forcing; field analysis of stream morphology and hydrology in the Mendocino triple junction region, Northern California. Geomorphology, 53(1-2), 97-127.

Stark, C. P., and Guzzetti, F., 2009. Landslide rupture and the probability distribution of mobilized debris volumes. Journal of Geophysical Research, 114, F00A02.

Syvitski, J. P. M., Voeroesmarty, C. J., Kettner, A. J. and Green, P., 2005. Impact of humans on the flux of terrestrial sediment to the global coastal ocean. Science 308 (5720), 376-380.

Upton, P., Koons, P. O. and Eberhart-Phillips, D., 2003. Extension and partitioning in an oblique subduction zone, New Zealand; constraints from three-dimensional numerical modeling. Tectonics 22(6), 14.

Upton, P., Kettner, A. J., Gomez, B., Orpin, A. R., Litchfield, N. and Page, M. J. In press. Simulating post-LGM riverine fluxes to the coastal zone: The Waipaoa River system, New Zealand., Computers & Geosciences, doi:10.1016/j.cageo.2012.02.001.

Van Den Eeckhaut, M., Poesen, J., Govers, G., Verstraeten, G. and Demoulin, A., 2007. Characteristics of the size distribution of recent and historical landslides in a populated hilly region. Earth and Planetary Science Letters 256(3-4), 588-603.

Vandergoes, M. J., Hogg, A. G., Lowe, D. J., Newnham, R. M., Denton, G. H., Southon, J., Barrell, D. J. A., Wilson, C. J. N., McGlone, M. S., Allan, A. S. R., Almond, P. C., Petchey, F., Dabell, K., Dieffenbacher-Krall, A. C., Blaauw, M., In press. A revised age for the Kawakawa/Oruanui tephra, a key marker for the Last Glacial Maximum in New Zealand, Quaternary Science Reviews, http://dx.doi.org/10.1016/j.quascirev.2012.11.006

von Blanckenburg, F., 2005. The control mechanisms of erosion and weathering at basin scale from cosmogenic nuclides in river sediment. Earth and Planetary Science Letters 237(3-4), 462-479.

Vucetich, C. G. and Pullar, W. A., 1964. Stratigraphy and chronology of late Quaternary volcanic ash in Taupo, Rotorua, and Gisborne districts, Part 2. Stratigraphy of Holocene ash in the Rotorua and Gisborne districts. New Zealand Geological Survey Bulletin. 73,43-78.

Vucetich, C. G. and Pullar, W. A., 1969. Stratigraphy and chronology of late Pleistocene volcanic ash beds in central North Island, New Zealand. New Zealand Journal of Geology and Geophysics 12 (4), 784-821.

Walcott, R. I., 1987. Geodetic strain and the deformational history of the North Island of New Zealand during the late Cenozoic. Royal Society of London, London, United Kingdom (GBR), Jan 20, 163 pp.

Walling, D.E. and Webb, B.W., 1996. Erosion and sediment yield: a global overview. IAHS Publications 236, 3-19.

Warton, D.I., Wright, I.J., Falster, D.S. and Westoby, M., 2006. Bivariate line-fitting methods for allometry. Biological Reviews 81 (2), 259-291. Wilson, K., Berryman, R., Litchfield, N. and Little, T., 2006. A revision of mid-late Holocene marine terrace distribution and chronology at the Pakarae River mouth, North Island, New Zealand. New Zealand Journal of the Geological Society 49, 477-489.

Whipple, K. X., and Tucker, G. E., 1999. Dynamics of the stream-power river incision model; implications for height limits of mountain ranges, landscape response timescales, and research needs. Journal of Geophysical Research, 104, 17-17,674.

Whiteford, C. M. and Lumb, J. T., 1975. A Catalogue of physical properties of rocks. Volume 2: Listing by geographic location. Geophysics Division DSIR report 106.

Wilmshurst, J. M., Eden, D. N. and Froggatt, P. C., 1999. Late Holocene forest disturbance in Gisborne, New Zealand: a comparison of terrestrial and marine pollen records. New Zealand Journal of Botany 37, 523-540.

Wilmshurst, J. M., Hunt, T. L., Lipo, C. P. and Anderson, A. J., 2011. High-precision radiocarbon dating shows recent and rapid initial human colonization of East Polynesia. Proceedings of the National Academy of Sciences of the United States of America 108(5), 1815-1820.

Wilson, K., Berryman, R., Litchfield, N. and Little, T., 2006. A revision of mid-late Holocene marine terrace distribution and chronology at the Pakarae River mouth, North Island, New Zealand. New Zealand Journal of the Geological Society 49, 477-489.

Wobus, C., Whipple, K., Kirby, E., Snyder, N., Johnson, J., Spyropolou, K., Crosby, B. and Sheehan, D., 2006. Tectonics from topography; procedures, promise, and pitfalls. Special Paper - Geological Society of America 398, 55-74.

Wolinsky, M. A., Swenson, J. B., Litchfield, N. J. and McNinch, J.E., 2010. Coastal progradation and sediment partitioning in the Holocene Waipaoa Sedimentary System, New Zealand. Marine Geology 270, 94-107.

Wu, W. and Wang, S. S. Y. , 2006. Formulas for sediment porosity and settling velocity. Journal of Hydraulic Engineering 132 (8), 858- 862.

Young and Ashford, S. A., 2006. Application of airborne LIDAR for seacliff volumetric change and beach-sediment budget contributions. Journal of Coastal Research 22(2), 307-318.